UNIVERSIDADE FEDERAL DE MINAS GERAIS
Escola de Engenharia
Programa de Pós-graduação em Engenharia Metalúrgica, Materiais e de Minas

Marina Luisa Silva Coelho

Arsenic and sulfate release from sulfide minerals: effect of galvanic interaction and soluble iron

Belo Horizonte
2022

Marina Luisa Silva Coelho

ARSENIC AND SULFATE RELEASE FROM SULFIDE MINERALS: **effect of galvanic interaction and soluble iron**

Dissertação de mestrado apresentado ao Programa de Pós-Graduação em Engenharia Metalúrgica, Materiais e de Minas da Universidade Federal de Minas Gerais, como requisito parcial para obtenção do título de Mestra em Engenharia Metalúrgica, Materiais e de Minas.

Orientadora: Profa. Virgínia Sampaio Teixeira Ciminelli

Coorientador: Prof. Daniel Majuste

Belo Horizonte
2022

Coelho, Marina Luisa Silva.
C672a Arsenic and sulfate release from sulfide minerals [recurso eletrônico] : effect of galvanic interaction and soluble iron / Marina Luisa Silva Coelho . - 2022.
1 recurso online (116 f.: il., color.) : pdf.

Orientadora: Virginia Sampaio Teixeira Ciminelli.
Coorientador: Daniel Majuste.

Dissertação (mestrado) - Universidade Federal de Minas Gerais, Escola de Engenharia.

Apêndices: f. 102-116.

Bibliografia: f. 92-101.

1. Engenharia metalúrgica - Teses. 2. Metalurgia extrativa - Teses. 3. Sulfetos - Teses. 4. Arsênio - Teses. 5. Oxidação - Teses. I. Ciminelli, V. S. T. (Virginia Sampaio Teixeira) II. Majuste, Daniel. III. Universidade Federal de Minas Gerais. Escola de Engenharia. IV. Título.

CDU: 669(043)

Ficha catalográfica elaborada pelo bibliotecário Reginaldo César Vital dos Santos CRB/6 2165
Biblioteca Prof. Mário Werneck, Escola de Engenharia da UFMG

UNIVERSIDADE FEDERAL DE MINAS GERAIS
ESCOLA DE ENGENHARIA
Programa de Pós-Graduação em Engenharia Metalúrgica, Materiais e de Minas

A dissertação intitulada **"*Arsenic and sulfate release from sulfide minerals: effect of galvanic interaction and soluble iron*"**, área de concentração: Metalurgia Extrativa e Meio Ambiente, apresentada pela candidata **Marina Luisa Silva Coelho**, para obtenção do grau de Mestre em Engenharia Metalúrgica, Materiais e de Minas, foi aprovada pela comissão examinadora constituída pelos seguintes membros:

Documento assinado digitalmente
gov.br VIRGINIA SAMPAIO TEIXEIRA CIMINELLI
Data: 07/06/2023 14:55:27-0300
Verifique em https://validar.iti.gov.br

Dra. Virginia Sampaio Teixeira Ciminelli
Orientadora (UFMG)

Documento assinado digitalmente
gov.br DANIEL MAJUSTE
Data: 09/06/2023 21:30:19-0300
Verifique em https://validar.iti.gov.br

Dr. Daniel Majuste
(UFMG)

Documento assinado digitalmente
gov.br HELIO ANDERSON DUARTE
Data: 07/06/2023 16:32:26-0300
Verifique em https://validar.iti.gov.br

Dr. Hélio Anderson Duarte
(UFMG)

Documento assinado digitalmente
gov.br CLAUDIA LIMA CALDEIRA
Data: 12/06/2023 11:17:46-0300
Verifique em https://validar.iti.gov.br

Dra. Cláudia Lima Caldeira
(UFMG)

Documento assinado digitalmente
gov.br EDUARDO HENRIQUE MARTINS NUNES
Data: 09/08/2023 21:07:34-0300
Verifique em https://validar.iti.gov.br

_____

Coordenador do Programa de Pós-Graduação em Engenharia Metalúrgica, Materiais e de Minas/UFMG

Belo Horizonte, 19 de dezembro de 2022

AGRADECIMENTOS

À minha mãe, Vilma Regina Coelho, por não medir esforços para me fazer feliz. Verdadeiramente a principal responsável para meu acesso a uma boa educação escolar. Minha maior admiração! Gratidão imensa por todo suporte e amor maternal.

À minha avó, Irene da Silva Coelho, guerreira e amável. Uma mulher à frente do seu tempo. Fonte de inspiração. Sinceros agradecimentos pelo cuidado e carinho. Saudades eternas.

Ao meu pai, José Francisco da Silva, e às minhas irmãs por serem ponte de apoio e por sempre acreditarem em mim.

Às minhas tias Maria de Fátima de Jesus e Luiza Helena Coelho. Muito obrigada pelo suporte ao longo de todos esses anos e por todo incentivo aos meus estudos. Vocês são pilares estruturais de minha formação.

Ao meu companheiro, também melhor amigo, Gabriel Damião.

À orientadora Virginia Ciminelli, por seu imenso conhecimento e bagagem acadêmica. Pela imensurável contribuição a esta pesquisa, pelo direcionamento e pela credibilidade depositada em mim para realização desse trabalho.

Ao coorientador Daniel Majuste pelas incisivas pontuações neste trabalho.

A todas as amizades adquiridas no Laboratório de Processamento Aquoso. Em especial à Nelson Freire e à Taiane Guedes. Obrigada pelo apoio, ideias ao trabalho, ajuda na execução de experimentos e pelos agradáveis momentos juntos compartilhados – fundamentais para enfrentamento do período de pandemia de forma mais leve.
Meu muito obrigada também à Thaiara Cristina, pela efetuação de experimentos de bancada em meu período ausente, e à Daísa Alves, Cláudia Caldeira e Maria Sylvia Dantas. Vocês todas foram imprescindíveis para conclusão deste trabalho.

A todos os professores que contribuíram para minha formação.

À Escola Madre Paula de Ensino Infantil e Fundamental, quanta lembrança boa, quanto aprendizado. Agradecimentos especiais à professora Regina (ensino infantil), à Ana Paula e Luiza – professoras de português, Davidson e Patrícia – professores de matemática, Amilde – professora de Ciências, Karla e Lizandra – professoras de Geografia e História – Harielma, professora de inglês, João Paulo – professor de Educação Física, Maria Luiza – professora de artes.

Aos professores do Colégio São José.
Às inesquecíveis aulas de matemática lecionadas pelo professor Reginaldo, de física com professor o Gabriel e de química com Eliane Bambirra. Sinceros agradecimentos. Vocês possuem enorme contribuição em minha escolha profissional e acesso à universidade pública. Agradeço também à Janaína, professora de português e ao Geraldo, professor de História.

À equipe do Laboratório de análises químicas do Departamento de Engenharia de Metalúrgica e de Materiais da UFMG . Em especial à Hellen Andrade e Filipe Alves.

Às agências de fomento, Capes, CNPq e FAPEMIG pelo apoio financeiro que viabilizou esta pesquisa.

ABSTRACT

The oxidation of mineral samples rich in arsenopyrite (>90%) has been extensively studied by a continuous flow system under oxygen saturation or depletion conditions. Considering the tailings dam context, several effects were evaluated to better determine the rate of arsenopyrite oxidation in a circumneutral medium. These effects involve: the evaluation of the presence of iron oxide products on the mineral surface, the influence of pH (range 4 -10) and dissolved oxygen and the effect of ferric ions and iron complexing agents. This work also studied, for the first time, the influence of the physical association between arsenopyrite/pyrrhotite sulfides on the release of As, Fe S. Two distinct proportions were investigated: i) Apy: Pyh - 1:1; i.e., 50% of each sample; ii) Apy: Pyh - 1:3; i.e., 25% arsenopyrite and 75% pyrrhotite. Under steady-state conditions, the rate of oxidation of arsenopyrite is about 200% higher when the particles are covered by a layer of iron oxidation products compared to the rate at the fresh surface. It is suggested that the iron product layer increases the availability of soluble Fe(III) - a strong oxidant - even at pH conditions close to neutral. Regarding the influence of pH and dissolved oxygen, arsenopyrite has a lower reaction rate at pH 7 ($3.54 \times 10^{-10} \pm 0.03$ mol $m^{-2}.s^{-1}$, and $7.93 \times 10^{-11} \pm 0.08$ mol $m^{-2}.s^{-1}$ under oxygen-saturated and oxygen-depleted condition, respectively). The addition of 1mmol of citrate to the leaching medium showed a remarkable effect on arsenopyrite oxidation – the release of As and S increased by about 300% –. This higher oxidation is associated in this study with the higher concentration of soluble ferric ions due to the formation and maintenance of the Fe(II)-citrate-/Fe(III)-citrate redox cycle in the presence of oxygen. The complexing effect of chloride ions (1 mmol) increases to a lesser extent (35%) the oxidation of FeAsS Under oxygen-depleted conditions, As and S release is significantly reduced (more than 75% for any pH range) in the presence or absence of iron complexing agents. Regardless of the proportion and sample of pyrrhotite used, the association of arsenopyrite/pyrrhotite pairs showed no galvanic effect, that is, insignificant differences were observed concerning the oxidation of individual sulfides, which allows us to conclude that arsenopyrite is not catholically protected during association with pyrrhotite.

Keywords: arsenic; oxidation; sulfides; galvanic interaction; soluble iron.

RESUMO

A oxidação de amostras minerais ricas em arsenopirita (>90%) foi extensivamente estudada por um sistema de fluxo contínuo sob condições de saturação ou depleção de oxigênio. Considerando o contexto de barragem de rejeitos, vários efeitos foram avaliados para melhor determinar a taxa de oxidação da arsenopirita em meio circumneutro. Estes efeitos envolvem: avaliação da presença de produtos de óxidos de ferro na superfície do mineral, influência do pH (faixa de 4 -10) e de oxigênio dissolvido, efeito de íons férricos e agentes complexantes com ferro. Este trabalho também estudou, pela primeira vez, a influência da associação física entre os sulfetos arsenopirita/pirrotita na liberação de As, Fe S. Sob condições de estado estacionário, a taxa de oxidação da arsenopirita é cerca de 200% maior quando as partículas são cobertas por uma camada de produtos de oxidação de ferro em comparação com a taxa da superfície fresca. Sugere-se que a camada de produto de ferro aumenta a disponibilidade de Fe (III) solúvel - um oxidante forte - mesmo em condições de pH próximo da neutralidade. Em relação à influência do pH e de oxigênio dissolvido, a arsenopirita tem uma taxa de reação mais baixa em pH 7 ($3.54 \times 10^{-10} \pm 0.03$ mol $m^{-2}.s^{-1}$, e $7.93 \times 10^{-11} \pm 0.08$ mol $m^{-2}.s^{-1}$ em condições de saturação e depleção de oxigênio, respectivamente). O oxigênio tem um efeito positivo na liberação de arsênio em qualquer condição de pH. A adição de 1mmol de citrato ao meio lixiviante mostrou um efeito notável na oxidação da arsenopirita – a liberação de As e S aumentou cerca de 300% –. Essa maior oxidação é associada neste estudo à maior concentração de íons férricos solúveis devido formação e manutenção do ciclo Fe (II)-citrato^{-} /Fe (III)-citrato par redox na presença de oxigênio. O efeito complexante dos íons cloreto (1 mmol) é menor, mas aumenta a oxidação do FeAsS em cerca de 35%. Sob condições de depleção de oxigênio, a liberação de As e S é significativamente reduzida (mais de 75% para qualquer faixa de pH) na presença ou na ausência de agentes complexantes de ferro. Independente da proporção e da amostra de pirrotita usada, a associação dos pares arsenopirita/pirrotita não mostrou efeito galvânico, ou seja, diferenças insignificantes foram observadas em relação à oxidação dos sulfetos individuais, o que permite concluir que a arsenopirita não é catodicamente protegida durante associação dos sulfetos.

Palavras-chave: arsênio; oxidação; sulfetos; interação galvânica; ferro solúvel.

FIGURES

TABLES

SUMMARY

1. INTRODUCTION

Ranked as the twentieth most abundant element in the earth's crust and found in more than 245 minerals (Mandal and Suzuki, 2002), arsenic (As) is toxic to human health. The weathering of arsenic minerals disposed of in tailing impoundments or in waste-rock dumps can become a crucial source of water contamination by arsenic and sulfate (Araujo *et al*., 2019).

Arsenopyrite (FeAsS) is the main arsenic-bearing mineral. Due to its low economic value, arsenopyrite usually is disposed of as solid waste during metal extraction (Corkhill and Vaughan, 2009). Under reducing conditions, arsenopyrite is stable. However, this mineral readily oxidizes by the weathering of rocks, leading to the formation of acid mine drainage and mobilization of arsenic in the aqueous medium (YU *et al*, 2007; Ciminelli, 2014). When oxidized, arsenic is found at tri- and pentavalent states (H_3AsO_3 and H_3AsO_4). Their dissociation products also occur in aqueous media. Both oxidation states, but especially the trivalent form, are harmful and might cause cancer, skin changes, respiratory problems (bronchitis, rhinitis, lung diseases), and cardiovascular diseases (Mandal and Suzuki, 2002; Bhattacharya *et al.*, 2007).

The occurrence of natural processes, such as weathering, biological activity, and volcanic emissions, are predominant in the As mobilization. These processes occur in different parts of the world - especially in Southeast Asia and Latin America (Bundschuh *et al*., 2010). However, anthropogenic activities, especially mining, also represent a potential risk of environmental contamination and to human health, mainly due to the mobilization of As present in large volumes of tailings and wastes (Smedley and Kinniburgh, 2002). Thus, the extraction of sulfide ore deposits requires risk control and adequate tailings disposal. In this context, toxic elements that do not have industrial applications, such as arsenic, are the center of attention in environmental licensing processes (Ciminelli, 2014).

To inhibit and understand the limiting steps of the arsenopyrite oxidation reaction, the mechanisms of oxidation of this sulfide have been extensively investigated in the literature. Thus, factors related to the influence of temperature, pH, oxygen concentration, and Fe(III) oxidation have been studied (Craw *et a*l., 2003; Walker *et al*., 2006; YU *et al.*, 2007;

Mckibben *et al*., 2008, Asta *et al*. 2010, Singh *et al*., 2015). Density Functional Theory (DFT) calculations were also performed to better understanding the arsenopyrite oxidation mechanism (Silva *et al*., 2015; Dos Santos *et al*., 2017; Silva *et al.,* 2017). Nevertheless, as highlighted in the review of Corkhill and Vaughan (2009), there are relevant gaps regarding the oxidation kinetics of arsenopyrite. Furthermore, there is a scarcity of studies about the behavior of this mineral at circumneutral pH (typical condition found in tailings). Therefore, the present work aims at further elucidation regarding the oxidation of this arsenic sulfide under pH conditions close to neutrality.

Sulfate is also a constant concern in the environmental scenario. Although not toxic to human health, sulfates can cause dehydration and diarrhea in humans (WHO, 2018). Sharma and Kumar (2020) highlight the salinization of freshwater bodies, pipes corrosion, and pipes incrustation (blockage of fluids passage) as the main problems owing to the high concentration of sulfate in an aqueous medium.

Ordinance 518/2004 of the Ministry of Health of Brazil and the Environmental Protection Agency of the United States (EPA) determines the maximum sulfate limit in drinking water to be 250 mg /L. Despite that, Fernando et al., 2018 state that most mine effluents present SO_4^{2-} ions higher than the allowable. Hence, several studies aim to remove sulfate ions from these wastes (Moosa *et al*., 2002; Kosutic *et al*., 2003; Madzivire *et al*., 2011; Cao *et al*., 2011; Torres *et al*., 2018; Araujo *et al*., 2019). The most used technique for sulfate removal is gypsum precipitation. Therefore, a decrease in sulfate production in extractive processes has, among others, the advantage for decreasing the waste disposal costs and the environmental liabilities.

The oxidation of metallic sulfides is the main factor contributing to the introduction of sulfates into waterways (Fernando *et al.*, 2018). Pyrite (FeS_2) and pyrrhotite ($Fe_{1-x}S$) are the most common iron sulfides in tailings and waste rock deposits of precious and base metals. While pyrite oxidation kinetics has been widely studied in the literature, studies on fundamental mechanisms and chemistry associated with pyrrhotite oxidation are scarce (Mycroft, 1995; Janzen *et al*., 2000). Despite this, pyrrhotite is one of the most reactive sulfides (Bezile *et al*., 2004) and thus, it is an important contributor to sulfate production in an aqueous medium and to the formation of acid mine drainage (AMD). In addition, the conditions accelerating the dissolution of the pyrrhotite mineral - such as pH, oxygen concentration, and the galvanic effect due to contact with other sulfides - are not established

in the literature. For this reason, the identification of these conditions is one of the objectives of the present work.

Pyrite, arsenopyrite, and pyrrhotite are sulfides generally found associated, so galvanic interactions can occur in tailings piles. Pyrite has the highest rest potential (E_R = 0.405 V - SHE) among primary sulfides at pH conditions close to neutrality. A recent work (Ferreira *et al.*, 2021) found that the galvanic interaction between pyrite and arsenopyrite particles at pH 7 increases the oxidation rate of the sulfide containing arsenic due to the lower value (0.277 V-SHE) of arsenopyrite compared to pyrite (Pozzo and Iwasaki, 1989; Iwasaki, 1989). Nonetheless, among the most common sulfides (pyrite, pyrrhotite, sphalerite, galena, arsenopyrite, and chalcopyrite), pyrrhotite is the mineral with the lowest rest potential at circumneutral pH. (E_R = 0.125 V). Therefore, contrary to the association with pyrite, arsenopyrite is expected to react cathodically in the arsenopyrite/pyrrhotite galvanic couple, leading to a reduction of arsenic release in the aqueous environment.

This work aims to investigate the behavior of the release of arsenic from the oxidation of a rich arsenopyrite mineral sample and the generation of sulfate from the oxidation of a pyrrhotite sample. Hence, the samples will be subjected to oxidation under circumneutral pH in the presence and absence of oxygen. Considering the common association of sulfide minerals in tailings dams, the galvanic interaction of the arsenopyrite/pyrrhotite and pyrite/pyrrhotite couples will also be analyzed. The main objectives are:

- To study the effect of pH, oxygen, and soluble iron on arsenic release from arsenopyrite oxidation at circumneutral conditions.
- To understand the effect of increasing the soluble iron on arsenopyrite oxidation by means of adding iron complexing agents - soluble citrate and chloride.
- To study the effect of galvanic interaction on sulfate release and to confirm lower arsenic release from sulfide mixtures (arsenopyrite/pyrrhotite couple).
- To investigate the effect of oxygen on sulfate release from pyrrhotite oxidation at pH 7.

By investigating the behavior of arsenopyrite and pyrrhotite under circumneutral conditions, the current project intends to contribute to reducing the release of arsenic and sulfate in aqueous medium, and thus, attenuating the environmental impact from the oxidation of these sulfides.

2. LITERATURE REVIEW

Arsenopyrite (FeAsS) is usually exploited along with precious and non-ferrous metals and discarded as solid waste in the environment (Wang *et al*., 2018). The arsenopyrite is unstable in aqueous and oxidizing environments and its oxidation products are of great concern to public health and environmental protection, since species containing S and As are produced (H_2SO_4, H_3AsO_3, H_3AsO_4, and their derivatives), causing the release of arsenic in an aqueous medium and possible occurrence of acid mine drainage (Nesbbit *et al*., 1995). Given these factors, the study of the rate and the oxidation mechanisms of this sulfide is of fundamental importance to elucidate the conditions of stability and mobilization of arsenic in the environment.

Arsenic (As) occurrence in groundwater is a worldwide concern due to the toxic characteristics of this element to human health (Matschullat, 2000; Basu *et al*., 2001; Hughes, 2002; Smedley and Kinniburgh, 2002; Bhattacharya *et al*., 2007). Consequently, the maximum concentration of arsenic in drinking water established by the World Health Organization (WHO) is 10µg.L^{-1} (WHO, 2011). Considering the provisional WHO guideline, a world population of more than 100 million people is at risk - especially in regions of natural contamination of water bodies, such as Bangladesh, Taiwan, India, Mexico, and Argentina - among these, more than 45 million are exposed to concentrations above 50µg. L^{-1} of arsenic (Singh *et al*., 2015). In addition to water intake, food intake, mainly in urban areas (Ciminelli *et al*., 2017), and inhalation/ingestion of dust, *e.g.* from coal burning, (Mandal and Suzuki, 2002) are important forms of exposure to arsenic.

Arsenic has four oxidation states, -3 (arsenic or arsenic hydride, AsH_3, or arsenides), 0 (arsenic), +3 (arsenite) and +5 (arsenate). Each arsenic species shows different physicochemical properties and bioavailability (Mandal and Suzuki, 2002). Thus, the toxicity and risks to human health depend on arsenic speciation. In the case of environmental exposure, toxicologists are primarily concerned with arsenic in the inorganic form (trivalent and pentavalent oxidation) with arsenite being considered 60 times more toxic than arsenate (Hughes, 2002). The species As (III) and As (V) are also classified by the International Agency for Research on Cancer (IARC, 1987) as carcinogen for humans (WHO, 2011).

Figure 2-1 shows the Eh-pH diagram of the dominant inorganic arsenic species in aqueous solutions and arsenopyrite under conditions of 25 ° C and 1 bar. In oxidizing environments, the dominant aqueous species are As(V) whereas in reducing environments As (III) species predominate.

The As (V) species are present as H_3AsO_4 in a strongly acidic pH, and dissociates into $H_2AsO_4^-$, $HAsO_4^{2-}$ and AsO_4^{3-}, respectively at pH 2.2, 7.0, and 11.5 (Figure 2-1). The As (III) is stable under reducing conditions, predominantly in the form of H_3AsO_3, and dissociates in $H_2AsO_3^-$, $HAsO_3^{2-}$ and AsO_3^{3-}, respectively at pH 9.2, 12.1 e 13.4.

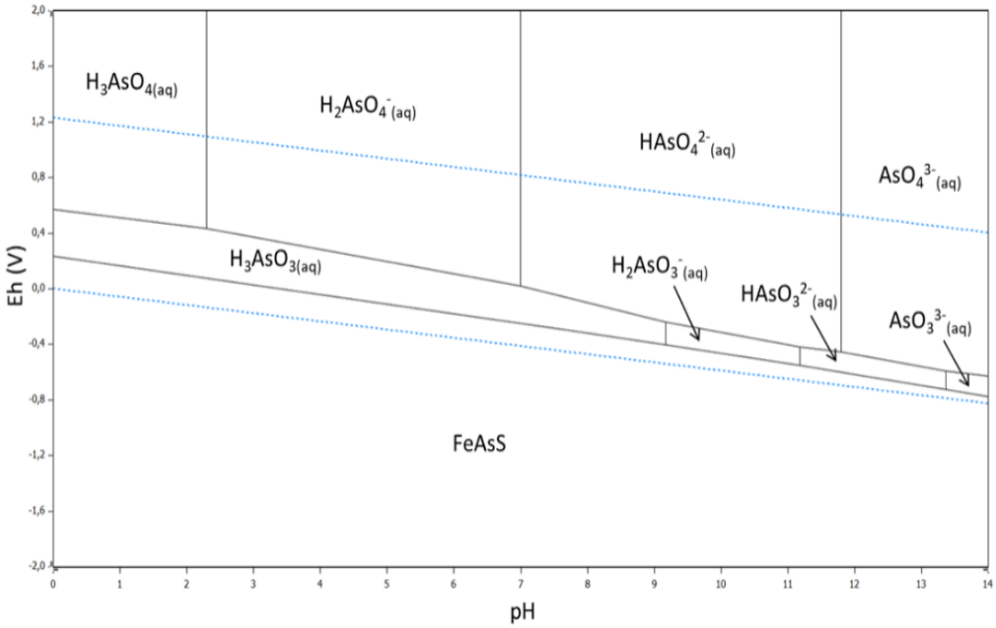

Figure 2-1 : Eh-pH diagram of aqueous species of inorganic arsenic at 25ºC and arsenopyrite, 1bar, for total [As] = 10µmol.L^{-1}. Built using the HSC Chemistry 9.0 software. The dotted lines limit the region of water stability.

Table 2-1: Dissociation reactions for As (III) e As (V). CHEN et *al.* (2009).

Speciation	Dissociation reactions	pKa
Arsenite As (III)	$H_3AsO_{3\,(aq)} \leftrightarrow H^+_{(aq)} + H_2AsO^-_{3\,(aq)}$	9.2
	$H_2AsO^-_{3\,(aq)} \leftrightarrow H^+_{(aq)} + HAsO^{2-}_{3\,(aq)}$	12.1
	$HAsO^{2-}_{3\,(aq)} \leftrightarrow H^+_{(aq)} + AsO^{3-}_{3\,(aq)}$	13.4
Arsenate As (V)	$H_3AsO_{4\,(aq)} \leftrightarrow H^+_{(aq)} + H_2AsO^-_{4\,(aq)}$	2.2
	$H_2AsO^-_{4\,(aq)} \leftrightarrow H^+_{(aq)} + HAsO^{2-}_{4\,(aq)}$	7.0
	$HAsO^{2-}_{4\,(aq)} \leftrightarrow H^+_{(aq)} + AsO^{3-}_{4\,(aq)}$	11.5

Arsenic is commonly found in mineral sulfides prevailing in gold, copper, nickel, lead, cobalt ores, among others (Nazari *et al*., 2017). In nature, arsenic is rarely found as a native element. Owing to the frequent association of As with geological sources, the mobilization of this element occurs mainly due to natural processes (weathering, biological activity, and volcanic emissions). However, anthropogenic activities, especially mining, represent a potential risk to environmental contamination by arsenic present in tailings dams and mining wastes (Smedley and Kinniburgh, 2002). The most abundant arsenic mineral – arsenopyrite – will be the focus of this work.

2.1. Oxidation of Arsenopyrite

Under environmental conditions, the mobilization of arsenic from sulfides occurs in an aqueous medium. Therefore, the pH and the oxidant concentration are important factors to be evaluated when investigating arsenopyrite oxidation. In general, acidic conditions favor the growth of microorganisms, such as *Acidithiobacillus ferrooxidans*, which will catalyze the

formation of ferric ion and thus, the dissolution of arsenopyrite (Jones *et al*., 2003; Johnson and Hallberg, 2005). As pH increases, the solubility of ferric and ferrous ions decreases, and iron precipitates. The conditions generally adopted in the disposal of mineral wastes containing sulfides are circumneutral to slightly alkaline pH, to avoid an environment favorable to the generation of acid drainage. Oxygen and ferric ions are the main oxidants employed in the kinetic studies of arsenopyrite oxidation in aqueous media.

1.1.1 Effect of pH on the oxidation rate of arsenopyrite

The dissolution of arsenopyrite was studied using continuous flow column experiments under pH range 1 to 9 in different concentrations of dissolved oxygen by Asta *et al.* (2010). YU *et al*. (2007), using a continuous flow reactor, also studied the oxidation of arsenopyrite in solution with dissolved oxygen over a wide pH range (1.8 - 12.6). The conclusions regarding the behavior and oxidation of arsenopyrite were divided between acidic and alkaline media. The main reason for this division is because, at pH below 4, iron is stable as soluble Fe (II) and at pH above 5-6 the authors claim that ferrous iron is quickly oxidized and precipitates as Fe oxyhydroxide, allowing the formation of a product layer and the adsorption of As in the Fe secondary phases formed.

The main reactions are summarized by YU *et al*. (2007). At pH <4, the general oxidation of arsenopyrite (equation 2.1) releases ferrous iron, arsenite as $H_3AsO_{3(aq)}$, and sulfate (considering the complete oxidation of the sulfide ion).

$$FeAsS_{(s)} + \frac{11}{4}O_2 + \frac{3}{2}H_2O_{(l)} = Fe^{2+}_{(aq)} + H_3AsO_{3\,(aq)} + SO^{2-}_{4\,(aq)} \quad (2.1)$$

The ferrous ion is further oxidized to ferric ion in the presence of oxygen. Since Fe (III) is soluble under high acidity, the presence of this species can induce arsenopyrite oxidation:

$$FeAsS_{(s)} + 7H_2O_{(l)} + 11Fe^{3+}_{(aq)} = 12Fe^{2+}_{(aq)} + H_3AsO_{3\,(aq)} + SO^{2-}_{4\,(aq)} + 11H^{+}_{(aq)} \quad (2.2)$$

As reaction 2.2 consumes a large amount of Fe (III), this reagent will be rapidly depleted, unless it is regenerated by the oxidation of Fe (II) to Fe (III):

$$Fe^{2+}_{(aq)} + H^{+}_{(aq)} + \frac{1}{4}O_{2\,(aq)} = Fe^{3+}_{(aq)} + \frac{1}{2}H_2O_{\,(l)} \quad (2.3)$$

At pH > 5-6, Fe (II) is rapidly oxidized to Fe (III) and precipitates:

$$FeAsS_{(s)} + 3O_{2\,(aq)} + 4H_2O = Fe(OH)_{3\,(s)} + H_3AsO_{3\,(aq)} + SO_{4\,(aq)}^{2-} + 2H_{(aq)}^{+} \quad (2.4)$$

.Since the pK_{a2} of As (V) is 7.0, in a circumneutral environment oxidation from arsenite to arsenate will produce $H_2AsO_4^-$ and $HAsO_4^{2-}$:

$$2H_3AsO_{3\,(aq)} + O_{2\,(aq)} = 2HAsO_{4\,(aq)}^{2-} + 4H_{(aq)}^{+} \quad (2.5)$$

$$2H_3AsO_{3\,(aq)} + O_{2\,(aq)} = 2H_2AsO_{4\,(aq)}^{-} + 2H_{(aq)}^{+} \quad (2.6)$$

Although thermodynamically favorable, the kinetics of reactions 2.5 and 2.6 are relatively slow, so in most laboratory experiments the arsenite species may still predominate. However, in natural weathering conditions (time in months), As (V) becomes predominant (YU *et al*., 2007).

Regarding the pH influence on the dissolution rate of arsenopyrite, Asta *et al*. (2010) determined similar values in a pH range from 1 to 6, with the average rate equal to log ~ -10.1 ± 0.2 mol m^{-2} s^{-1}. Therefore, the authors suggest that the effect of the hydrogen ion concentration on the dissolution rate of arsenopyrite at acid pH is very low. By studying the dissolution of two different samples arsenopyrite rich (> 80%), Coutinho *et al*. (2019) did not observe significant differences in the oxidation rates for experiments at pH 5 and 7. These results are consistent with the little pH dependence for arsenopyrite oxidation rate reported by YU *et al*. (2007) (pH 1.8 - 5.9) but disagree with the pH dependence reported by McKibben *et al*. (2008) in the pH range 2 - 4.5 (rate = k $(M_{H+})^{0,27}$), who indicated a decrease in the oxidation rate when increasing pH (Figure 2-2). However, the effect of pH reported by McKibben *et al*. (2008) occurred when the rate was measured based on iron concentration. The rate based on As release did not show pH dependence.

For the pH range 6 to 9, Asta *et al*. (2010) observed a slight increase in dissolution rates as the pH increases. The increase in the oxidation rate, in an alkaline medium, with the increase at pH, was also observed by Koslides and Ciminelli (1992) for the pH range 10-13.5 for a sample of 60% arsenopyrite and 40% pyrite. Coutinho *et al.* (2019) reported a small decrease in the oxidation rate of arsenopyrite for experiments performed at pH 11 when compared to the values obtained for pH 5 (Figure 2-2).

The apparent dissolution rates for arsenopyrite obtained by YU *et al*. (2007) reached a minimum value at pH close to 7-8, followed by an increase in higher pH values. This

behavior agrees with the studies by Craw *et al*. (2003). Figure 2-2 summarizes the effect of pH on arsenic release (log rate r = $mol.m^{-2}. s^{-1}$) for most of the works mentioned in this section. The discrepancies are more evident at pH below 7. The work of McKibben *et al.* (2008), which used the dissolution of Fe (III) to determine the rate, is unique as the rate decreases with increasing pH in an acid medium. Also, the high rates found by them, may be related to the short time adopted in the experiments.

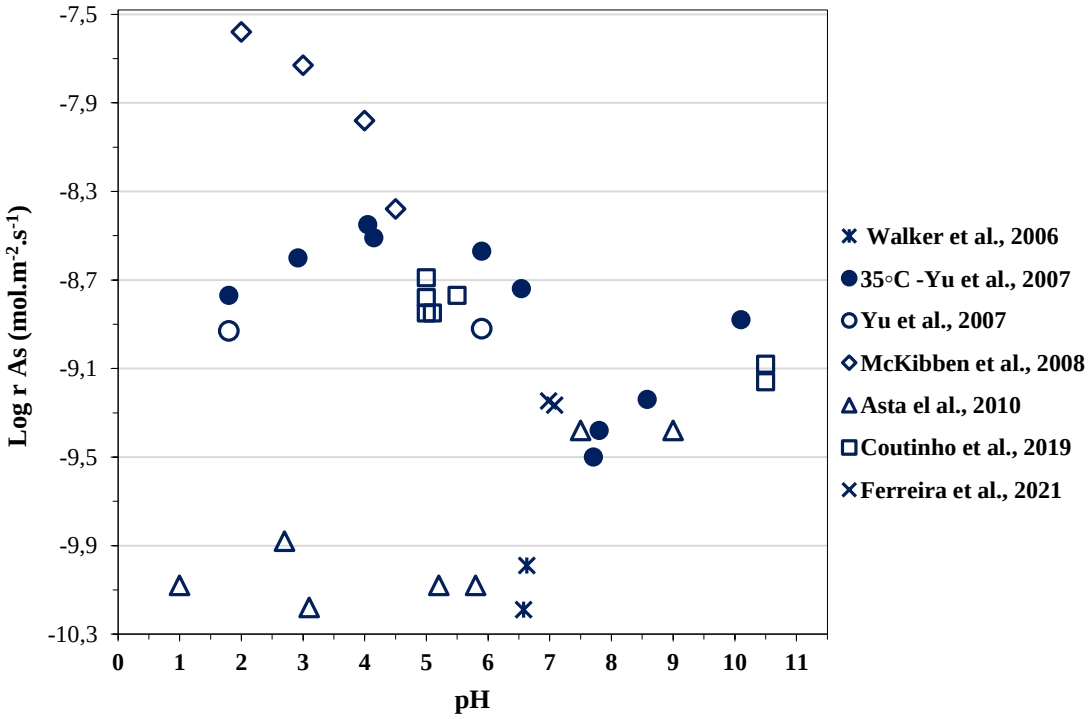

Figure 2-2: Comparison of arsenopyrite oxidation rates as a function of the pH obtained from previous studies, O_2 concentration between 6-22 $mg.L^{-1}$. The studies were carried out at a constant temperature of 25ºC, except those indicated in the figure (modified by Asta *et al*., 2010; Coutinho et al., 2009).

It is noteworthy the existence of few studies at circumneutral pH, probably due to experimental difficulties associated with the formation of solid iron species. However, there is no consensus regarding the features and role of precipitated secondary species. It is suggested that the nature and the amount number of precipitates will depend on the extent of arsenopyrite oxidation, pH, and the composition of the leach solution (Corkhill and Vaughan, 2009).

1.1.2 Oxygen effect

YU *et al.* (2007) demonstrated the dependence of dissolved oxygen on the oxidation rates of arsenopyrite in acidic medium (pH 1.8-5.9), i.e., their values increased when the O_2 concentration was increased. The effect of the dissolved oxygen concentration on the arsenic release obtained by those authors is represented in Figure 2-3. The O_2 dependence has also been reported by Asta *et al.* (2010) in the pH range 1- 4 and McKibben *et al.* (2008) at pH 2 - 4.5. From Table 2-2, the reaction order with respect to oxygen concentration determined by YU *et al.* (2007) (mO_2 = 0.45) is inferior to that determined by Asta *et al.* (2010) (mO_2 = 0.76) and higher than those of McKibben *et al*. (2008) (mO_2 = 0.33) for arsenopyrite.

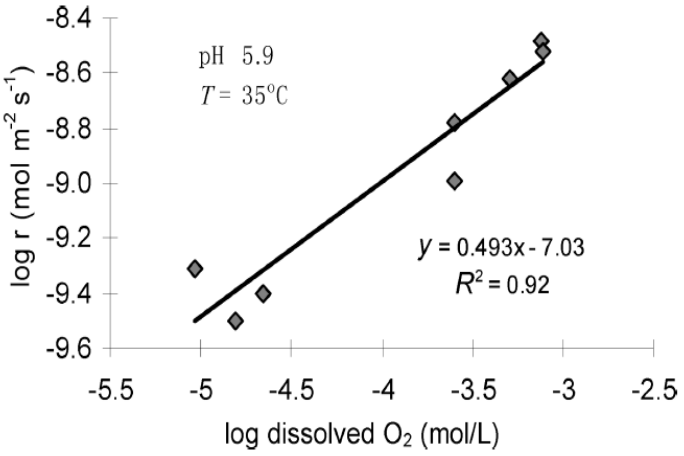

Figure 2-3: The effect of dissolved oxygen concentration on the rate of arsenic release during oxidation of arsenopyrite *at* 35ºC, pH 5.9, OD = 0.25 and 1mM (YU *et al*., 2007).

i) Circumneutral- Alkaline medium

Under circumneutral and alkaline conditions, the effect oxygen concentration on arsenopyrite oxidation is less noteworthy. Walker *et al*. (2006) reported no oxygen dependence on the oxidation rate in the pH range of 6.3 to 6.7. Likewise, Ferreira *et al.* (2021) reported an insignificant effect of oxygen at pH 7 (ranging from 100% N_2 to 100% O_2, the release of arsenic from FeAsS underwent a slight increase of about 1%) (Table 2-2). This behavior agrees with that reported by Koslides and Ciminelli (1992), who stated that the oxidation rate of arsenopyrite, in an alkaline medium (pH 10-13.5), is weakly affected by the partial pressure of oxygen in the range of 202.6 - 10000 KPa.

Although Asta *et al*. (2010) have studied the dissolution rate of arsenopyrite in the pH range 1-9, the dissolution rate considering the activity of oxygen was only calculated for pH below

4. YU *et al*. (2007) also defined the oxidation rate for acidic medium (pH < 6). In these studies, as described in the section above, oxygen favored the sulfide oxidation. The authors argue that the hydrated ferric oxide (HFO) precipitation at alkaline pH introduces considerable uncertainties in the theoretical interpretations of the experimental reaction rates under these conditions. Thus, the effect of oxygen on the oxidation rate of arsenopyrite in an alkaline medium is rarely discussed in the literature, despite the important role of this variable in tailings impoundments.

Table 2-2: Oxidation rates of arsenopyrite particles. Adapted from Ferreira et *al.* (2021).

Reference	Experimental Conditions	Rate law expression/ Rates ($mol.m^{-2}.s^{-1}$)
Walker et al. (2006)	Mixed flow reactor; FeAsS particles (177–250 μm); (pH 6.3–6.7); room temperature; DO (0.3–17 mg L^{-1}); flow rate (~0.33mL min^{-1}); 24 h; Rate calculation base: As release.	$r = 10^{-10,14\pm0,03}\ a_{O2(aq)}^{0,01(\pm0,02)}$ (pH 6.3-6.7)
Yu *et al.* (2007)	Mixed flow reactor. FeAsS particles (177–250 μm); pH 1.8–12.6; DO (0.2–32 mg L^{-1}); flow rate (5–8 mL min^{-1});15-45 °C; 6 - 8h. Rate calculation base: total As in solution	$r = 10^{-2211\pm57/T} a_{O2(aq)}^{0,45(\pm0,05)}$ (pH 1.8-6.4; 35°C)
McKibben *et al*. (2008)	Reator em batelada; FeAsS particles 150 - 250 μm; pH 2 – 4.5; DO = 10-100% O_2; Rate calculation base: Fe (III) release.	$r = -10^{-6,11}\ a_{O2(aq)}^{0,33\pm18}\ a_{H+}^{0,27\pm0,09}$ (pH 2 – 4.5; 25°C)
Asta *et al.* (2010)	Flow-through reactor; FeAsS particles <100 μm, pH 1-9; DO (~0.2–8.7 mgL^{-1}); flow rate (0.01–0.4 $mL.min^{-1}$); 25-70 °C; 600-4500 h. Rate calculation base: As release.	$r = 10^{-7,41(\pm0,47)} a_{O2(aq)}^{0,76(\pm0,11)} a_{H+}^{0,12(\pm0,07)}$ (pH 1-4; 25°C)
Ferreira *et al.* (2021)	Flow-through reactor; FeAsS particles (d50 = 3.6 μm); pH ~7; DO (~0.4–22 mg L-1); flowrate(1mL.min^{-1}); 25°C; 24h. Rate calculation base: As release.	$r = 2.4\times10^{-10}$ (pH 7; 25°C; DO 0.4mgL^{-1}); $r = 4.9\times10^{-10}$ (pH 7; 25°C; DO 21.6 mgL^{-1})

The arsenopyrite oxidation mechanism is not fully elucidated. SILVA et al. (2017) propose a mechanism for the oxidation of arsenopyrite in the presence of water based on the Density functional/plane-wave calculation method. According to the authors, the process initiates with

the dissociative adsorption of an O_2 molecule on the arsenopyrite surface. The O atom binds to Fe and As atoms forming a bridge (Figure 2-4) and Fe e As are readily oxidized to Fe (III) e As^0. Afterwards, a water molecule approaches the O adsorbed. This water donates hydrogen ion to the O adsorbed (forming Fe (III) – OH) and the $OH^{\bullet}$ radical binds to the neighbor As oxidizing it to +1 and forming the As−OH bond.

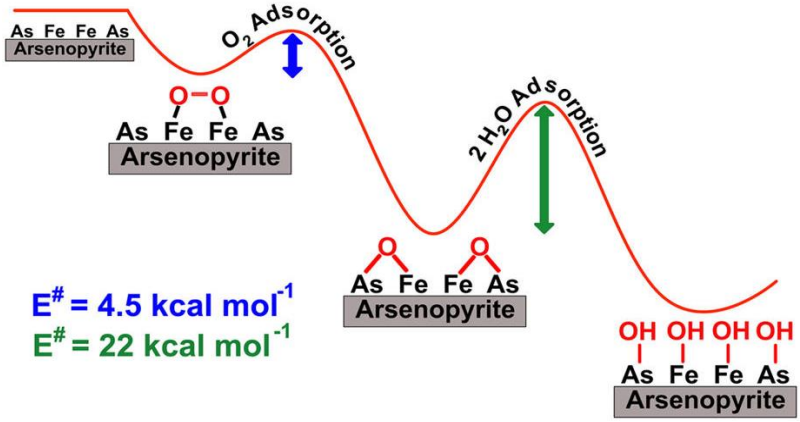

Figure 2-4: Arsenopyrite surface oxidation reaction proposed by SILVA et al. (2017).

The coadsorption of water is necessary for the next oxidation steps. Then, another water molecule adsorbs to a neighbor Fe atom, donates a hydrogen atom to the adsorbed OH group, forming water and reducing the initial oxidized Fe (III) to Fe (II). In this step, arsenite (As(III)) is also formed. This mechanism demonstrates why the removal of the humidity is necessary to avoid the oxidation of arsenopyrites in aerobic conditions. A variation of this mechanism includes the bonding of the OH groups to the S atom instead of the As atom. This is less stable than in the case of As bond. Therefore, the first steps in the arsenopyrite oxidation must involve As reaction. Silva et al. (2017) emphasize that this mechanism is in accordance with equation 2.1, where Fe (II) is formed and with the experimental results found by Corkhill et al. (2008), Nesbitt et al. (1995) and Schaufuss et al. (2000) who observed that As is more readily oxidized than Fe and S.

The energy barrier for the above reaction mechanism descript is relatively low compared to that of pyrite oxidation mechanism, where the oxygen is molecularly adsorbed. Because the oxygen molecules readily dissociate on the surface, leading to the oxidation of the Fe (II) and As sites, many steps observed for the pyrite oxidation mechanism are avoided. The presence of more reactive arsenic sites on the surface is the most important difference compared to pyrite found by Silva et al. (2017).

1.1.3 The Fe (III) effect

YU *et al*. (2004) investigated the oxidation of arsenopyrite in acidic solution (pH = 1.8, bubbled with N_2) with $Fe_2(SO_4)_3$ concentrations varying between $1x10^{-5}$ and $1x10^{-2}$ $mol.kg^{-1}$. The oxidation rate was calculated using the conversion rate from As (III) to As (V). The authors determined that the oxidation of the sulfide grows exponentially with the increase in the concentration of Fe (III) and temperature. The reaction order varied between 0.41 (from 15 to 35 °C) and 0.64 (at 45 °C). To evaluate the effect of the anionic component of the oxidant, the oxidation rate of arsenopyrite was also determined from the dissolution of $FeCl_3$ at pH 1.8. The results indicated that the oxidation rate of arsenopyrite with $FeCl_3$ is considerably higher (5 times) than with $Fe_2(SO_4)_3$.

> Compared with the $Fe_2(SO_4)_3$ solutions, the relative amounts of Fe (III), $FeOH^{2+}$ and $FeCl^{2+}$ are greater in the $FeCl_3$ solutions. For example, at 25 °C the distribution of species is Fe (III) (66.4%), $FeOH^{2+}$(14.1%) and $FeCl^{2+}$(16.3%) in $FeCl_3$ solutions, compared to Fe (III) (7.4%), $FeOH^{2+}$ (1.4%) and $FeSO_4^{+}$ (84.7%) in $Fe_2(SO_4)_3$ solutions. According to Hug (2001) and Emett and Khoe (2001), in acidic solutions (pH<5), the $FeOH^{2+}$ and $FeCl^{2+}$ species absorb photons and produce hydroxyl radicals (OH) and dichloro radicals (Cl_2^{-}) which are very strong oxidants. In contrast, $FeSO_4^{+}$ does not produce free radicals when illuminated by ultraviolet light (YU *et al*., 2004).

After 7 hours practically all the arsenic in the solution was oxidized to As (V) when $FeCl_3$ was used, whereas in the ferric sulfate system only 6.7% of the As (III) was oxidized to As (V) for the same period of time (YU *et al*., 2004).

McKibben *et al*. (2008) evaluated the effect of ferric ions on the oxidation of arsenopyrite at pH 2 using a batch reactor with a concentration of Fe (III) between 10-100 mg L^{-1} (source of Fe (III) not indicated). The authors found that aqueous Fe (III) oxidizes arsenopyrite at least an order of magnitude faster than dissolved O_2. Williamson and Rimstidt (1994) determined the oxidation rate of arsenopyrite using $FeCl_3$ at pH 2. The results agree with those

determined by McKibben *et al*. (2008). Both obtained a reaction order of 1 with respect to Fe (III) concentration.

Studies regarding the effect of Fe (III) on the oxidative dissolution rate of arsenopyrite in conditions close to neutrality are scarce due to the precipitation of this species. Some relevant findings from investigations carried out with pyrite will be discussed. Moses *et al*. (1987) studied the effect of ferric ions on the oxidation of pyrite in the pH range 2-9. The authors suggest that Fe (III) is the main oxidizer of pyrite even in a circumneutral pH, where the solubility of the species is very low. According to the authors, at pH 7, the oxidation rate of pyrite in solutions saturated with Fe (III) is at least similar to those saturated with DO (dissolved oxygen). At pH 9, the oxidation rate was one order of magnitude higher, and in an acid medium, the reaction rate with Fe (III) was at least 2 times higher than the rates with DO.

Further experiments carried out by Moses and Herman (1991) indicated that, indeed, Fe (III) is an effective oxidizer of pyrite, however, the reaction cannot be sustained in the absence of DO since the oxidation of the mineral depends on the continuous oxidation of Fe (II) to Fe (III). According to the authors, in an acidic environment, the oxidation of Fe (II) by oxygen is slower than the oxidation of pyrite by Fe (III). In a circumneutral environment, Fe (II) is adsorbed on the surface of the pyrite, blocking the access of Fe (III) or DO. Then, Fe (II) must be oxidized by oxygen to generate Fe (III) on the surface of pyrite. Thus, the authors suggest that the oxidation of Fe (II) limits the rate of oxidation of pyrite in acid and circumneutral medium.

Caldeira *et al*. (2010) also propose Fe (III) as the main oxidizer of pyrite in an alkaline medium. The authors indicate that the presence of carbonate ions generates soluble iron-carbonate complexes, favoring the kinetics of pyrite oxidation from the formation of the redox pair Fe (II)-pyrite / Fe (III)-carbonate on the surface of the pyrite. The conclusions obtained by Caldeira *et al*. (2010) also warn about the influence of the composition of the leaching medium on the oxidation of sulfides.

From the study of the oxidative dissolution of arsenopyrite in a circumneutral pH, Neil and Jun (2016) showed for the first time that, despite the low solubility of Fe (III) in an alkaline medium, the addition of this ion results in a higher dissolution of arsenic. It is important to emphasize that although the authors claim to have worked in conditions close to neutrality, the specific pH was not reported.

Their study was conducted under aerobic and anaerobic conditions in systems containing 10mM sodium nitrate or sodium chloride and 1.5 µM Fe (III). Under aerobic conditions, an 18% increase in arsenic concentration was observed in the nitrate system and a 36% increase in the chloride system compared to systems without Fe (III) (Figure 2-5). For the systems with chloride, in addition to greater As dissolution, greater iron oxide/hydroxide precipitation was also noted. As reported by Moses and Herman (1991), under anaerobic conditions no significant variations regarding the presence of Fe (III) were observed for both systems (chloride and nitrate).

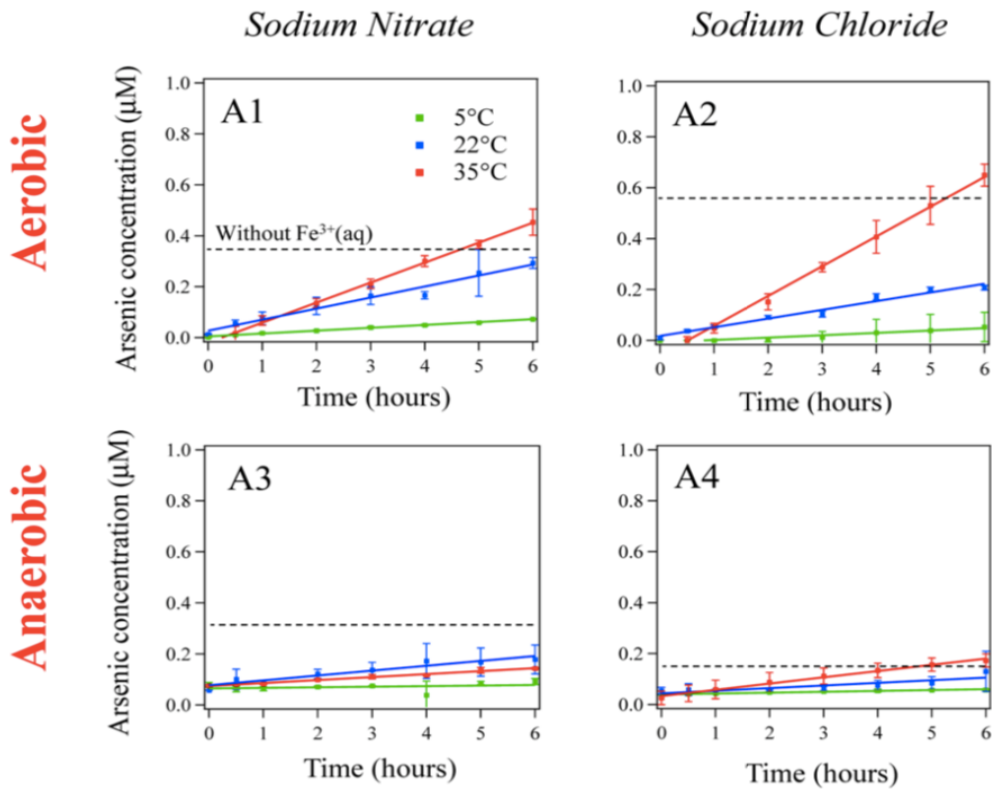

Figure 2-5: Arsenic concentration evolution for batch reactors containing arsenopyrite and 1.5 µM Fe (III) during a 6 h reaction period for aerobic sodium nitrate (A1), aerobic sodium chloride (A2), anaerobic sodium nitrate (A3), and anaerobic sodium chloride (A4). The dotted lines indicate the maximum concentrations observed for the reactors without added Fe (III) at 35 °C for each system, pH not disclosed. Source: Neil and Jun (2016).

During the oxidation process, arsenic dissolves from the exposed arsenopyrite surface. Neil and Jun (2016) observed, by Raman spectroscopy, that even after 14 days there was still some arsenopyrite surface exposed to the solution. The addition of Fe salts increased the precipitation of secondary minerals – the total amounts of precipitated Fe (III) phases in these systems was about four times higher. This increase, however, did not entirely mitigate arsenic

mobility, but rather an increase in As concentrations was observed. The authors explain that the amounts of mobilized arsenic can exceed what can be attenuated by secondary minerals.

Neil and Jun (2016) propose a mechanism for the interaction of ferric ions with FeAsS (Figure 2-6). The Fe^{3+} species (any reactive hydroxo−Fe^{3+} aqueous complexes, such as $Fe(OH)_2^+$ and $Fe(OH)_3(aq)$ or colloidal Fe(III) phases) is initially adsorbed on arsenopyrite surface. $Fe\ (II)_{FeAsS}$ then donates an electron to $Fe^{3+}{}_{ads}$, forming $Fe\ (III)_{FeAsS}$ and directly reducing Fe^{3+} to Fe^{2+} or forming a Fe^{2+}/ Fe^{3+}complex with a delocalized electron. This complex (Fe^{2+} or Fe^{2+}/Fe^{3+}) will donate electron to dissolved oxygen forming Fe^{3+} species again and repeating the cycle. It should be noted that this mechanism is only sustained in an oxidizing environment since continuous reduction and oxidation of iron is necessary. With time, Fe (III) on the surface will form precipitates of Fe (III) oxyhydroxides.

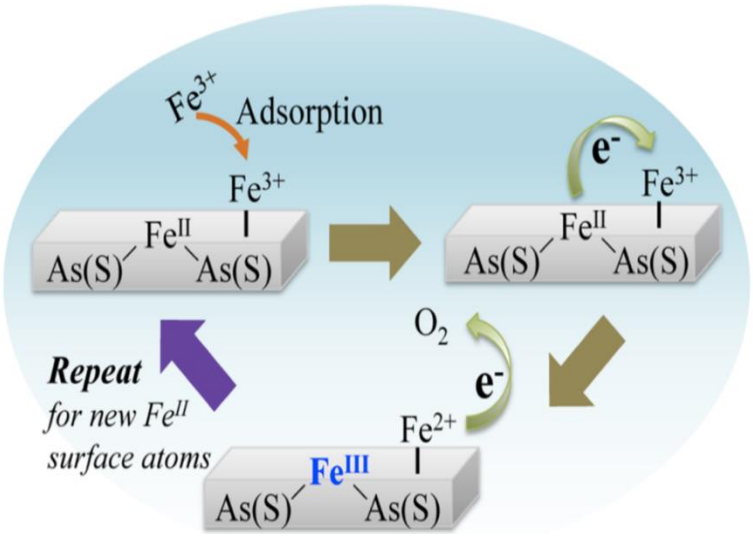

Figure 2-6: Interaction mechanism of Fe (III) ions with arsenopyrite at circumneutral medium proposed by Neil and Jun (2016).

By Raman spectroscopy, Neil and Jun (2016), identified the presence of maghemite and hematite as Fe precipitates. However, the authors did not assess the pathway of arsenic and sulfur after their release from arsenopyrite. Corkhill and Vaughan (2009) state that "there is no consensus on the surface chemistry of oxidized arsenopyrite, and this can be attributed to the lack of agreement on the composition of the layers close to the surface". In contrast, I emphasize that there is an agreement between the authors concerning the formation of Fe (III) oxide/hydroxide products and the formation of arsenates/arsenites on the mineral surface.

In conclusion, despite the existence of numerous studies on the oxidation of arsenopyrite in an aqueous medium, the effect of Fe (III) in the circumneutral medium is still insufficiently understood. Moreover, the diverse experimental conditions adopted among the studies might have contributed to the discrepancies found in the literature on the oxidation kinetics of the mineral. Consequently, there is no agreement on the combined influence of pH, oxygen, and ferric ions on the release of arsenic. This lack of agreement hinders, therefore, the identification of the conditions associated with the greater stability of arsenopyrite.

1.2 The pyrrhotite mineral

The pyrrhotite mineral is one of the most reactive and the second most abundant sulfide on the earth's crust (Belzile *et al*., 2004; Cai *et al*., 2005). This sulfide, $Fe_{1-x}S$, has a non-stoichiometric composition with x ranging from 0 (FeS) to 0.125 (Fe_7S_8). Due to the various compositions that pyrrhotite can present, different crystalline structures are found. The crystal structures of all forms are based on a layered NiAs-type substructure, on which superstructures occurs due to the distortion of the coordination of stoichiometric troilite (FeS) or by the ordering of Fe-site vacancies (non-stoichiometric pyrrhotites) (Harries *et al.*, 2013). The most iron-deficient compound, Fe_7S_8, is magnetic and has monoclinic symmetry, while the equimolar structure (FeS) is hexagonal. The intermediates (*e.g.*, Fe_9S_{10}, $Fe_{10}S_{11}$ and $Fe_{11}S_{12}$) might exhibit monoclinic, hexagonal, or orthorhombic symmetry, as showed in Table 2-3.

Table 2-3: The structure types for naturally occurring pyrrhotites. Adapted from Muzeum, 1990.

Composition (at. % Fe)	Symmetry	Superstructure type (cell size, Å)	Remarks
50.0 (FeS)	Hexagonal	A, 2C a = 5.96, c=11.75	2C - natural troilite
~ 46.7 (Fe_7S_8)	Monoclinic	2A, 2B, 4C a = 11.90, b = 6.87, c=22.87	4C - magnetic pyrrhotite
~ 47.4 (Fe_9S_{10})	Hexagonal	2A, 5C a= 6.88, c = 28.7	5C - pyrrhotite
~ 47.8 ($Fe_{11}S_{12}$)	Hexagonal	2A, 6C a= 6.89, c = 34.48	6C - pyrrhotite
~ 47.6 ($Fe_{10}S_{11}$)	Orthorhombic	2A, 2B, 11C a= 6.89, b= 11.95, c = 63.18	11C - pyrrhotite
47.4 - 47.8 (Fe_9S_{10}→$Fe_{11}S_{12}$)	Orthorhombic or Monoclinic	2A, 2B, nC where n is a non-integer between 4.8 - 6	nC - pyrrhotite

* NC (2C, 4C, 5C, 6C, 11C and nC) describe the multiplicity of the superstructure period along the hexagonal c axis relative to the NiAs substructure Harries et al., 2013). For example: 4C indicates that iron vacancies define a superlattice that is 4 times larger than the unit cell in the "C" direction.

The monoclinic 4C-magnetic pyrrhotite is the best characterized and understood superstructure (Harries, 2012). Bertaut (1953) was the first to define the pyrrhotite superstructure as a variation from NiAs structure with iron layers normal to the c axis and showed that it contains an ordered sequence of vacancies (Elliot, 2010). Based on a NiAs type structure of FeS, the 4C structure is derived by removing 1/4 of Fe atoms from every second Fe layer, leading to Fe_7S_8 composition (Harries, 2012). Bertaut (1953) proposed the following sequence for a 4C superstructure: FAFDFBFC, where A, B, C and D are spatially different configurations of two vacancies in eight positions and F represents a full layer of Fe atoms, as illustrated in Figure 2-7 (a) (Elliot, 2010). This structure was later confirmed and refined by Tokonami et al. (1972). The spacing between vacancy layers of the same type is four times the c-axis repeat of the NiAs substructure (Harries, 2012).

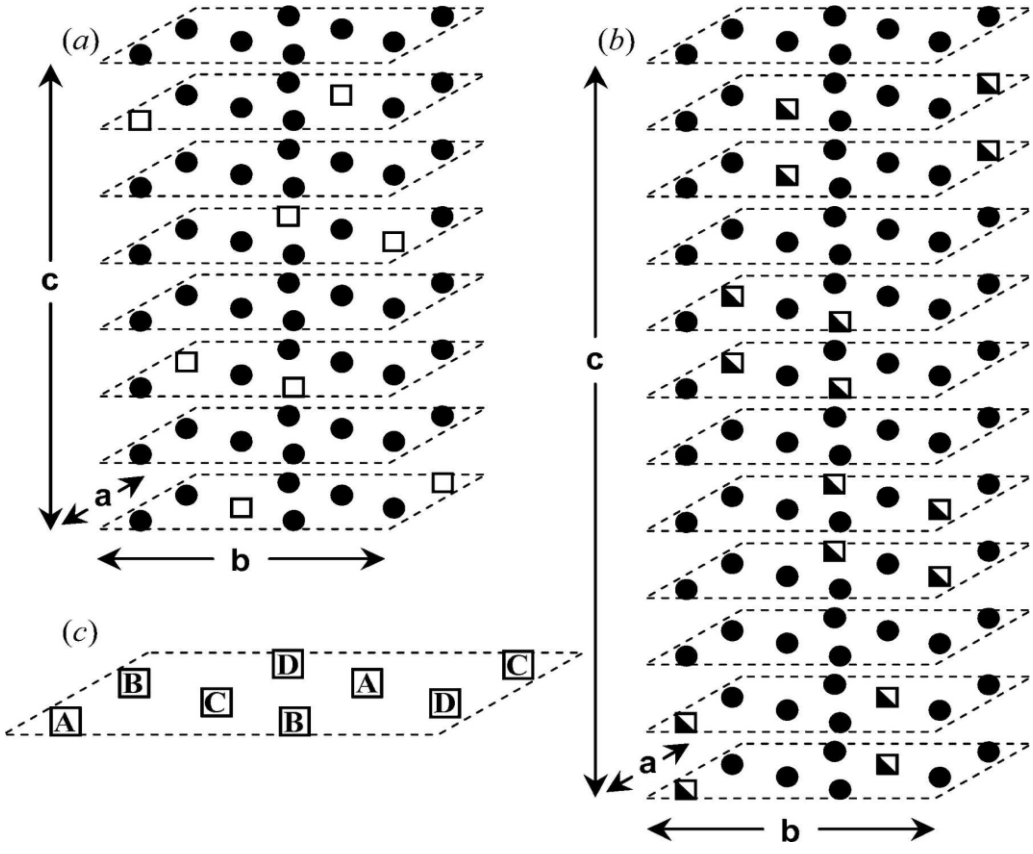

Figure 2-7: The superstructures for (*a*) the ideal 4*C*-type pyrrhotite (Fe_7S_8) proposed by Bertaut (1953) and (*b*) the 6*C*-type pyrrhotite ($Fe_{11}S_{12}$) described by Koto *et al.* (1975). Only the iron layers have been illustrated with sulfur layers omitted, where empty squares represent vacant sites and half-filled squares represent half an Fe atom. (*c*) Illustration of the nomenclature for vacant site positions (for the case of two vacancies in eight positions). (Elliot, 2010).

Koto *et al.* (1975) determined and refined the 6*C* superstructure ($Fe_{11}S_{12}$) as a statistical distribution of vacancies with every third iron layer full and with half iron occupancies in-between (*FC½C½FB½B½FD½D½FA½A½F*) (Elliot, 2010). Figure 2-7 shows the distribution of Fe sites in 4C (a) and 6C (b) pyrrhotite superstructures.

de Villiers et al. (2009) defined the 5C superstructure with vacant sites present in two of the 10 layers. The remaining eight layers contains Fe sites partially occupied (each containing less that one vacancy in eight positions), (de Villiers et al., 2009 and Elliot, 2010. Figure 2-8 shows the distribution of Fe sites in 5C pyrrhotite (left) and compares with the distribution of vacant sites in monoclinic 4C pyrrhotite (right), described by Tokonami et al. (1972). The cell for monoclinic pyrrhotite shown in Figure 2-8 is not the true unit cell, but one formed by connecting the Fe atoms in the layers as shown (de Villiers et al., 2009).

The nC superstructure, are intermediate or non-integral pyrrhotites with compositions that vary between 5C and 6C. Marimoto et al. (1975) showed that this group comprises low-temperature metastable structures that do not persist in nature (Elliot, 2010).

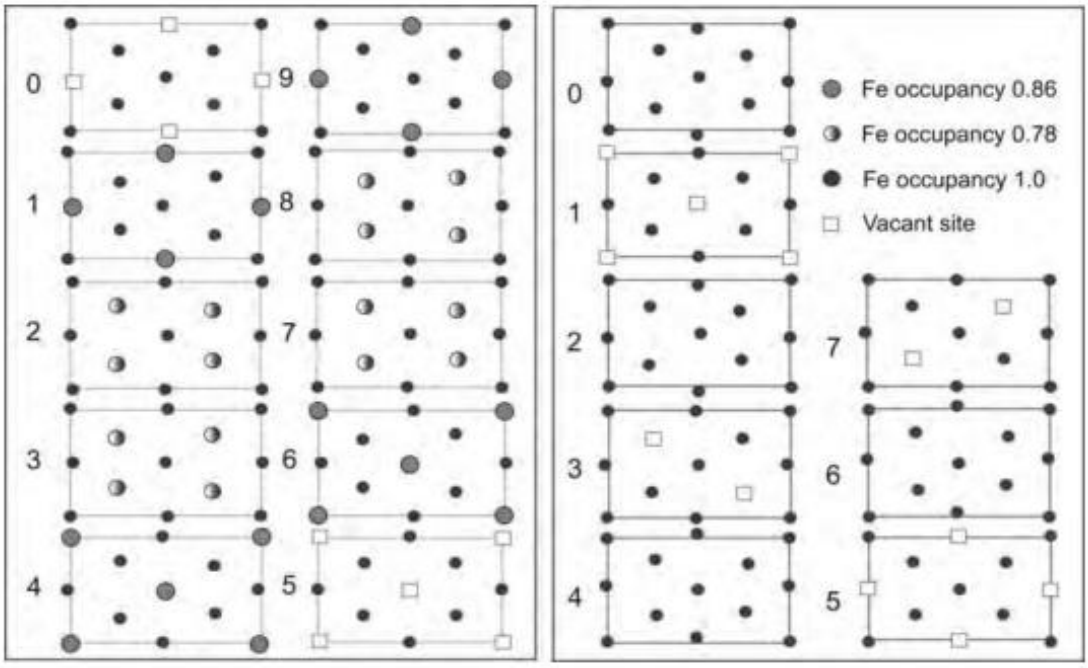

Figure 2-8: Distribution of vacant and partially occupied sites in 5C pyrrhotite (left diagram) as compared to the vacancy distribution in monoclinic pyrrhotite (right). The layers are labeled from 0 to 9 for 5C pyrrhotite and from 0 to 7 in 4C pyrrhotite. The sites with the partial occupancies are shown in different shades of gray. layers 1, 3, 5, and 7 in 4C pyrrhotite are also described as the A, B, C, and D configurations (de Villers et al., 2009).

A series of reactions occur when pyrrhotite is exposed to the atmosphere and water. Sulfur products (e.g.,) sulfate, iron ions, and hydrogen ions are usual products that eventually can be converted to iron oxyhydroxides and sulfuric acid (Chirita and Rimstidt, 2014). The elucidation regarding the reactivity of pyrrhotite and the factors that accelerate or delay its oxidation kinetics is necessary to improve the processing and disposal of this sulfide in the environment, aiming at reducing the release of sulfate ions in mining effluents and acid mine drainage (Belzile *et al*., 2004). According to Chirita and Rimstidt (2014), the pyrrhotite oxidation process is complex and consists of parallel and consecutive elementary reactions, with multiple reaction steps. The authors state that a full understanding of the nature of the overall oxidation process requires detailed knowledge of each elemental step of oxidative dissolution.

Thermodynamically, pyrrhotite is not stable and reacts relatively quickly with its environment (Buckley and Woods, 1985; Belzile *et al*., 2004; Miller *et al*., 2005). Many abiotic factors influence the dissolution kinetics of pyrrhotite: crystalline structure, temperature, pH, presence of oxidants, and the formation of galvanic couples.

Regarding the crystalline structure, the studies by Pratt *et al*. (1996) indicate that because pyrrhotite is submitted to pressures and stresses in mine tailings, modified structures occur and can increase this iron sulfide's susceptibility to the oxidation processes. Nicholson and Scharer (1994) attribute the reactivity of pyrrhotite to the lower symmetry caused by the vacancy of iron atoms in the crystal structure. In accordance with this premise, Harries *et al*. (2013) observed a large difference in reactivity between monoclinic 4C-pyrrhotite and hexagonal NC-pyrrhotite. The authors argued that these discrepancies originate from different arrangements at Fe vacancy sites.

Janzen *et al* (2000) reported that the specific surface area of pyrrhotite is about 2 to 10 times greater than that of pyrite with the same grain size. The authors explain that this difference is due to the presence of fractures that occur along the cleavage planes of the pyrrhotite particles. "The fractures are not merely near surface effects; rather, they extend into the pyrrhotite grains" (Janzen, 1996). The high reactivity of pyrrhotite was attributable to the high specific surface area compared to other mineral sulfides, such as pyrite. The authors also infer that specific surface area was not related to crystal type or trace metal content.

The effect of temperature on the oxidative rate of pyrrhotite is well established and it follows Arrhenius law (Belzile *et al*., 2004). However, the influence of pH is not conclusive in the literature. Nicholson and Scharer (1994) report an inconsistent effect of this variable in the pH range between 2 and 6 at three different temperatures (Belzile *et al*., 2004). The work of Kwong (1995) also did not find a trend in the oxidation of pyrrhotite as a function of pH.

The higher reactivity of pyrrhotite, when compared to other sulfides, is proven in the studies by Chopard *et al*. (2015) (Table 2-4). The authors analyzed the oxidation rates of sixteen mineral sulfides and one sulfosalt by leaching the sample with deionized water in a modified weathering cell. The experiments run for 55 to 70 cycles (stopped upon reaching steady state) and the rate of sulfate production was used as a direct indicator of the acid generation rate and the sulfide oxidation rate. However, the authors did not consider the specific surface area to assess the reactivity between the sulfides, which discredits this comparison.

Table 2-4: Experimental oxidation rates for common sulfides. Adapted from Chopard et al. (2015).

Oxidation rates (mg of S/kg/day)			
Iron-sulfides		***Base-metals sulfides***	
Pyrrhotite 1 ($Fe_{(1-x)}S$)	**8.2**	Bornite (Cu_5FeS_4)	0.23
Pyrrhotite-Ni ($Fe_{(1-x)}S$	2.6	Chalcocite (Cu_2S)	0.28
Pyrite 1 (FeS_2)	**2.4**	Chalcopyrite 1 ($CuFeS_2$)	2.0
Pyrite 2 (FeS_2)	**4.8**	Chalcopyrite 2 ($CuFeS_2$)	1.0
Pyrite 3 (FeS_2)	**4.6**	Covellite (CuS)	2.7
		Galena (PbS)	0.53
As/Sb - bearing sulfides		Sphalerite (ZnS)	2.3
Arsenopyrite (FeAsS)	**6.9**	Sphalerite-Fe ((Zn,Fe)S)	3.2
Gersdorffite (NiAsS)	93.6		
Fahlore $(Cu,Fe,Ag,Zn)_{12}(Sb,As)_4S_{13}$)	3.2		
Stibnite (Sb_2S_3)	0.49		

After gersdorffite, which is a sulfosalt and presents geochemical behavior different from sulfides as this mineral dissolve like a salt, pyrrhotite was the mineral with the highest oxidation rate, followed by arsenopyrite and pyrite. It is important to highlight that the pyrrhotite-Ni sample is not pure and contains 10 % of pentlandite $(Fe,Ni)_9S_8$. Moreover, Chopard *et al*. (2015) emphasize that this pyrrhotite contains Ni trace, certainly in its crystal network (about 1%), which explains the lowest reactivity of *pyrrhotite- Ni* when compared to *pyrrhotite 1*. In addition to showing the high reactivity of pyrrhotite, this result highlights the

importance of trace element composition in the stability of individual sulfides. A trend of decreasing reaction rates as trace metal content increases was also noticed by Kwong (1995) and Janzen *et al*. (2000) for pyrrhotite. This may relate to either the lower solubility of solid solution phases or the lack of oxidation of the trace constituents. (Janzen *et al*., 2000).

Regarding the influence of temperature, oxidants, and galvanic couples on the reactivity of pyrrhotite, such aspects will be discussed in greater detail in the following sections.

1.2.1 Non-oxidative dissolution

The dissolution of pyrrhotite in natural or mining environments proceeds via acidic dissolution under anoxic conditions or via oxidative dissolution when oxygen can access the reaction site (Harries *et al*., 2013). Dissolution of a solid is defined as nonoxidative when the formal oxidation states of the solute species are identical in solution and the solid phase (Nicol and Scott, 1979).

Because pyrrhotites are iron deficient, their non-oxidative dissolution can produce zero valence sulfur in the form of disulfide, polysulfide, or elemental sulfur (Chirita and Rimstidt, 2014):

$$Fe_{1-x}S_{(s)} + 2(1-x)H^+ = (1-x)Fe^{2+} + (1-x)\,H_2S + xS^0 \qquad (2.7)$$

According to Janzen *et al*. (2000), the nonoxidative dissolution rate of pyrrhotite is a potential contributor of ferrous iron release in pyrrhotite weathering in acidic solutions when the oxidation reactions are not dominant.

Chirita and Rimstidt (2014) developed a rate equation for non-oxidative pyrrhotite dissolution in acidic medium by combining 16 rate data obtained in their study with 46 additional rates from previous publications (Bugajinski and Gamsjager, 1982; Janzen *et al*., 2000; Gleisner, 2005; Thomas *et al*., 2000; Thomas *et al*., 2001). The compilation covered a pH range from 0 to 5 and temperatures from 20 to 90 °C. The reaction order determined concerning H^+ concentration was 1.46, indicating a pH dependence:

$$r_{H^+}(mol/m^2s) = 1.58x10^7 e^{\frac{-65,900}{RT}} M_{H^+}^{1.46} \qquad (2.8)$$

Most of the data used to determine equation 2.8 was measured at a pH lower than 2.75. Gleisner (2005) was the only study to investigate the non-oxidative dissolution in the range of

pH 4 – 5. Hence, these authors found a reaction rate considerably inferior (mean = 1,77 x 10^{-12} $mol.m^{-2}.\ s^{-1}$) than the rates for studies at higher acidity. Also, when considering the experiments conducted at 25 °C, the rate for experiments in the range of pH 4-5 are at least five orders of magnitude lower when compared to the rate determined from other studies at pH 1.

The activation energy shown in equation (2.8), calculated by Chirita and Rimstidt (2014), is 65.9 kJ/mol. The authors argued that because reaction under diffusion control have activation energy values near 15 kJ/mol, this high activation energy indicates that the reaction is not limited by ion transport through the solution. Fractional reaction orders also do not indicate diffusion control.

Considering a tailing environment, nonoxidative dissolution is expected to be a significant mechanism only at low oxygen concentrations (i.e., far from water/air interface). When pyrrhotite is exposed to air, a series of complex oxidation reactions occur (Gunsinger *et al*., 2006; Janzen *et al*., 2000). Therefore, anoxic dissolution should be considered in predictive models for underwater storage of pyrrhotite wastes. It is also important to notice the lack of data within circumneutral to alkaline conditions, typical of tailings impoundments.

1.2.2 Oxidative dissolution

As for arsenopyrite, both oxygen and ferric ion are important oxidants of pyrrhotite. When oxygen is the primary oxidant, the oxidation reaction may be represented by the following reactions:

$$Fe_{1-x}S_{(s)} + \left(2 - \frac{1}{2}x\right)O_2 + xH_2O = (1-x)Fe^{2+} + SO_4^{2-} + 2xH^+ \quad (2.9)$$

$$Fe^{2+}_{(aq)} + H^+_{(aq)} + \frac{1}{4}\,O_{2\,(aq)} = Fe^{3+}_{(aq)} + \frac{1}{2}\,H_2O_{\,(l)} \quad (2.10)$$

$$Fe_{1-x}S_{(s)} + (8-2x)Fe^{3+} + 4H_2O = (9-3x)Fe^{2+} + SO_4^{2-} + 8H^+ \quad (2.11)$$

However, if pH is not sufficiently low, reaction (2.12) will concomitantly occur with the precipitation of ferric hydroxides or oxyhydroxides (Harries *et al*., 2013):

$$Fe^{3+} + 3H_2O = Fe(OH)_{3\,(s)} + 3H^+ \quad (2.12)$$

Jambor (1986) and Nicholson and Scharer (1994) indicate that the initial oxidation of sulfide to sulfate is often not complete as implied by reactions (2.9) and (2.11) but generates elemental sulfur instead. However, by using voltammetry and XPS, Buckley *et al*. (1988) found that the initial oxidation products of pyrrhotite generate metal-deficient sulfides rather than elemental sulfur. Also, Jones *et al*. (1992) confirmed by XPS and XRD the presence of sulfate species, iron (III) oxyhydroxides, and iron-deficient sulfide species when ground pyrrhotite is oxidized by air and water (Belzile *et al*., 2004).

Janzen *et al*. (2000) investigated the oxidation rates by oxygen and ferric iron for twelve samples of pyrrhotite. Regarding the rates obtained by oxygen, these were performed at pH 2.75 in terms of Fe (II) and sulfate release. The results showed that the rates of oxidation based on iron release (4×10^{-9} mol.m^{-2}.s^{-1}) are substantially higher than the oxidation rates based on sulfate production (2×10^{-10} mol.m^{-2}.s^{-1}) (Table 2-5). These findings agree with Mikhlin *et al*. (2000) and Mikhlin *et al*. (2002) studies who reported the formation of a non-stoichiometric metastable layer (NL) as a result of the preferential release of iron relative to sulfur in the oxidation or dissolution of pyrrhotite.

Few studies have determined reaction order with respect to oxygen for the oxidative dissolution of pyrrhotite. For pyrite, the rate is shown to be proportional to the square root of the O_2 partial pressure by McKibben and Barnes (1986) and Williamson and Rimstidt (1994). Romano (2012) determined, for pyrrhotite, a reaction order for oxygen as 0.30 ± 0.07 at 25ºC and pH 3. In the range of pH 2-4, the author did not identify the influence of pH on the oxidation rate.

For pyrrhotite oxidation by ferric iron, the mean rate obtained by Janzen *et al*. (2000) was 3,5 $\times 10^{-8}$ mol.m^{-2}.s $^{-1}$ at pH 2.75, which means that the oxidation rate increased one order of magnitude when compared to the oxidation by oxygen. This result matches the studies for pyrite oxidation conducted by Moses *et al*., (1987) who showed that ferric iron is a more reactive oxidizing agent than oxygen. It should be emphasized that sulfide conversion to sulfate by ferric iron was less complete (18% conversion) than in the case of pyrrhotite oxidation by oxygen (20 – 34% conversion). “These partial oxidation trends for pyrrhotite are consistent with the general oxidative mechanism proposed by Loten and Wesker (1987) for monosulfide minerals. A single electron transfer agent (Fe (III)) should react more rapidly but produce more elemental sulfur (i.e., less sulfate) than a two-electron transfer agent (O_2), because different hydrolysis reactions should take place” (Janzen *et al*, 2000). The mean

reaction order to ferric iron determined by the authors was 0.56 ± 0.09. McKibben and Barnes (1986) also observed a half order dependence for pyrite oxidation by ferric ions.

Table 2-5: Oxidation rates and activation energies of pyrrhotite based on iron release.

Reference	Sample	Oxidant	Conditions pH/ T(°C)	Rate ($molm^{-2}\ s^{-1}$)	Activation energy ($kJ\ mol^{-1}$)
Nicholson and Scharer, 1994[a]	Museum grade	Air	2-6/10	3.1×10^{-9}	58.1 (pH 2)
			2-6/22	8.5×10^{-9}	52.4 (pH 4)
			2-6/33	3.3×10^{-8}	100.4 (pH 6)
Janzen et al.(2000)[a b]	Several locations in N. America (12 samples)	Air	2.75/25	4×10^{-9} 2×10^{-10} [(c)]	53.4 92.6 [(c)]
		Fe^{3+}(2×10^{-4} $molL^{-1}$)	2.75/25	3.5×10^{-8}	
		Fe^{3+}(2×10^{-4} $molL^{-1}$)	2.50/25	3.1×10^{-8}	48.6
		Fe^{3+} (1×10^{-3} $molL^{-1}$)	2.50/25	6.8×10^{-8}	
Belzile et al. (2004)	Museum grade	Air	2/22	2.28×10^{-9}	
		Fe^{3+} (1×10^{-3} $molL^{-1}$)	2/22	1.44×10^{-8}	
		Air	2/35	2.87×10^{-9}	
		Air	3/35	3.86×10^{-9}	
		Air	4/35	2.51×10^{-9}	
Cai et al. (2005)	PO-97 (Wards)	Fe^{3+} (1×10^{-3} $molL^{-1}$)	2/10	2.77×10^{-8}	
			2/20	4.12×10^{-8}	
			2/30	4.22×10^{-8}	
			2/40	9.28×10^{-8}	
Chirita et al. (2008)	Aldrich	Air	2.75/25	2.65×10^{-8}	41.6
			3/25	2.12×10^{-8}	
			3/35	9.85×10^{-8}	
			3/45	1.96×10^{-7}	

[a] Average value of oxidation rates
[b] Average value of activation energies
[c] Based on sulfate release

Chirita and Rimstidt (2014) gathered the results obtained by Janzen *et al*. (2000) with other data from the literature (Belzile *et al*., 2004; Cai *et al*., 2005; Chirita *et al*., 2008 and Romano, 2012) and developed rate equations for oxidative dissolution of pyrrhotite and determined a reaction order by Fe (III) and O_2. A total of 48 and 35 data was used for Fe (III) and O_2, respectively. The resulting rate equations are shown in equations (2.13) e (2.14). The Fe (III) experiments data collected span a narrow pH range of 2.0–2.75, while the O_2 rate experiments were performed over a pH range of 1.97–3.5.

$$r_{Fe(III)}(mol/m^2s) = 0.516e^{\frac{-33,600}{RT}} M_{Fe(III)}^{0.368} \quad (2.13)$$

$$r_{O2}(mol/m^2s) = 1.10x10^{-2}e^{\frac{-30,200}{RT}} P_{O2}^{0.352} \quad (2.14)$$

In an agreement with Romano (2012), Chirita and Rimstidt (2014) claim that, based on the multiple linear regression, pH has no significant effect on either reaction. The reaction order to oxygen determined by both studies was very close (0.30 - 0.352). However, the reaction order for the ferric iron equation found by Chirita and Rimstidt (2014) (m_{Fe} = 0.368) is relatively lower than those discussed by Janzen *et al*. (2000) (m_{Fe} = 0.560).

It is important to highlight that the correlation coefficients determined for the oxygen and iron rate equation were low (21% and 39%, respectively). The authors argue that:

> The random and systematic errors in the data are quite large compared to the effect of O_2 or Fe (III) concentrations on the observed rate. Nonetheless, these equations represent the current best estimates for the effect of O_2 and Fe (III) on pyrrhotite dissolution rates. This lack of fit may be the result of one or more uncontrolled variables such as reactor design, the extent of reaction, solution chemistry, pyrrhotite impurities or simply caused by the narrow range of experimental conditions and relatively small numbers of data (Chirita and Rimstidt, 2014).

The low correlation coefficients found means that the regression variables determined explain only 21% and 39% of the variance of the oxygen and ferric iron rates, respectively. This low adjustment obtained justifies the need for further studies on the influence of oxidants on the reaction rate of pyrrhotite. In addition, these studies need to be extended to circumneutral pH, typical of tailings impoundments. Belzile *et al*. (2004) also draw attention to the varied structures of pyrrhotite as an influence on rates differences between the experimental studies. However, the few studies reporting the oxidation rate of pyrrhotite in acidic medium seem to agree with the values in the range of 10^{-8} to 10^{-9} mol.m^{2}s^{-1}, generally based on the release of iron.

Figure 2-9 compares the rates of pyrrhotite dissolution for each of the three reactions equations developed by Chirita and Rimstidt (2014) (equations 2.8; 2.13 and 2.14) and shows

how complex the pyrrhotite dissolution mechanisms can be. The overlap of the rates for these experimental conditions suggests that the rates determined by some of the experiments are a composite of two reactions at least. The O_2 rate experiments are presented by the large rectangle over a pH range of 2 - 3.5. It is possible to note that the rates at low pH are similar to the H^+ rates, which indicates that they are a composite of both the H^+ and O_2 reactions. The Fe (III) experiments are presented by the small rectangle in a narrow pH range of 2.0 - 2.75 and the overlap between this range and the H^+ rates suggest that the rates measured near pH 2 represent a combination of rates from the H^+ and Fe (III) reactions. Also, the measured rates for O_2 and Fe (III) reactions overlap, implying that in O_2 rich atmospheres the measured Fe (III) oxidation rates may contain a significant contribution from O_2 oxidation.

The oxidation mechanisms of pyrrhotite are still unclear. Despite this, many studies agree on a progressive enrichment of the surface with sulfur when pyrrhotite is oxidized (Belzile *et al*., 2004). Buckley and Woods (1985), Jones *et al*, (1992) and Mycroft *et al*. (1995) evaluated the oxidation of pyrrhotite by air at room temperature using X-ray photoelectrons and Auger electron spectroscopy. The authors agree with a rapid oxidation, about seconds, when pyrrhotite is exposed to air and suggest that after oxidation two distinct compositional zones are formed. As a result of Fe diffusion to the surface, Mycroft *et al*. (1995) by using Angle resolved X-ray photoelectron spectroscopy (ARXPS) identified that the outermost zone is composed of iron oxyhydroxide, and the underlying zone is rich in sulfur and depleted of Fe in relation to the pyrrhotite bulk.

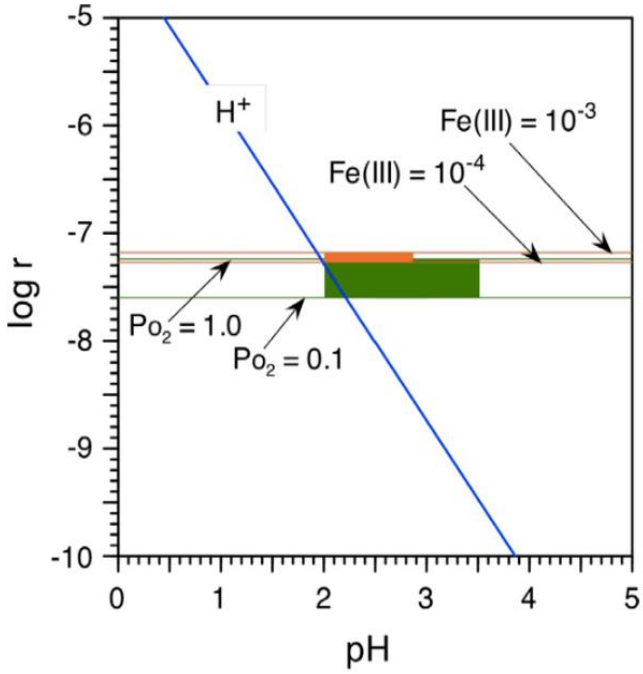

Figure 2-9: Rates (mol.m^2.s^{-1} of the H$^+$, O_2, and Fe (III) predicted by the rate equations of nonoxidative (2.8), and oxidative reactions by ferric ion (2.13) and oxygen (2.14) of pyrrhotite for the experimental conditions (25 °C) where the rate data were derived (shaded areas and H$^+$ line). The shaded rectangles represent ranges of pH and oxidant concentrations for the rate data used to develop equations (2.13) and (2.14). Obtained from Chirita and Rimstidt (2014).

The studies by Jones *et al*. (1992) indicate that in air or water, the surfaces depict amorphous layers containing carbonate; sulfate, iron (III) oxides/hydroxides, and iron-deficient sulfide species. Thomas *et al*. (1998) infers that during the oxidative dissolution of pyrrhotite at acid conditions, the kinetics are diffusion-controlled due to iron diffusion through the metal-deficient layer (sulfur-rich layer - SRL). The results obtained by Thomas *et al*. (2001) agree with their previous studies and confirms the idea of a sulfur-rich layer as a barrier to iron diffusion, which is supported by the activation energy obtained, around 12 kJ mol^{-1} at 20 to 40 °C. Chirita *et al*. (2008) and Chirita (2009) also claim that the pyrrhotite dissolution rates are limited by diffusion of reactants through a passive SRL.

Similar activation energy for Fe (III) oxidized pyrrhotite (33.6 kJ.mol^{-1}) and oxygen (30.2 kJ.mol^{-1} were determined by Chirita and Rimstidt (2014). These values are lower than those reported by Janzen *et al*. (2000) who found 48.6 kJ.mol^{-1} and 53.4 kJ.mol^{-1} as mean activation energy values for oxidation with ferric ions and oxygen, respectively at pH 2.5 (Table 2-5). However, according to Chirita and Rimstidt (2014), the values are substantially higher than expected by a diffusion process (10-20 kJ/mol). Nicholson (1994) found 50 kJ.mol^{-1} as

activation energies for pyrrhotite oxidation at pH 2 and 4, and 100 kJ·mol^{-1} at pH 6. Thus, the author claims that the rate-controlling step is a chemical reaction rather than control by diffusive processes. Agreeing with chemical control, Janzen *et al*. (2000) propose that the fractional order dependence (~0.56) of the rate with ferric ions determined at low reactant concentrations (2 x 10^{-4} mol. L^{-1} Fe (III)) implies a reaction mechanism involving control by sorption or desorption processes. The authors also observed that at high initial ferric concentrations, the order dependence substantially decreases, which is also consistent with an adsorption mechanism.

In the review by Belzile *et al*. (2004) the authors conclude that at low pH oxidative and non-oxidative dissolution processes compete. Also, Chirita and Rimstidt (2014) reported that similar rates for H^+, O_2, and Fe (III) were determined near pH 2, leading to concerns that some of the experiments may have measured combined rates. However, since acid mine drainage solutions rarely reach pH <2.5 (Chirita and Rimstidt, 2014), it is inferred that the pyrrhotite oxidation process is dominated by the O_2 reaction at pH> 3. I draw attention to the absence of studies at circumneutral or mildly alkaline medium, common conditions for disposing of sulfides in tailings (Ritcey, 2005). Therefore, in this work, the oxidation of pyrrhotite will be investigated in this pH range.

In summary, Pyrrhotite ($Fe_{1-x}S$) has iron vacancies that originate different crystallographic superstructures. The most common and best understood is the 4C (composition Fe_7S_8, monoclinic symmetry, and magnetic). Pyrrhotite is known to be one of the most reactive sulfides. The authors attribute this higher reactivity to the lower symmetry caused by the vacancy of iron atoms in the crystal structure and higher specific surface area compared to other mineral sulfides (Nicholson and Scharer, 1994; Janzen et al., 2000). Pyrrhotite can exhibit non-oxidative and oxidative dissolution. However, for conditions close to neutrality, the oxidative reaction predominates. The oxidative rate based on the iron release is usually higher than the oxidation rates based on sulfate production (in the range of 10^{-8} - 10^{-9} versus 10^{-10} mol.m^{-2}.s^{-1}, respectively) (Table 2-5). Also, pyrrhotite oxidation by ferric iron is about one order of magnitude greater than oxidation by oxygen. The pH has no significant effect on either reaction (ferric iron or oxygen).

1.3 Galvanic Interaction

Qing You *et al*. (2007) suggest that oxidative dissolution of metal sulfides due to galvanic interaction is a critical factor that contributes to environmental pollution in the mining of metal sulfide ores (Byerley and Scharer, 1992; Lin, 1997; Dinelli and Tateo, 2002; Salomons, 1995; Subrahmanyam and Forssberg, 1993; Cruz *et al*., 2001). Because most metal sulfide minerals have semiconductor properties, a galvanic cell is created when two sulfides are in intimate contact in solution (Liu *et al*., 2008). The expected magnitude of this effect can be estimated by comparing mineral's rest potential (Table 2-6).

Table 2-6: Rest potential of sulfide minerals at ambient temperature (Fallon *et al*., 2017).

Mineral	pH	Rest Potential (V) vs. SHE				References
			Bubbled with N_2	Bubbled with O_2	Exposure to air	
Pyrite (FeS_2)	4	0.66				Majima (1969) and references therein
	Distilled water (~ pH 7)		0.405	0.445	0.485	Pozzo and Iwasaki (1989)
Marcasite (FeS_2)	4	0.63				Majima (1969) and references therein
Arsenopyrite (FeAsS)	Distilled water (~ pH 7)		0.277	0.303	0.323	Iwasaki (1989)
Pyrrhotite ($Fe_{(1-x)}S$)	Distilled water (~ pH 7)		0.055	0.160	0.173	Adam *et al*. (1984)
	Distilled water (~ pH 7)		0.125	0.262	0.295	Iwasaki (1989)
Chalcopyrite ($CuFeS_2$)	4	0.56				Majima (1969) and references therein
	Distilled water (~ pH 7)		0.190	0.355	0.371	Hu *et al*. (2010) and references therein
Covellite (CuS)	4	0.45				Majima (1969) and references therein
Bornite (Cu_5FeS_4)	4	0.42				Majima (1969) and references therein
Sphalerite (ZnS)	4	0.46				Majima (1969) and references therein
Galena (PbS)	4	0.4				Majima (1969) and references therein
	Distilled water (~ pH 7)		0.142	0.172	0.218	Learmont and Iwasaki (1984)

The sulfides with the lowest rest potential act as anodes and have their oxidation rate favored, while the sulfides with the highest potential are protected from oxidation (Abraitis *et al*., 2004; Holmes and Crundwell, 1995). Since pyrite is a ubiquitous mineral on earth, it is commonly found associated with other minerals. Pyrite has the highest rest potential among the common sulfides (Mehta and Murr, 1983; Majima, 1969). Thus, pyrite reacts cathodically in the galvanic couple, and, consequently, it will rule the oxidation process of the other associated minerals.

The effect of the formation of galvanic couples between sulfides has been investigated in the literature for different purposes: i) influence on the leaching of the metal of interest in hydrometallurgical systems; ii) influence on flotation; iii) environmental concerns mainly related to acid generation and release of toxic metals.

According to Majima and Peters (1968) "The galvanic effect may be one of the most important electrochemical factors which govern the dissolution rate of sulfide minerals in hydrometallurgical systems" (apud Holmes and Crundwell, 1995, p. 354). Therefore, many authors have investigated the galvanic effect in aqueous leaching or bioleaching systems (Mehta and Murr, 1983; Abraits *et al*., 2004; Majuste *et al*., 2012; Deng *et al*., 2018; Deng *et al*., 2020).

The catalyst effect of pyrite in the oxidation of the sulfides due to the galvanic interaction can be very well noted in Figure 2-10 from the work of Abraitis *et al*. (2004). The authors studied, under identical conditions (pH 2.5 and 25 °C), the oxidation of the isolated phases and in the presence of pyrite for the following systems: galena/pyrite, chalcopyrite/pyrite, sphalerite/pyrite, pyrite, galena, and chalcopyrite. The studies lasted 200 min. As expected, all minerals presented a higher dissolution rate in the presence of pyrite due to the occurrence of galvanic interaction. The rates of dissolution of galena, chalcopyrite and sphalerite were 31, 18 and, 1.5 times, respectively, more rapid than in single-mineral experiments. Majuste *et al*. (2012), using an innovative approach with pyrite inclusions naturally found in chalcopyrite samples, also evaluated, through electrochemical studies, the magnitude of the galvanic interaction involving these two sulfides under oxidizing conditions aiming to improve the chalcopyrite leaching rate from low-grade ores. An increase in the mixed potential value and in the dissolution current density of the copper sulfide was noted in the presence of pyrite inclusions. The authors also conclude that the galvanic effect established between pyrite and chalcopyrite is magnified under less oxidizing conditions.

Some authors have also studied the galvanic effect in the flotation process (Adam *et al.*, 1984; Nakazawa and Iwasaki, 1985; Nakazawa and Iwasaki, 1986; Cheng and Iwasaki, 1992; Ekmekçi *et al*., 1997; Huang *et al*., 2006). According to Ekmekçi *et al*. (1997), the mineral surfaces may be altered when the galvanic current flows between the sulfides. The authors also conclude that the relative ratio between anode and cathode in the galvanic couple will determine the active surface area of electrodes, and the dominant reaction type in the pulp, such as the formation of hydrophobic sulfur-based or hydrophilic iron hydroxide species. Thus, the surface coating produced will directly affect the floatability of the sulfide minerals.

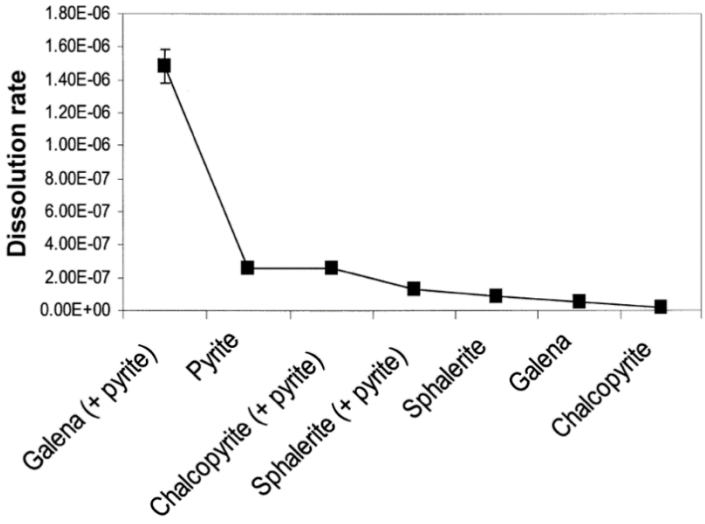

Figure 2-10: Dissolution rate (mol. m^{-2}. s^{-1}) in air-equilibrated solutions at pH 2.5 for single and two phases system. Obtained from Abraitis *et al.* (2004).

Regarding environmental problems, it is important to highlight the studies that investigated the impacts of galvanic interactions on metal contamination and acid generation in the mining of metal sulfide ores (Qing You *et al*., 2007; Liu *et al*., 2008; Qian *et al*., 2018; Ferreira *et al*., 2021).

Aiming to evaluate the effects of flowing media on metal pollution, Qing You *et al.* (2007) studied pyrite/chalcopyrite galvanic interaction in a flowing system by connecting a FeS_2 electrode and a $CuFeS_2$ electrode through copper wire. The authors investigated the effect of pH (5-7), Fe (III) ion concentration (10^{-2} - 10^{-4} mol. L^{-1}), and flow rate (0.06 – 0.36ms^{-1}). Qing You *et al*., 2007 concluded that a higher acidity, a higher ferric ion concentration, and a higher flow rate led to an increase in the corrosion current density, and to a more positive mixed potential of the galvanic cell. Therefore, when increasing these three parameters, the environmental pollution in the mining districts and surrounding areas becomes more serious.

Liu *et al*. (2008), using the same experimental design of Qing You *et al*. (2007), found that the presence of non-oxidizing and non-reducing ions (e.g., Na^+) have no evident influence on the galvanic cell. Qing You *et al*. (2007) and Liu *et al*. (2008) infer that because Fe (III) in the flowing solution can increase the speed of galvanic interactions, the mere fact of excluding oxygen from the system is not able to prevent galvanic interactions. Thus, building in-situ subsurface barriers will not improve the acidic wastewater discharged or heavy metal pollution in places where ore tailings and mining wastes contain a variety of sulfide minerals.

Qian *et al*. (2018) investigated the impacts of galvanic interaction on acid generation at low sulfide content representative of acid mine drainage wastes using kinetic leach columns (KLC). A total of five mineral systems were studied (pyrite, sphalerite, galena, pyrite-galena, and pyrite-sphalerite) for 76 weeks. In all KLCs, sulfides were added at a total of 2.0 wt% S. In the mixed sulfide KLCs, 10% of the total S from sulfide was contributed from sphalerite or galena and 90 % from pyrite (typical of AMD waste rocks). Quartz, K-feldspar, and chlorite were also added in the KLC experiments in weight percent of about 80, 10 and, 5%, respectively. It was observed that the presence of pyrite accelerated the leaching of galena and sphalerite in 24% and 15%, respectively.

In addition to acid mine drainage generation, galvanic interactions can also favor the dissolution of toxic metals in the environment. Pyrite, arsenopyrite and pyrrhotite are generally found associated. From samples collected from a gold beneficiation plant (BP) at Paracatu (Northwest of Minas Gerais State, Southeast Brazil), the studies by Morais *et al*. (2019) identified pyrite as the main constituent of the BP sample (277 at 33,328 particles) among the sulfide minerals. Arsenopyrite was the second major constituent of this sample followed by pyrrhotite (94 and 79 particles, respectively).

Greater generation of acids, sulfates, and greater release of toxic elements can occur due to galvanic interaction, as demonstrated by Ferreira *et al*. (2021). The authors used a flow-through reactor to study the galvanic effect of FeS_2 on FeAsS at circumneutral pH under conditions typically found in the tailings dam. In this system, the physical contact between the sulfides was kept permanent. The authors showed that 5% wt. of FeS_2 within the reactor is enough to increase the As released in 24 h around 73% and 75%, under oxygen-depleted and oxygen-saturated conditions, respectively. The positive effect on the release of the toxic element can be observed in Figure 2-11.

When studying the galvanic interaction between arsenopyrite and pyrite by Density Functional Theory (DFT) dos Santos *et al.* (2017) also concluded the anodic role of the former. According to the authors, the calculations indicate the valence band of pyrite in a region above the valence band of arsenopyrite, making pyrite an electron donor relative to arsenopyrite. The studies conducted by Urbano *et al*. (2008) and Deng *et al*. (2018) demonstrated the dissolution of arsenopyrite also can be enhanced in the presence of pyrite.

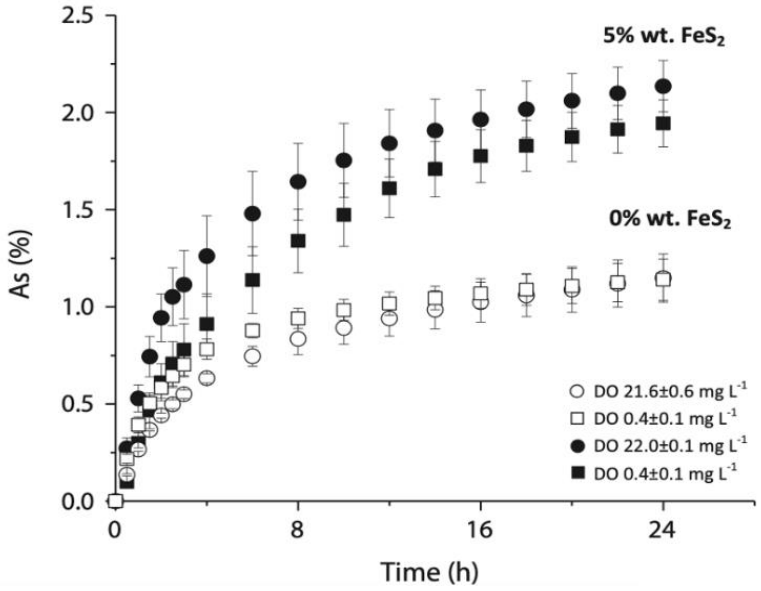

Figure 2-11: Effect of dissolved oxygen concentration and 5% wt. of pyrite on the accumulated As release from FeAsS oxidation as a function of time. Experimental conditions: pH initial (6.9–7.2); temperature (24.2–26.2) ◦C; flow rate (0.93–1.04) mL min^{-1}. Obtained from Ferreira *et al.*, 2021.

Although pyrrhotite commonly occurs in many refractory gold ores together with pyrite and arsenopyrite (Rabieh *et al.*, 2017), no publication is available, to the best of the author's knowledge, on the galvanic interaction between arsenopyrite and pyrrhotite. Besides, for the pyrite/pyrrhotite system the studies in the literature are most focused on the products formed and its effect on the mineral floatability (Nakazawa and Iwasaki, 1985; Pozzo and Iwasaki, 1989; Almeida and Giannetti, 2003).

Among the three sulfides (FeS_2, $Fe_{1-x}S$ and FeAsS) , pyrite has the highest rest potential and pyrrhotite the lowest, regardless of the pH of the solution, as shown in Table 2-6. Therefore, arsenopyrite is expected to react cathodically in the arsenopyrite/pyrrhotite couple and the As release be reduced. On the other hand, pyrrhotite oxidation will be favored in both galvanic couples (pyrite/pyrrhotite and arsenopyrite/pyrrhotite), possibly leading to an increase in the sulfate concentration.

3. Experimental

1.4 Preparation of the mineral samples

The mineral samples used in this work were acquired from Ward's Science as research grade samples of arsenopyrite (Gold Hill – Utah, USA), arsenopyrite ((49–5857; Yi Zhang, Hunan Province, China) and pyrrhotite (470025-752 – Galax – Virginia, USA) these sample will be named as Apy GH, Apy H and Pyh V, respectively, to simplify the identification. Moreover, pyrrhotite sample (d50 < 38 μm) of a magnetic pyrrhotite concentrate were provided by a gold cyanidation plant (MG – Brazil), named as Pyh MG. Pyrite sample (49–5884; Zacatecas, Mexico) from Ferreira et al. (2021) study was also used to conduct pyrite-pyrrhotite association experiments. (Results on Appendix).

The samples were initially ground in a cup and ring mill and sieved to size fractions below 100μm or 38μm. The pyrrhotite samples were separated into magnetic and non-magnetic fractions under the magnetic field intensity of 0.2 T using a magnetic separator (P/N S4925 Frantz Isodynamic Magnetic Separator Model L-1, USA). Afterwards, the samples were rinsed with 75% v/v ethanol (99.8° v/v) and placed in an ultrasonic bath (Nova instruments) for 3 min to remove ultrafine particles adhering to the surface of the mineral. To remove oxide phases and other acid-soluble impurities, the arsenopyrite samples were rinsed in 3 mol. L^{-1} hydrochloric acid, HCl, solution (37% PA, Química Moderna) at 45 °C for 3 h under stirring. Then, the mixtures were vacuum filtrated using nylon membranes (47 mm diameter, 0.45 μm pore size, Millipore®). The solid phases were thoroughly rinsed with Milli-Q water (resistivity of 18.2 MΩ cm, Millipore®) followed by rinsing with absolute ethyl alcohol (99.5% ACS, Synth). Next, the samples were thoroughly homogenized and, successively quartered (Quantachrome, Rotary Micro Riffler RR-4). Mineral samples containing around 1g were prepared and kept under vacuum.

1.5 Characterization of the mineral samples

The mineral samples were characterized according to the particle size distribution, specific surface area, mineral composition and quantitative chemical composition. The particle size

distribution analysis was conducted by dynamic light scattering using a CILAS (1064) granulometer. A dispersing agent (TRITONX 100) was added to the pulp during analysis. The results were expressed according to the cumulative percent diameters (d_{10}, d_{50} and d_{90}) and mean diameter, in μm.

The specific surface area (SSA) of the mineral samples was measured using a nitrogen gas sorption analyzer (Quantachrome, NOVA 1200e). Prior to the measurements, the samples were weighed, degassed by placing them into a glass cell under vacuum for 96 h at 40 °C and weighed again. Nitrogen gas adsorption occurred in relative pressures (P/P_0) within a range of 0.05–0.3. The SSA was calculated using the multipoint Brunauer, Emmett and Teller (BET) equation.

The main mineral phases were identified by X-ray diffraction (XRD) analysis using a PANalytical (Empyrean) X-ray diffractometer, with Cu Kα1 (λ = 1.5406 Å) radiation. The XRD patterns were measured in 2θ range from 3.03° to 89.94° using a step size of 0.04◦. The mineral composition was identified using COD (Crystallography Open Database) files as reference.

Raman spectroscopy was also used for the characterization of some mineralogical phases. Raman spectra were obtained with a LabRam-HR 800 (Horiba Jobin Yvon, USA) spectrograph equipped with helium-neon laser (λ = 632.8nm) and a microscope (Olympus BX-41, 100x). The back-scattered light collected was detected by a LN2 charged coupled device (CCD 3000 - Spectrum One). The spectra ranged within 100-1400cm-1 with a step size of $1cm^{-1}$.

The quantitative chemical composition of the mineral samples was determined after aqua regia digestion at moderate temperature (to avoid arsenic volatilization) by using inductively coupled plasma optical emission spectrometry (ICP- OES) and hydride generation. The procedure followed the same methodology utilized by Ferreira et al., 2021. Firstly, 0.1 g of each sample was weighed using an analytical balance (Mettler Toledo AE200) with readability of 0.1 mg and linearity of ± 0.3 mg. The samples were dissolved (in triplicate) in a hot block digester (Tecnal, TE-040/25) at 80 °C for 2 h using aqua regia (3HCl:HNO_3) solution (HCl 37% PA and HNO_3 65% PA, Química Moderna). After that, the mixtures were vacuum filtrated using nylon membranes (47 mm diameter, 0.45 μm pore size - Millipore®)

and properly diluted. The concentrations of the elements in the digested solutions and output solutions were analyzed by ICP-OES or hydride generation using a Perkin Elmer (Optima 7300 DV) spectrometer. The total sulfur content in the mineral samples was measured using a LECO (SC 632) induction furnace at 1400 °C.

1.6 Sulfide oxidation and Galvanic interaction - Flow-through reactor

The experiments for sulfide oxidation and galvanic interaction were carried out in a flow-through reactor made with polystyrene developed by Ferreira *et al*. (2021) (Figure 3-1). This cylindrical reactor was installed in a water-jacketed glass column. 0.5 or 1 g of mineral particles was confined in the inner chamber of the reactor (11.50 mm length × 5.00 mm height, 0.519 cm^3 total volume) between mixed cellulose ester membranes (0.45 μm pore size - Millipore®) and stainless steel meshes (5 mm). Thus, a permanent contact among the FeAsS, FeS_2 and $Fe_{1-x}S$ particles was ensured. O-rings were used for sealing and for keeping the reactor fixed in the glass column during the experiments. To evaluate the effect of soluble citrate and chloride ligands on arsenic and sulfate release from sulfide minerals, 1mmol of each ligand was added in the feed solution.

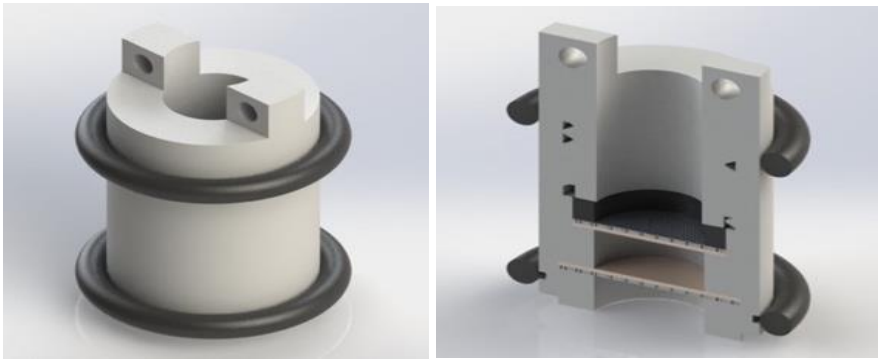

Figure 3-1 : Drawing of the flow-through reactor used in the oxidation experiments: (a) trimetric view; and (b) trimetric section, by Solid Works.

1.6.1 Experimental apparatus and procedures

The experimental procedure consisted in the continuous flow of oxygen-depleted or oxygen-saturated solutions through the reactor during 24 h. In order to remove moisture and traces of

carbon dioxide (CO_2), the nitrogen (99.999% N_2, Air Products) and oxygen (99.99% O_2, White Martins) gases were percolated through U-type tubes containing anhydrous calcium sulfate – DrieriteTM (1–3 mm, Fluka) and sodium hydroxide-coated silica – AscariteTM (8–20 mesh, Fluka). Next, the gases were continuously bubbled in a 4 L Pyrex flask that contained the input solution with the pH adjusted. This solution was prepared by dissolving sodium hydroxide, NaOH (97% PA, Vetec) or HCl (Vetec)in Milli-Q water.

The input solution was pumped to the flow-through reactor in up-ward flow using a peristaltic pump (MasterFlex® L/S, 7521–50) at fixed flow rate (1.0 ± 0.1 mL min^{-1}). The temperature of the input solution was controlled using a temperature-controlled water bath (Lauda®, Alpha). During the experiments, aliquots (30 mL) of the output solution were regularly collected in polyetilene tubes by an automatic sampler device (Pharmacia LKB, Superfrac Fraction Collector). A schematic of the column system assembly is shown in Figure 3-2.

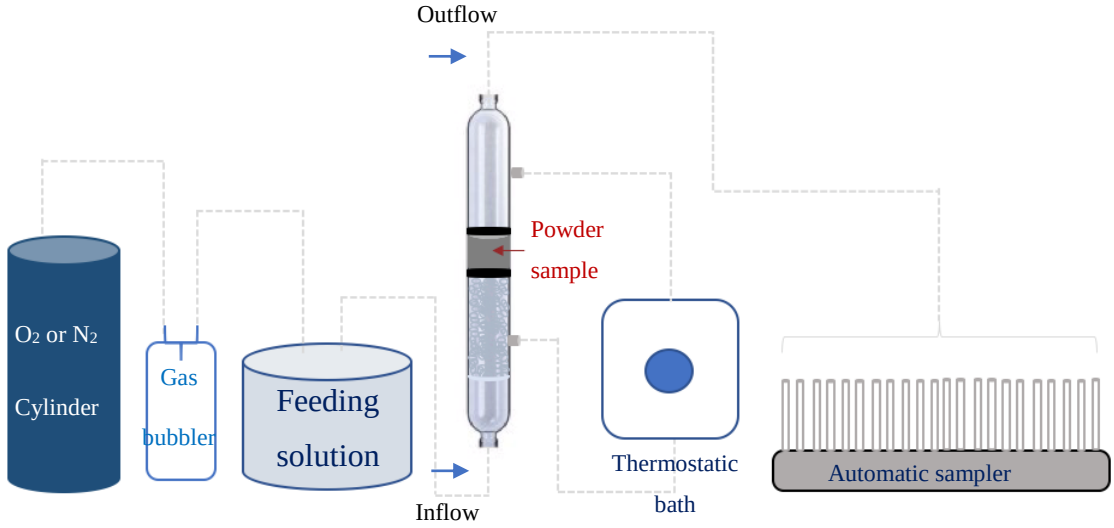

Figure 3-2 : System assembly for sulfide oxidation experiments in column.

The concentrations of Fe and As in the output solution were analyzed by ICP-OES for FeAsS Yi Zhang, Hunan Province sample. Certified aqueous standards (Arsenic 1000 mg L^{-1} and Iron 1000 mg. L^{-1} SPEX CertPrep, NJ, USA) were used and replicate readings carried out during the ICP-OES measurements. The sulfur, iron and arsenic quantities released from FeAsS (Gold Hill) sample and from $Fe_{1-x}S$ sample were analyzed by ICP-MS (Inductively coupled plasma – mass spectrometry) model PerkinElmer - NexION 300X. Germanium (5 ppb) was used as internal standards for reading AsO and Fe species, and indium (1ppb) for SO analysis. The pH of both the input and output solutions was measured using a pH electrode (Digimed DM-23, DME-CV2P). Previous calibrations were conducted with certified buffers. All

reagents and experiments were prepared using Milli-Q water (18 MΩ.cm Milli-Q water purification system, Millipore Corporation, Bedford, USA).

The calculated limits of detection (LOD) are 0.12; 2.40 ; and 9.92 μg L^{-1} for As, Fe and S, respectively, and the limits of quantification (LOQ) are 0.59; 12.00 and 49.60 μg L^{-1} for arsenic, iron and sulfur in this sequence. The limit of detection and quantification were determined by analysing the calibration curve and 7 analytical blanks. The blanks are a solution of double-distilled nitric acid at a concentration of 2% V/V (diluted with Milli-Q water), which is the same mean for preparing the curve and the samples. The internal standards (Ge 5 ppb and In 1 ppb) are also added to the blanks. The (LOD) was calculated by multiplying the standard deviation of the reading intensities of the 7 blanks by 3. The quantification limit is five times the LOD, as it considers the minimum dilution of samples for reading in the ICP-MS. This dilution was determined experimentally, considering the matrix complexity and analyte concentrations.

Duplicates and replicates were carried out in each batch. As for quality assurance and control, analytical blanks, and Certified aqueous standards (Arsenic 1000 μg L^{-1} , Iron 1000 μg. L^{-1} and Sulfur 1000 μg. L^{-}SPEX CertPrep, NJ, USA - diluted to 20x to reach 50 μg L^{-1} for each analyte) were analyzed for each batch of 8 samples. All blank extractions returned values below the detection limits. The Standard Reference Material -SRM- NIST 1643e were also analyzed during ICP-MS procedure. The recovery ranged from 80 to 87% and 98 to 104% for arsenic and iron, respectively. Detailed analytical procedures are provided in the Supplementary Material.

At the end of each experiment, the mineral particles were collected from the flow-through reactor and rinsed with absolute ethyl alcohol (99.5% ACS, Synth) under vacuum. The samples were then stored in closed desiccator under vacuum until examination.

1.6.2 Experimental conditions

The effect of the following variables was evaluated: DO concentration in the input solution (oxygen-depleted (<1 mg L^{-1}) and oxygen-saturated (around 22 mg L^{-1})), pH of the input solution (4 -10), the amount of pyrrhotite added, that is, the content of $Fe_{1-x}S$ particles mixed to FeAsS or FeS_2 particles (50% wt., 75% wt.), and the effect of complexing ligands ions in

the solution (citrate and chloride – 1mmol). The main parameters monitored in this work were the As, Fe and S released in the output solution from sulfides oxidation and As release rate.

The rate (mol.m^{-2}.s $^{-1}$) was calculated by:

$$r_{As} = \frac{[C] * Q}{SSA * m_i}$$

where [C] represents the As concentration in the output solution (mol kg $^{-1}$), Q the solution flow rate (kg s^{-1}), SSA the specific surface area (m^2 g^{-1}) of the mineral particles and mi the initial mass of arsenopyrite (g).

1.7 Iron effect - Shaker experiments

Preliminary experiments in shaker systems were carried out to evaluate the effect of the addition of Fe (II) and Fe (III) on the arsenic release from arsenopyrite sample. Thus, 0.1 g of the material was added to 50 ml of a solution (pH = 5) without iron addition (control experiments) or with 100 mg.kg^{-1} (concentration based on studies by McKibben *et al*. (2008)) of ferrous or ferric sulphate. The experiments were carried out at 25°C and under agitation of 200 min^{-1} for 48 hours. Periodic solution samples were taken from each system (control; with addition of Fe (II) and with addition of Fe (III) for pH measurements, as well as As and Fe concentration analyses by ICP-OES (Results on Appendix).

4. RESULTS

1.8 Sample characterization

The XRD pattern (Figure 4-1) and the chemical composition (Table 4.1) indicates the high grade of both arsenopyrite samples Apy - H and Apy - GH. Trace amounts of: (i) pyrite (FeS_2); (ii) sphalerite (ZnS) in the sample GH were also identified by XRD and confirmed by Raman spectroscopy (results no shown).

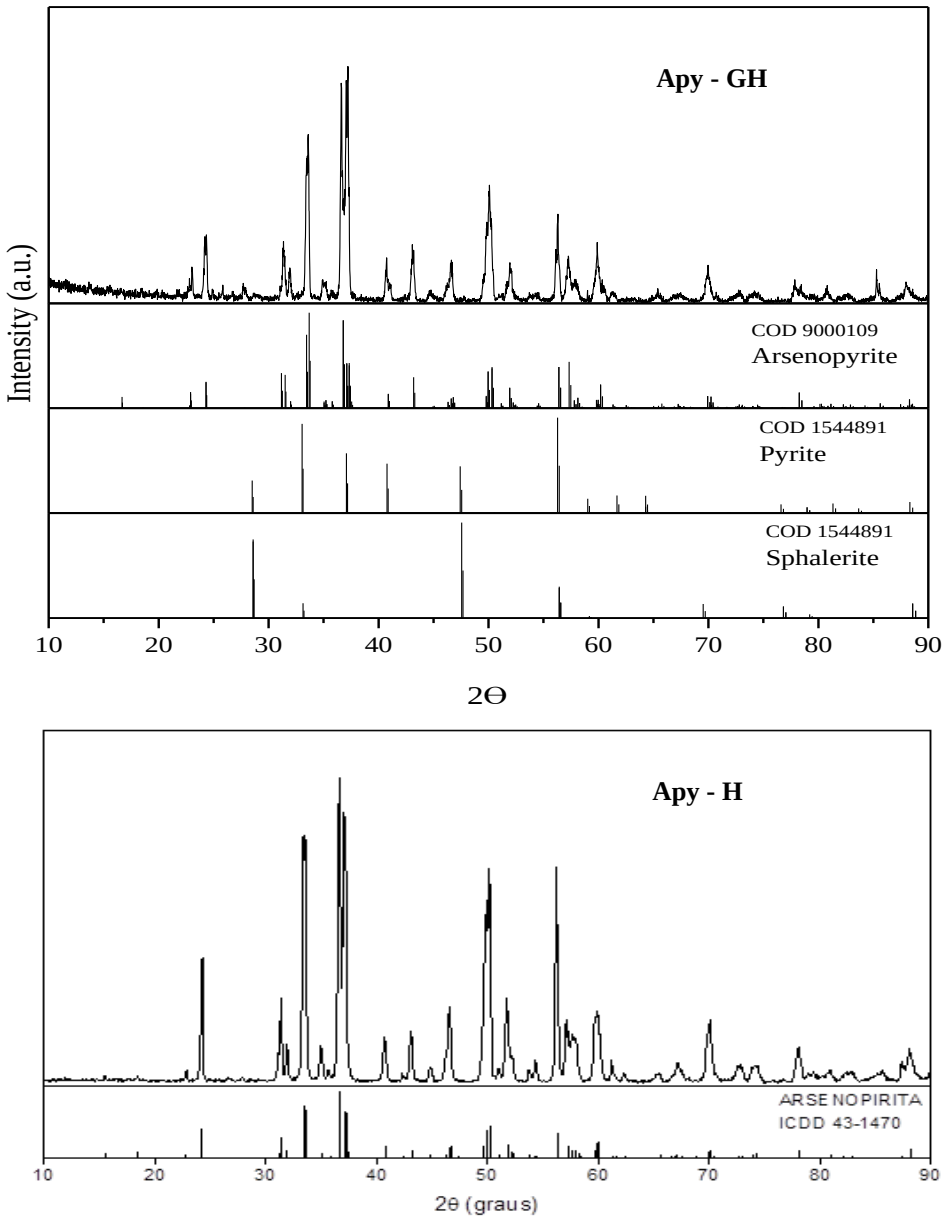

Figure 4-1: X-ray diffraction patterns for the arsenopyrite samples Apy-GH (a) and Apy-H (b). The Apy – H pattern is from Ferreira et al. (2021).

The arsenopyrite sample FeAsS (GH) contains 31.0 % Fe; 23.6% S; and 45.1 % As whereas FeAsS (H) consists of 33.5% Fe; 19.7% S; and 46.0% As. From the arsenopyrite theoretical composition (*i.e.*, 34.3% wt. Fe; 46.0% wt. As; 19.7% wt. S) one can estimate 97.7% wt. FeAsS in sample (H) and 97.9% wt. FeAsS in sample (GH).

Table 4-1: Chemical composition of the mineral samples (% wt.).

	Apy - GH	Apy - H	Pyh - V	Pyh - MG	Pyrite
[2]**Fe**	30.95 ± 1.97	33.5 ± 1.4	59.69 ± 1.19	59.02 ± 1.56	49.01 ±0.9
[3]**S**	22.56 ± 0.77	19.7 ± 1.1	38.73 ± 0.06	40.02 ± 0.90	51.5 ±2.5
[1]**As**	45.05 ± 1.05	46.0 ± 2.8	0.024 ± 0.005	0.11 ± 0.01	0.085 ±0.003
[1]Ni	[a]	[a]	a	0.15 ± 0.01	-
[2]**Si**	0.005 ± 0.001	0.30 ± 0.01	0.018 ± 0.000	0.031 ± 0.002	0.04 ± 0.02
[2]**Ca**	0.01 ± 0.00	[a]	0.39 ± 0.01	0.12 ± 0.01	-
[1]**Cu**	0.004 ± 0.000	0.016 ± 0.001	0.37 ± 0.01	a	0.020 ±0.001
[1]**Zn**	0.36 ± 0.01	0.15 ± 0.01	0.28 ± 0.01	0.022 ± 0.001	-
[1]**Pb**	0.035 ± 0.003	0.034 ± 0.001	0.05 ± 0.01	0.009 ± 0.001	a
[2]**Mg**	0.003 ± 0.000	[a]	0.42 ± 0.01	0.32 ± 0.01	-

[a] Below the detection limit (0.005 mg/L) of the analytical technique
[1] Digestion of the sample in aqua regia and closed system in a digester block
[2] Digestion of the sample after lithium metaborate fusion
[3] Solid sample analyses in LECO

Figure 4-2 shows the X-ray diffraction pattern for the pyrrhotite samples Pyh – V. Only pyrrhotite and possibly talc ($Mg_3Si_4O_{10}(OH)_2$) were identified in the sample. Chalcopyrite ($CuFeS_2$) and calcite ($CaCO_3$) were only identified on the XRD pattern of the raw sample (before magnetic separation - not shown). However, since Cu and Ca were detected by chemical analysis, a small amount of chalcopyrite and of calcite is still present in the sample even after magnetic separation in amounts less than 5%, which makes detection difficult by XRD.

Pyrrhotite Pyh-V sample contain 59.69 % Fe and 38.73% S. By considering and excluding Fe and S from chalcopyrite, the stoichiometric composition determined for Pyh-V was $Fe_{7.0}S_{8.1,}$ which is consistent with the magnetic monoclinic symmetry (4C superstructure – Fe_7S_8) (Table 2-3).

X-ray diffraction pattern (Figure 4-2) Sample Pyh - MG has arsenopyrite (FeAsS), siderite (FeCO3) and dolomite (CaMgCO3) as minor impurities.

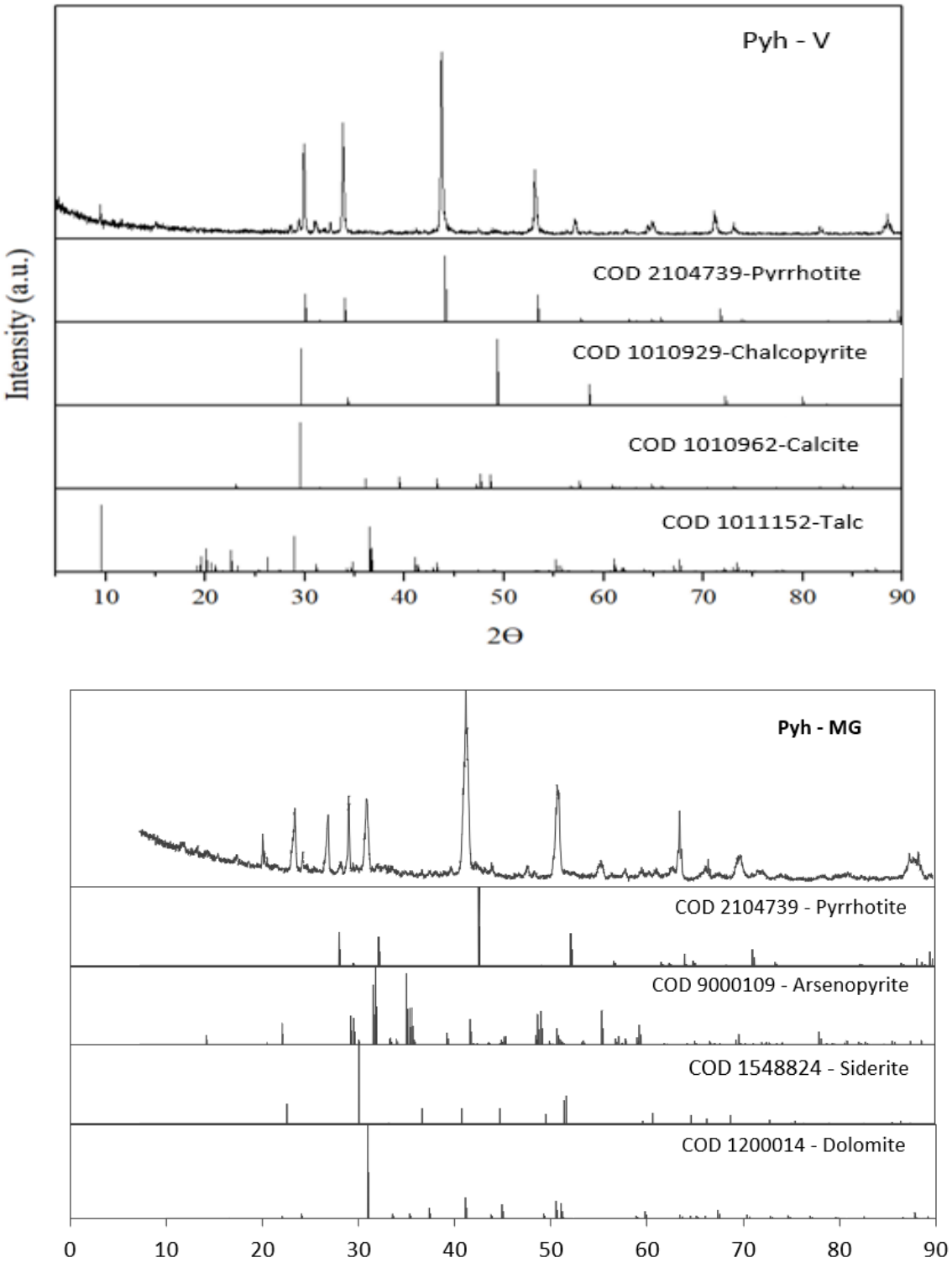

Figure 4-2: X-Ray diffraction patterns for prepared pyrrhotite samples after magnetic separation (Pyh-V (a) and Pyh – MG).

A detailed investigation of the pyrrhotite surface was carried out by Micro Raman spectroscopy. Figure 4-3 exhibits Raman spectra for the sample Pyh-V. From bottom to top: red curve - represents pyrrhotite particle with practically non-oxidized surface; green curve: pyrrhotite particle with oxidized surface, showing the formation of elemental sulfur (153, 220, 474 cm^{-1}), Marcasite (320 and 385cm^{-1}) and amorphous iron oxyhydroxides (~700cm^{-1}); blue curve: talc particle: 113, 200, 366, 680 cm^{-1}.Pyrrhotite has no bands, it only shows this rise in the curve below 200cm^{-1} (Belzile et al 2004 and Urashima 2022). Visually, this pyrrhotite sample shows most of the particles in a gray color with no oxidation products. Few regions were found in green, yellow, or red colors that indicate some degree of oxidation. Sulfate and iron sulfate compounds were not detected.

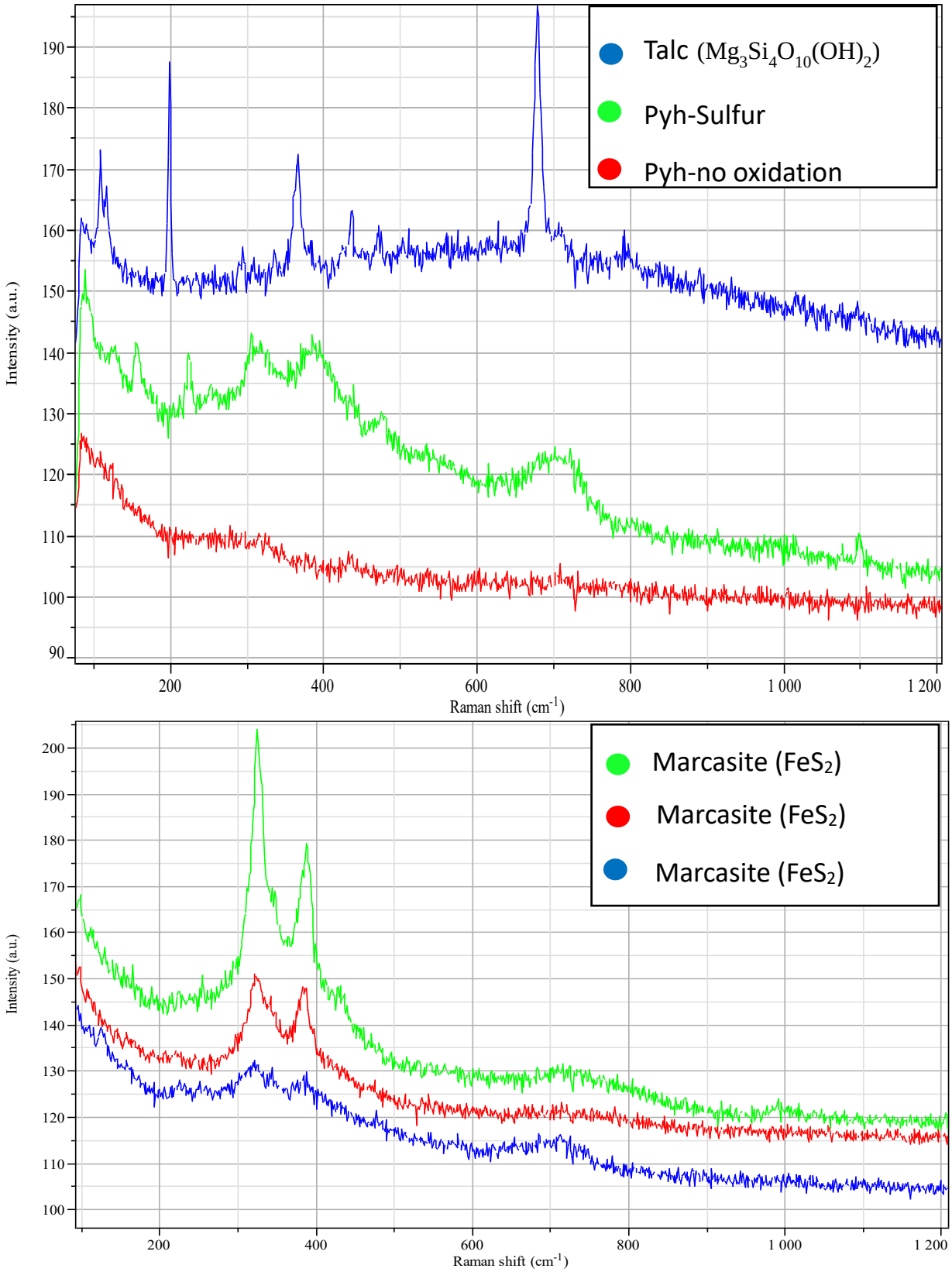

Figure 4-3: Raman spectra of Pyh V sample showing pyrrhotite (weak signal) at 334 and 399 cm^{-1} and Fe-oxyhydroxides (670-740 cm^{-1}) (a), marcasite (FeS_2) at 325 and 390 cm^{-1} (b) and elemental sulfur (470 cm^{-1}) (c).

According to the Raman investigation, the Pyh - MG sample depicted most of the particles with a thin greenish layer, some yellowish spots (indicating elemental sulfur, peaks 156, 220, 474 cm^{-1}), and other red spots (characteristic of regions where amorphous iron oxides form). Marcasite (FeS_2), siderite ($FeCO_3$), hematite (Fe_2O_3) and maghemite (γ-Fe_2O_3) were also identified (Figure 4-4) as trace compounds. There was no identification of phases containing sulfate in the region of 980-1200 cm^{-1}. Iron oxyhydroxides were observed around 690-720 cm^{-1} in most of the spectra. Other displacements (198, 227, 301 cm^{-1}) may indicate iron lattice modes like Fe-O_x and Fe-S (polysulfide) phases.

Pyrrhotite Pyh- MG is composed of 59.02 % Fe and 40.02% S (Table 4.1). The presence of pyrite which contain the same elements as pyrrhotite, makes it difficult to estimate the purity of the sample Pyh – MG. However, dolomite is estimated to be about 2.5%.

The presence of sulfur and iron oxides indicates surface layer oxidation for MG pyrrhotite and agrees with the higher surface area determined in the BET analysis (as discussed further) for this sample since the oxidation products are characterized by having very fine granulometry, which increases the surface area of the mineral.

Figure 4-5 shows secondary electron images generated by scanning electron microscopy for arsenopyrite (sample GH) from the fresh sample (submitted to acid washing a few hours before analysis) before (a) and after (b) flow-through reactor experiment for 24h under an oxygen atmosphere. It can be noticed for both conditions, heterogeneous particle sizes, with fines adhered to the larger particles. No significant differences were seen regarding the surface characteristic after the oxidation experiment.

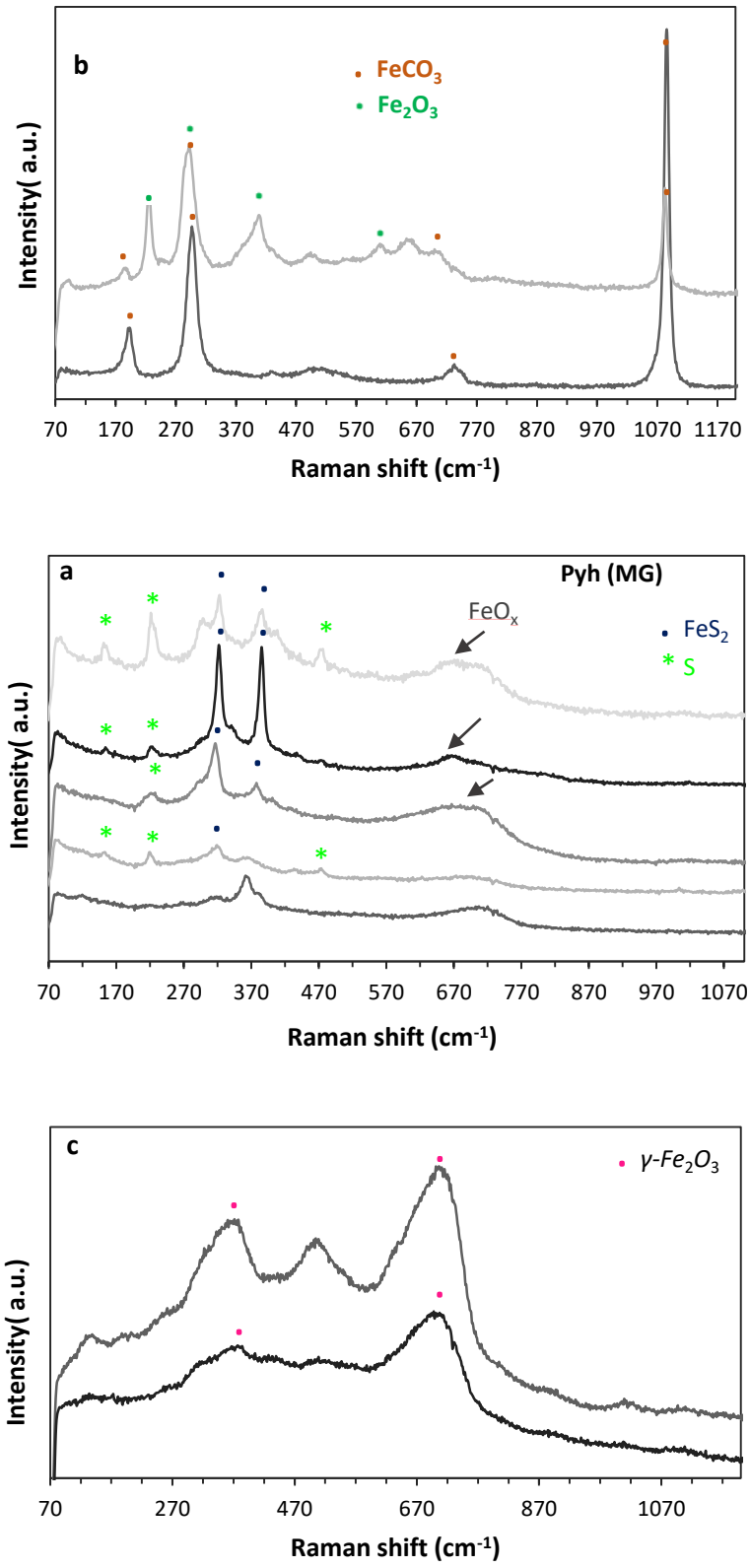

Figure 4-4: Raman spectra of the Pyh sample MG showing marcasite (FeS2) at 334 and 399 cm^{-1}, Fe-oxyhydroxides (670-740 cm^{-1}) and elemental sulfur (153, 220, 477 cm^{-1}) (a) siderite (FeCO3) at 189, 295, 507, 736 and 1088 cm^{-1} and hematite (Fe2O3) at 225, 290, 408, 610 cm^{-1} (b) and maghemite (γ-Fe_2O_3) at 380 and 705 cm^{-1}.

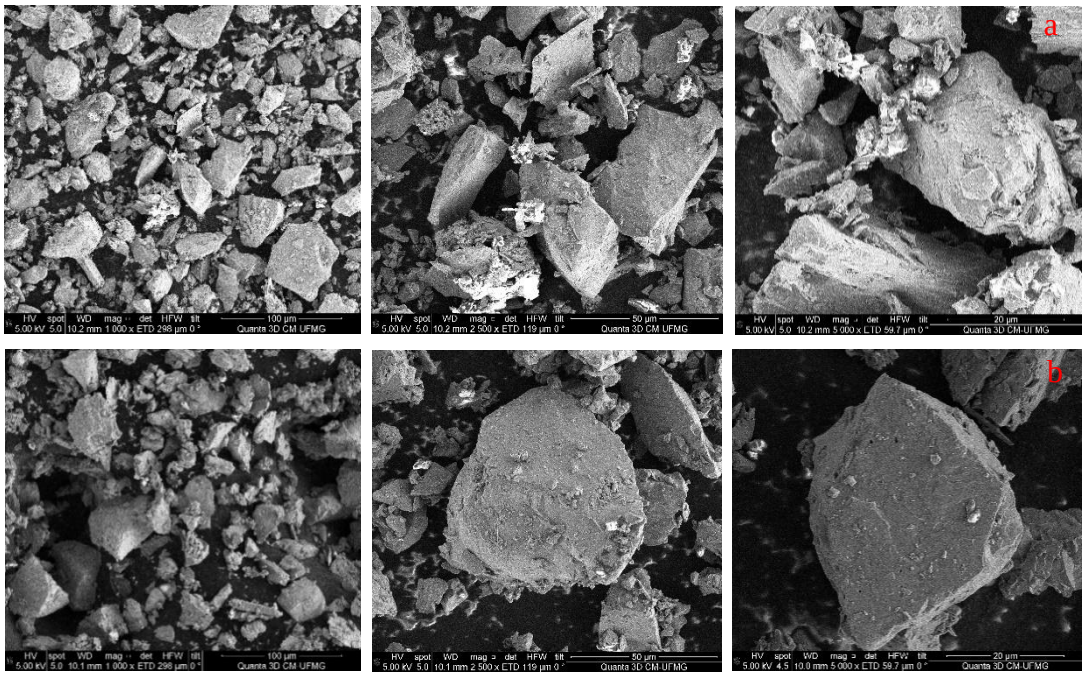

Figure 4-5: Secondary electron images by scanning electron microscopy for the Apy H sample. (A) fresh sample; (B) Fresh sample after oxidation experiments on the flow-through reactor – 24h under oxygen medium. Scale: 100 µm, 50, and 20, respectively.

Particle size features (d_{medium} and d_{50}) and BET specific surface areas are shown in Table 4-2. The particle distribution varied in a range of 2.6 ± 0.1 (d_{10}) to 23.9 ± 0.5 (d_{90}), and from of 0.6 ± 0.0 (d_{10}) to 13.1 ± 0.5 (d_{90}) for the arsenopyrite samples GH and H, respectively. The medium diameters were 13.0 ± 0.2 (sample GH) and 5.3 ± 0.2 (sample H). The larger SSA for the arsenopyrite H sample (0.500 $m^2.g^{-1}$) compared to that of the GH sample (0.411 $m^2.g^{-1}$) is consistent with the smaller particle size of the former. The higher SSA for the pyrrhotite sample MG (1.904 $m^2.g^{-1}$) compared to sample V (0.550 $m^2.g^-1$) is consistent with the presence of fine particles.

Pyrite has the smallest specific surface area, which agrees with Janzen et al. (2000). The authors imply that the specific surface area of pyrrhotite is about 2 to 10 times greater than that of pyrite and state that this is a contributing factor to the higher reactivity of pyrrhotite in relation to the other sulfides. However, in this study, the surface areas of Pyh V and both arsenopyrite samples are very similar.

Table 4-2: Main physical characteristics of the mineral particles.

Mineral	*d*10 (mm)	*d*50 (mm)	*d*90 (mm)	SSA ($m^2 g^{-1}$)
Arsenopyrite (H)	0.6 ± 0.0	3.6 ± 0.1	13.1 ± 0.5	0.500
Arsenopyrite (GH)	2.6 ± 0.1	12.2 ± 0.1	23.9 ± 0.5	0.411
Pyrrhotite (V)	2.6 ± 0.0	17.5± 0.2	32.12 ± 0.4	0.550
Pyrrhotite (MG)	5.6 ± 0.3	22.5 ± 0.4	34.9 ± 0.5	1.904
Pyrite	2.4 ±0.1	9.8 ±0.6	20.1±0.4	0.25

In summary, the arsenopyrite samples studied in this work are highly pure (greater than 97%) with sphalerite and pyrite as the main impurities in the GH sample. No contaminants were identified in the H sample by XRD, only traces (<0.6%) of likely quartz (Si) and sphalerite (Zn) are indicated by chemical analysis.

Pyrite, and carbonates were the main impurities identified in the pyrrhotite samples (Pyh V and Pyh MG). The Pyh MG showed relatively high SSA (1.904 $m^2.g^{-1}$), and surface oxidation products composed of iron oxides and elemental sulfur, which were scarcely seen on the Pyh V sample. Both arsenopyrite samples and pyrrhotite V have particle sizes smaller than 38 µm and specific surface areas in the range of 0.40 - 0.55 $m^2.g^{-1}$.

1.9 Effect of iron oxyhydroxides layer and iron complexing agents on arsenopyrite oxidation at circumneutral medium

1.9.1 Influence of the product layer on arsenopyrite oxidation

The arsenic release is lower when oxidant products were removed with acids (HCl or HNO_3) prior (days) to the experiment. To simulate conditions close to the tailing dams, where particles are previously exposed to the oxygen during ore comminution, processing, and tailings disposal, arsenopyrite (H sample) was previously cleaned with HCl 3mol.L^{-1} and then stored for around six months in a closed box, but not under vacuum. Figure 4-6 exhibits the arsenic release (% wt) from the stored material and freshly washed mineral with 3mol.L^{-1} HCl and 1.8 mol.L^{-1} HNO_3. The difference is a remarkable - 230% - increase in arsenic release. The mean accumulated As release in 24h was 1.20% for the stored material and 0.35 - 0.38% for the fresh mineral cleaned with HCl and HNO_3 respectively, which indicates that the As release is about three times lower when the oxidation products were removed with acids (HCl or HNO_3) prior to the experiment. Parthasarathy (2014) highlights that because arsenopyrite dissolution is oxidative in nature, oxidized species can drive subsequent surface dissolution. The author also emphasizes the importance of correct sample preparation to avoid no reproducibility of the dissolution experiments.

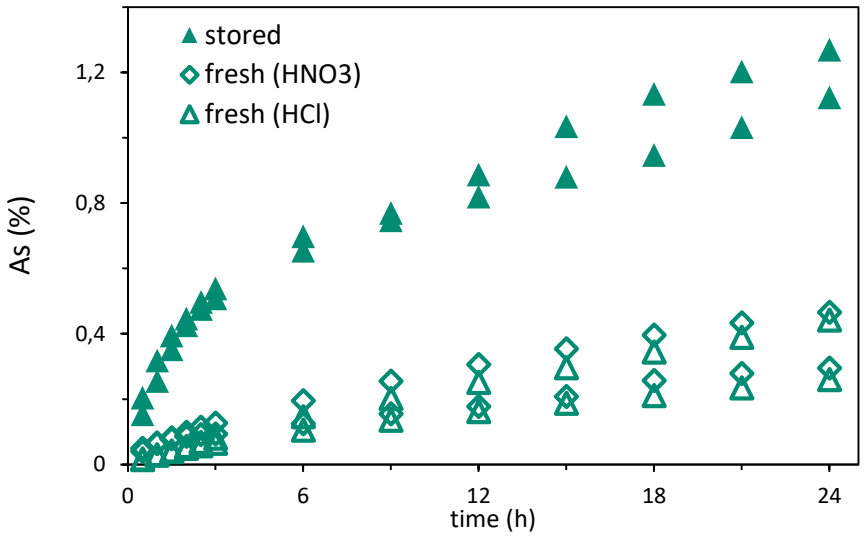

Figure 4-6 : Arsenic (%) released in duplicate experiments from the stored (approximately 6 months) and freshly washed (3mol.L^{-1} HCl or 1.8 mol.L^{-1} HNO_3) arsenopyrite sample (H) under an oxygen atmosphere. Experimental conditions: T=25±2°C, d50 = 13 µm, $pH_{initial}$ = 5.0 ± 0.2 and $pH_{steady\ state}$ = 4.8 ± 0.2.

The removal of the oxidation products before sulfide leaching has been extensively described in the literature (Ciminelli and Osseo-Asare, 1995 (a, b), McGuire et al., 2001), McKibben et al., 2008, Parthasarathy, 2014), but not the effect of the oxide coating on dissolution. Acid washing has been used to remove the oxides and therefore expose the fresh surfaces of sulfide minerals. The procedures to assure no contact with oxygen and then guarantee pristine surfaces may vary from simple to complex. Elsetinow *et al*., (2000) claim that acid-cleaned sulfide mineral surfaces exhibit similar reactivity to a freshly cleaved sample. In contrast, Ciminelli and Osseo-Asare (1995 a,b) observed no effect of acid cleaning on the dissolution of pyrite in alkaline solutions. With regards to the acids applied in this study, no significant difference was noted between experiments conducted using HCl 3mol.L^{-1} (30 min) or HNO_3 1.8 mol.L^{-1} (1 min) for surface cleaning of arsenopyrite (Figure 4-6). It suggests that both acids and concentrations applied are efficient to remove the oxide layer formed during sample preparation.

Figure 4-7 presents the arsenic and iron release % w.t. (a) and rate (b) from the stored and fresh material for experiments run 24h at pH 5 under an oxygen atmosphere. The differences in the rates calculated for both arsenic and iron are noticed (experimental). The steady state was established at 18 hours, which is when no significant variations in dissolution rates are noticed. The calculated steady-state rates for arsenic release were $10^{-9.0}$ and $10^{-9.5}$ mol.m^{-2}.s^{-1} for the stored and fresh minerals, respectively, showing that the arsenic release rate for the fresh sulfide is about three times lower compared to the stored material. The difference in the initial rates is even greater – 16 times, if one considers the slope at time=o of the fitting equation to the curves shown in Figure 4-7(a). For iron, the calculated rates were $10^{-9.4}$ and $10^{-9.8}$ mol.m^{-2}.s^{-1} (stored and fresh material). The higher initial rates can be initially attributed to the dissolution of the oxidized product layer of As and Fe present on the arsenopyrite surface for the stored sample, as shown on the Raman spectrum (Figure 4-8). The fresh sample showed no evidence of oxidation products on the surface.

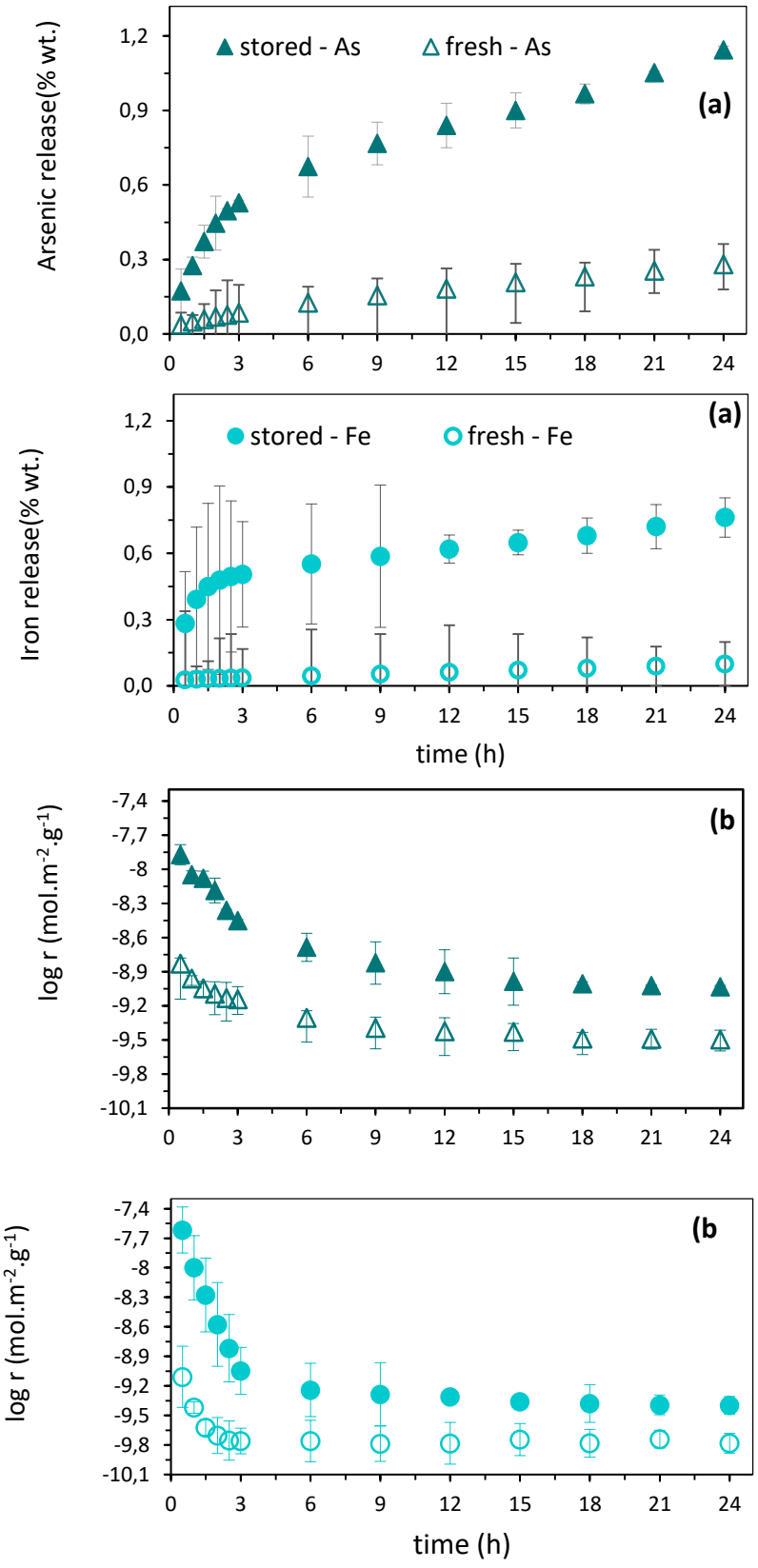

Figure 4-7: (a) Arsenic (%) released from stored (app. 6 months) and washed arsenopyrite sample (H) with 3mol.L^{-1} HCl under an oxygen saturated medium; (b) arsenic and iron release rate from the stored and fresh arsenopyrite (H). Experimental conditions: T=25±2°C, d50 = 13 µm, $pH_{initial}$ = 5.0 ± 0.2 and $pH_{steady\ state}$ = 4.8 ± 0.2.

McKibben et al. (2008) highlight that failure to remove fines, sharp edges, damaged zones, and oxidation products formed on the surfaces can result in anomalous initial dissolution rates in experiments. However, the difference in the calculated rate is unexpected. Under steady-state conditions (after 18 hours experiment run), the effect of product layer dissolution should not be relevant. The higher arsenic released from the stored sample was also verified at $pH_{initial}$ 7 and 11 (Figure 4-9), thus emphasizing the effect of the product layer on arsenopyrite oxidation.

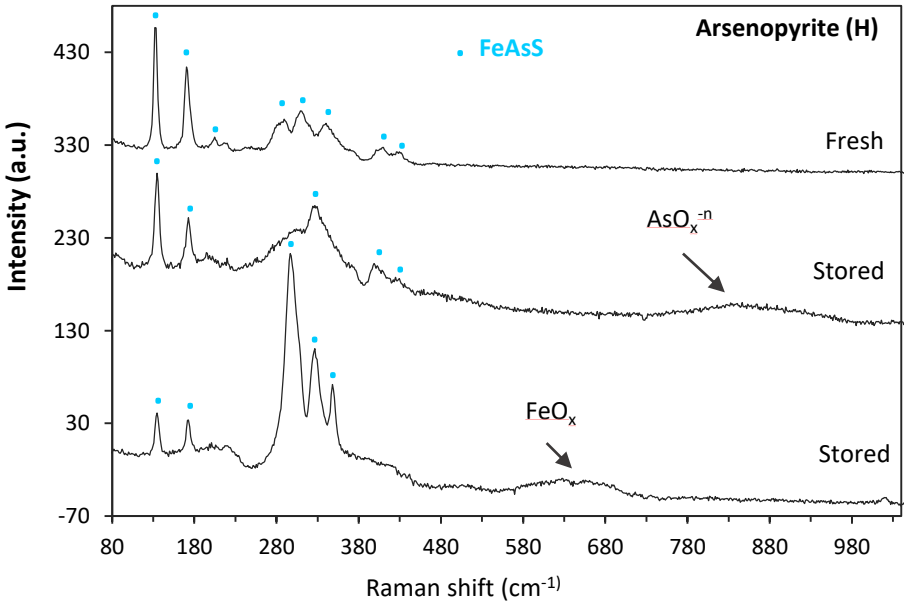

Figure 4-8: Raman spectra for fresh and stored samples of arsenopyrite (H). Arsenopyrite at 135 cm^{-1}, 175 cm^{-1}, 206 cm^{-1}, 290 cm^{-1}, 311 cm^{-1}, 340 cm^{-1}, 411 cm^{-1}, 431 cm^{-1}; Fe-oxyhydroxides at 660-730 cm^{-1}; AsOx-n (arsenate/arsenite) at 800-900 cm^{-1}.

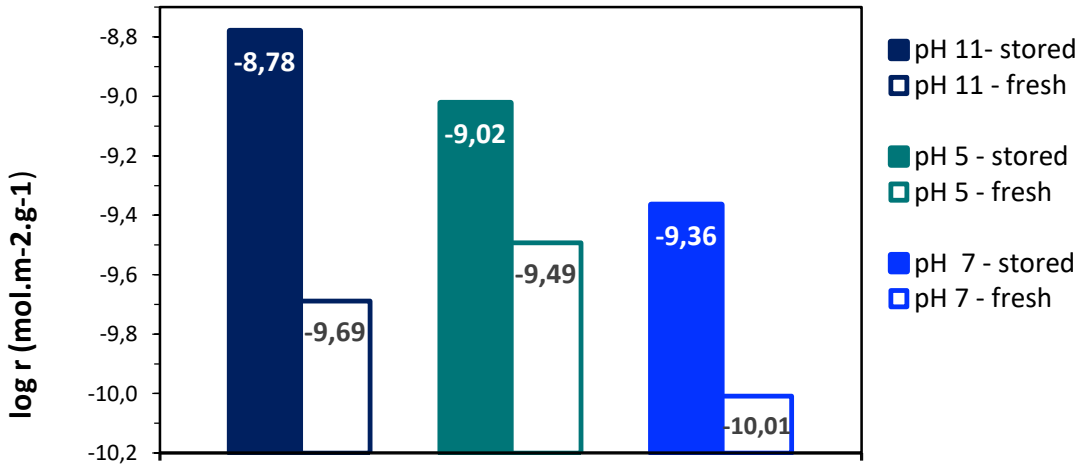

Figure 4-9: Arsenic (%) release from the stored and fresh arsenopyrite (H) washed with HCl 3mol.L^{-1} under oxygen saturated condition. Experimental condition: $pH_{initial}$ = 5.0 ± 0.2, 7 ± 0.2, 11 ± 0.1 and pH $_{steady\text{-}state}$ 4.8 ± 0.2, 5.7 ± 0.3 and 11.0 ± 0.1, respectively ; T = 25 ± 2°C.

To estimate the amount of arsenic released from the stored sample due to the dissolution of the product layer, the acidic solution (HCl 3 mol.L^{-1}) from the washing was analyzed by ICP-OES. The total As dissolved was quantified as 0.34% (Figure 4-10). Thus, since the total arsenic released from the stored sample was quantified as 1.12 % (Figure 4-7 a), the As removed from this sample was estimated to be 0.78%, excluding the arsenic from the oxidized layer. This value is still much higher than the dissolved As from the fresh sample (0.26%) and confirms that the greater dissolution of arsenic from the stored material is not only due to the dissolution of the product layer.

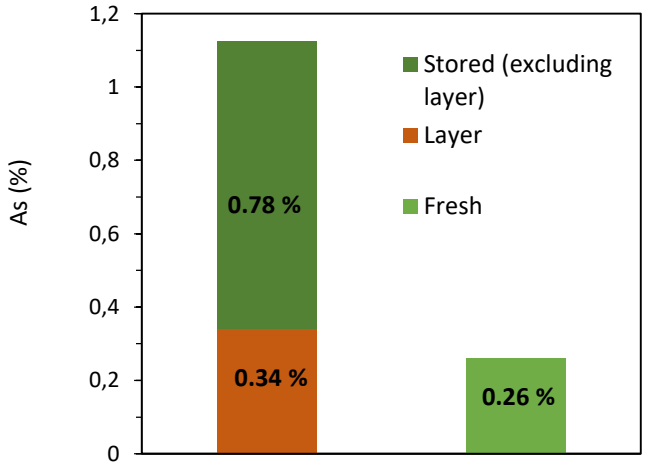

Figure 4-10: Arsenic (%) released from fresh and stored sample under flow-through experiments (O_2 saturated, 24h, pH initial 5.0 ± 0.2, T = 25 ± 2ºC), excluding the arsenic acidly removed (HCl 3 mol.L^{-1}) from the oxide layer present in the stored sample.

It is proposed that the presence of iron arsenates/arsenites and iron oxyhydroxides on the surfaces of the stored sample (seen in the Raman spectrum) act as sources of continuous supply of Fe(III) or Fe(II), the latter oxidized to Fe (III) by oxygen. The soluble iron, even at low concentrations, favors greater oxidation of the sulfide and consequently greater release of arsenic in an aqueous medium. McKibben et al. (2008) and YU et al. (2007) argue that the influence of Fe(III) on arsenopyrite oxidation at pH greater than 2 could not be evaluated due to the precipitation of Fe oxyhydroxide. However, from the study of the oxidative dissolution of arsenopyrite in a circumneutral pH, Neil & Jun (2016) showed that, despite the low solubility of Fe (III) in an alkaline medium, the addition of iron results in higher dissolution of arsenic. The effect of arsenopyrite oxidation by Fe(III) at circumneutral pH will be further investigated in this study.

1.9.2 Effect of complexings iron ligands

Figure 4-11 exhibits the single effect of chloride (1 mmol) on arsenopyrite oxidation for 24h in oxygen-saturated and oxygen-depleted solutions. The pH of the feed solution was 7.0 ± 0.2 and the output solution reached a plateau and remained constant at pH 6.2 ± 0.2.

With regards to As and S release, after 24h in an oxygen saturated, 1mmol Cl^- solution, the release of arsenic and sulfur increased to a maximum of (0.55 ± 0.07) % and (0.47 ± 0.06) % (Figure 4-11a and Figure 4-11c). These values represent an increase of 35% and 36% for As and S, respectively, compared to the system without adding any ligand. The higher As release might be relevant in the long-term disposal of the FeAsS, if chloride is present even in small concentrations. The slight increase in As and S dissolution might be related to the ability of chloride ions to penetrate the surface film and promote the dissolution of arsenopyrite (Zheng *et al.*, 2020). The depletion of oxygen (e.g., disposal under water column) clearly inhibits As and S release, as expected. The initial rate in oxygen-saturated is 3 times greater than in oxygen-depleted solutions.

The accumulated iron release was (0.18 ± 0.02) % and (0.15 ± 0.02)% for experiments containing 1 mmol Cl^- and without any ligand, respectively, (Figure 4-11b) under oxygen medium (filled symbols). The slight increase in iron release is consistent with the low concentrations applied in this study (100 µmol of dissolved Fe (result from ICP-MS analysis and 1mmol Cl^-). As shown in the Eh-pH, for these iron and Cl^- concentrations, $FeCl_2^+$ is stable in the pH range of 0-4 (Figure 4-12a). For conditions close to neutrality, $FeCl_2^+$ becomes stable at chloride concentrations close to $1 mol.L^{-1}$ (Figure 4-12b).

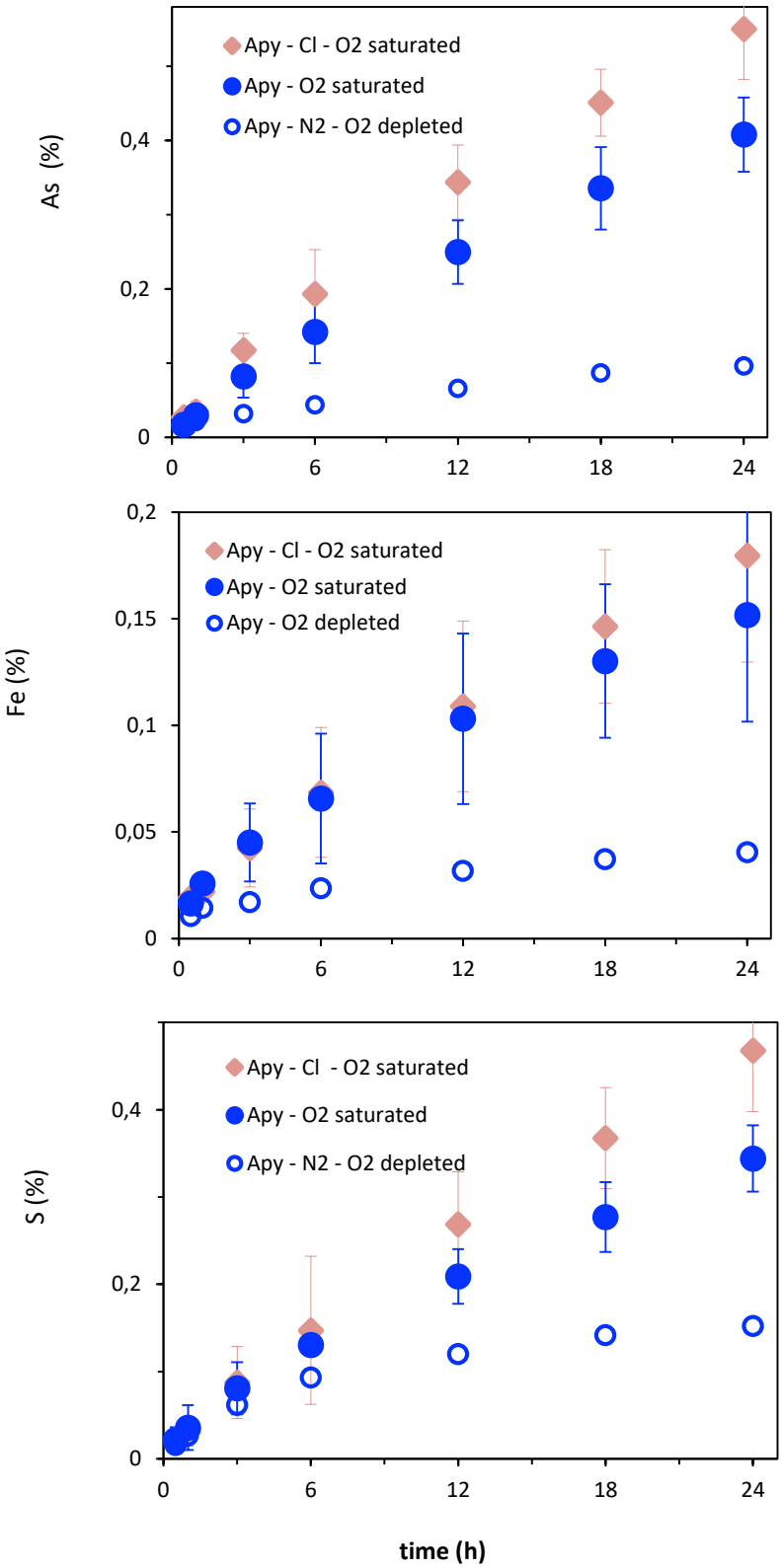

Figure 4-11: Effect of chloride (1mmol) on accumulated iron (a) arsenic (b) sulfur release (c) under oxygen- saturated and oxygen-depleted from FeAsS (sample GH) oxidation as a function of time. Experimental conditions: $pH_{initial}$ 7.0 ± 0.2 and $pH_{steady\ state}$ 6.2 + 0.2 ; temperature 25 ± 2°C; flow rate 1.00 $ml.min^{-1}$ ± 0.05. Calculated rate (As) : $10^{-9,81}$, $10^{-9,28}$ and $10^{-9,16}$ for Apy - N2, Apy - O_2 and Apy-Cl O_2 experiments, respectively.

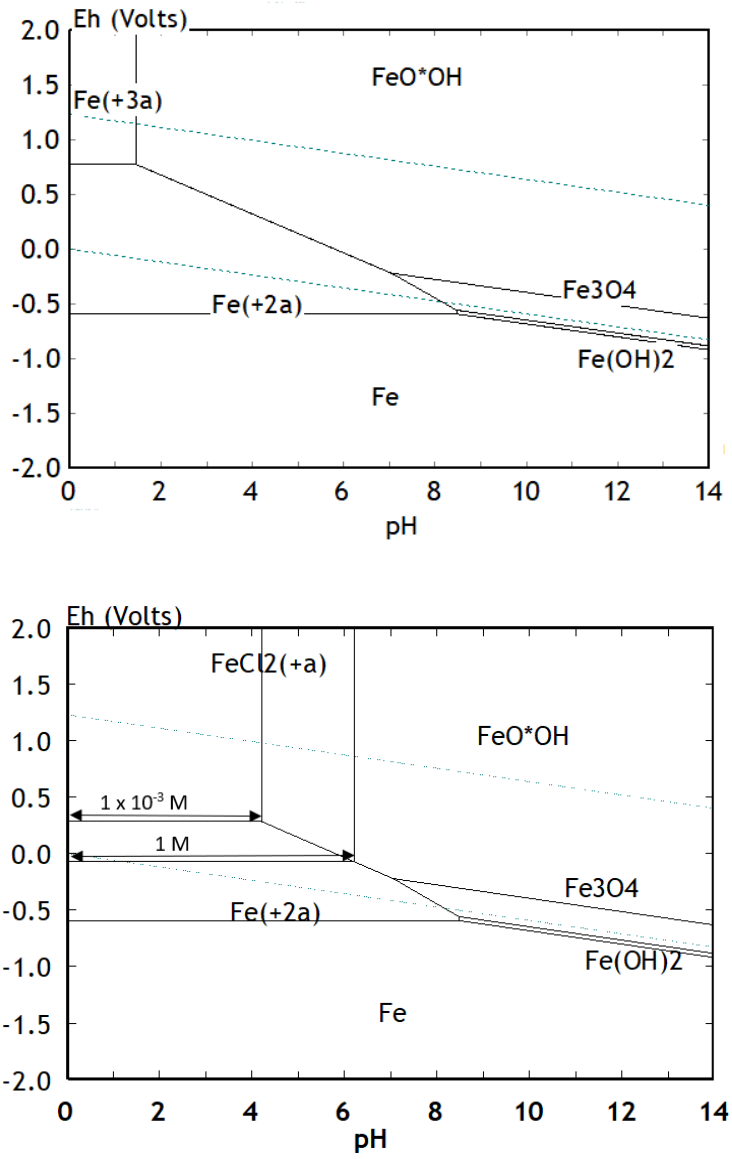

Figure 4-12: Eh-pH diagram at 25 ºC, 1 bar. (a) Fe-H_2O $[Fe]_{(aq)} = 10^{-4}$ M systems (b) Fe-Cl- H_2O systems $[Fe]_{(aq)} = 1 \times 10^{-4}$ mol.L^{-1} ; $[Cl]_{(aq)} = 1 \times 10^{-3}$ and 1 mol.L^{-1} ideal solutions. Eh (V). HSCv7.0.

To magnify iron dissolution and, in turn, its effect on arsenopyrite oxidation, the addition of citrate was also investigated. As shown in Figure 4-13, citrate showed a remarkable effect on arsenopyrite oxidation for the experiments conducted under an oxygen atmosphere (filled symbols). The accumulated arsenic (Figure 4-13b) and sulfur (Figure 4-13c) progressed from (0.40 ± 0.05) % to (1.56 ±0.08) % and from (0.34 ± 0.04) % to (1.42 ±0.07) %, respectively. Both changes imply an increase in arsenopyrite oxidation greater than 280%. Iron complexation is clearly indicated by the increase in the soluble iron (1.13 ± 0.07%) in the citrate system – more than seven times higher compared to the system without any ligand. It is also important to highlight that citrate acts as a buffer in the solution, so the pH of the outlet solution was maintained throughout the experiments (24h) with an average of 7.0 ± 0.2.

Calculated rates under steady-state for the release of As are $10^{-8.60}$, $10^{-9,28}$ and $10^{-9,81}$ $mol.m^{-2}.g^{-1}$ for the Apy-Cit O_2, Apy - O_2 and Apy - N_2 experiments, respectively. In oxygen-saturated solutions, the presence of citrate makes the rate of arsenic release (steady-state) 4.7 times greater than in the ligand's absence. But the effect is negligible in the absence of oxygen (i.e., 5 times smaller considering the initial rates), according to the mechanism discussed below (Eq. (6)).

Citrate is a polycarboxylate molecule with more than one carboxylate functional group and can react with Fe(III) to form strong complexes (Zhang & Zhou, 2019). Mikutta *et al*. (2010) claims that the presence of citrate retards the production of Fe(III) hydroxide from ferric ion hydrolysis. Thus, the increase in As and S release is assumed to be a result of Fe (III)-citrate complexation, which in turn increases soluble ferric ion concentration - a strong oxidant - in the system. Peiffer & Stubert (1999) also determined the acceleration of pyrite oxidation in the presence of citrate. The authors of the present study are not aware of any previous investigation on the effect of citrate on arsenopyrite oxidation.

The complexation of ferric iron and citrate can occur through direct reaction between Fe^{3+} + Cit^{3-} or by the oxidation of Fe(II)-$citrate^{-}$. At pH 7.0, Zhang *et al*. (2017) observed a large increase on soluble Fe (II) when the citrate concentration increased from 0 mM to 5 mM. The authors explain that adsorbed Fe(II) on the mineral surface ($Fe(II)_{ad}$), produced from pyrite oxidation, complexes with citrate ligand to form Fe(II)-$citrate^{-}$ (eq. 5).

The percentage of free $Fe(II)_{ad}$ is oxidized to Fe^{3+} and rapidly precipitates as Fe(III) oxyhydroxides . Therefore, the complexation of soluble Fe^{2+} by citrate, rather than Fe^{3+}, primarily affects Fe(III)-citrate production, as Fe(III)-citrate is mainly produced from the oxidation of Fe(II)-$citrate^{-}$ (eq. 6) while the direct complexation (Eq. 7) has a minor role (Zhang, *et al*., 2017).

$$Fe(II)_{ad} + citrate \leftrightarrow Fe\ (II)\text{-}citrate^{-} \quad (5)$$

$$Fe(II)\text{-}Cit^{-} + O2 \leftrightarrow Fe(III)cit + {}^{\cdot}O2^{-} \quad (6)$$

$$Fe^{3+} + Cit^{3-} \leftrightarrow Fe(III)cit \quad (7)$$

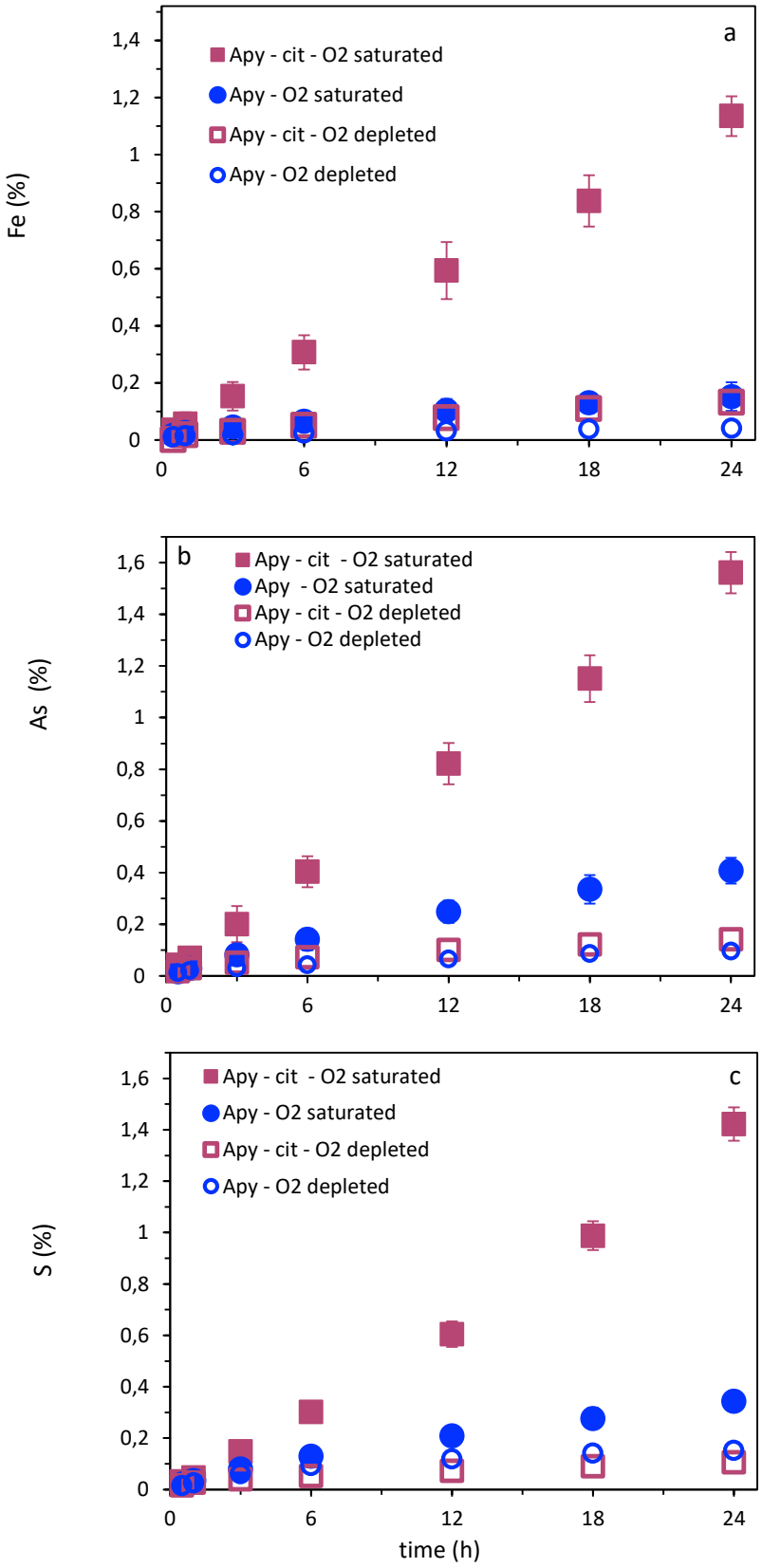

Figure 4-13: Effect of citrate (1mmol) on accumulated iron (a) arsenic (b) sulfur release (c) under oxygen-saturated and oxygen-depleted from FeAsS (sample GH) oxidation as a function of time.Experimental conditions: $pH_{initial}$ 7.0 ± 0.2, $pH_{steady\ state}$ 6.2 + 0.2 (experiments without citrate) and $pH_{steady\ state}$ 7.0 + 0.2 (citrate experiments); temperature 25 ± 2ºC; flow rate 1.00 ml.min^{-1} ± 0.05.

Although Zhang et al. (2017) conducted an extensive study of the complexation of citrate ions with Fe(II) and Fe(III) in an alkaline medium, the authors did not explore the thermodynamically formed species. Figure 4-14 shows the Fe(II)-cit species distribution diagram as a function of pH for 1mmol citrate concentration. Under these conditions, the same ones used in this study, the predominant species in the pH 6-8 range is $FeCit^-$, with a small contribution of the $FeCit_2^{4-}$ species. Hydroxides are formed only at pH>10 and the concentration of Fe^{2+} is negligible over the entire pH range. The studies by Pam and Waite (2017) also determined a predominance of $FeCit^-$ and $FeCit_2^{4-}$ species for concentrations of 5mM citrate and $[Fe]_t$ = 5µM.

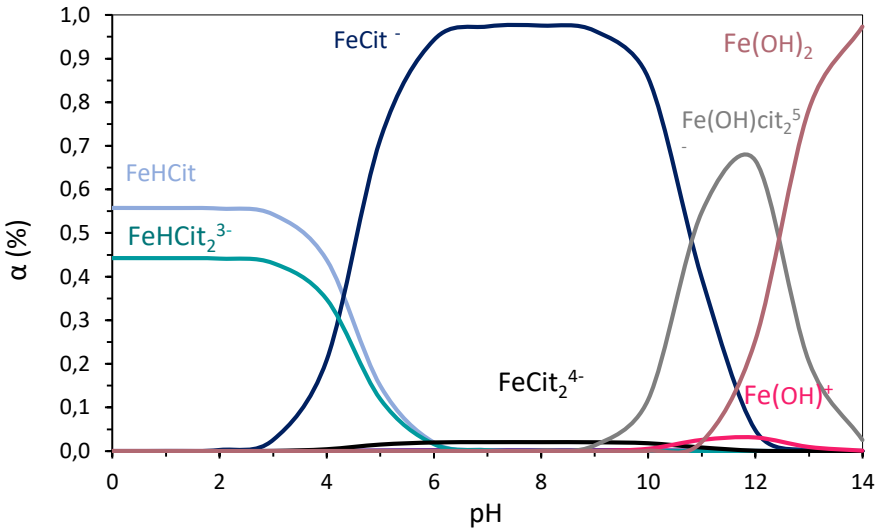

Figure 4-14: Distribution diagram Fe(II) - cit species as a function of pH for 1 x10^{-3} mol.L^{-1} citrate concentration. Thermodynamic data extracted from Pam and Waite, 2017. Species considered: Fe^{2+}, **$Fe(OH)^+$, $Fe(OH)_2$, FeHCit, $FeCit^-$, $FeHCit_2^{3-}$, $FeCit_2^{4-}$, $Fe(OH)cit_2^{5-}$.**

The species formed in the Fe(III) – citrate system are unclear. Ito et al. (2011) state that the literature diverges about citrate protonation. For example: in the stability calculations of the equilibrium constants in the Fe(III)-citrate system, the models by Konigsberger et al. (2000) and Ribas et al. (1989) consider citrate as triprotonated ligand and, while Silva et al. (2009) assume citrate as a tetraprotonated ligand. Chen, 2011 also emphasizes discrepancies in the literature regarding dominant aqueous species at different pH's in the Fe(III)-cit system. However, considering citrate a triprotonated ligand, the authors indicate that the main Fe(III)-cit species are: Fecit, $FeHcit^+$, $FeOHcit^-$, and $Fe_2(OH)_2(cit)_2^{2-}$.

Using data stability from Medusa software, studies by Chen et al. (2011) suggest $FeOHcit^-$ as the main specie, followed by $Fe2(OH)_2(cit)_2^{2-}$ in the pH range 6-8 ([Fe(III)] /[cit] = 10/150

ratio). The data values were not exposed by the authors. Considering de Konigsberger et al. (2000) equilibrium model, Ito et al., 2011 also determined $FeOHcit^-$ as the main specie at circumneutral medium ([Fe]t = 1µM and [Cit]t = 0.5 mM). However, considering Ribas et al. (1989) data, $Fe(OH)_2Cit_2^{5-}$ was calculated as the main stable species for the same concentrations of iron and citrate.

As carbonate in the article by Caldeira et al. (2010), citrate plays a key role in the Fe(II)-$citrate^-$/Fe(III)- citrate redox couple in neutral environments (Zhang *et al*., 2017), but only in the presence of oxygen. Under oxygen-depleted (unfilled symbols) conditions, the percentage of the release of As, Fe and S scarcely changes when comparing the system without ligand, suggesting a negligible influence of citrate in the absence of oxygen. This finding is aligned with the Moses & Herman (1991) hypotheses that Fe (III) is an effective oxidizer of pyrite at circumneutral pH. However, the reaction cannot be sustained in the absence of dissolved oxygen, since the oxidation of the mineral depends on the continuous oxidation of Fe (II) to Fe (III).

1.10 Arsenopyrite oxidation

1.10.1 Effect of pH and dissolved oxygen

The lower reactivity of arsenopyrite (GH) at circumneutral pH is shown by the arsenic release rate at 25 °C under different pH conditions (4, 5, 7, 8, and 9) in an oxygen-saturated medium (Figure 4-15). The greatest reactivity of the sulfide occurs under acidic conditions (1.33 x 10^{-9} and 1.07 x 10^{-9} ± 0.06 mol.m^{-2}.s^{-1}, at pH 4 and 5, respectively) and the lowest at pH 7. At this pH, the calculated rate was 3.54 x 10^{-10} ± 0.03 mol m^{-2}.s^{-1} (4 replicates), which is about two-fold lower than the As release rate at pH 8 (6.93 x 10^{-10} ± 0.06 mol.m^{-2}.s^{-1}). This finding is similar to that reported by Yu et al. (2007), and Ferreira et al. (2021) (Figure 4-16), as both determined log (r) in the range of -(9.3 to 9.4) (mol.m^{-2}.s^{-1}), under oxygen saturated condition at pH close to 7.

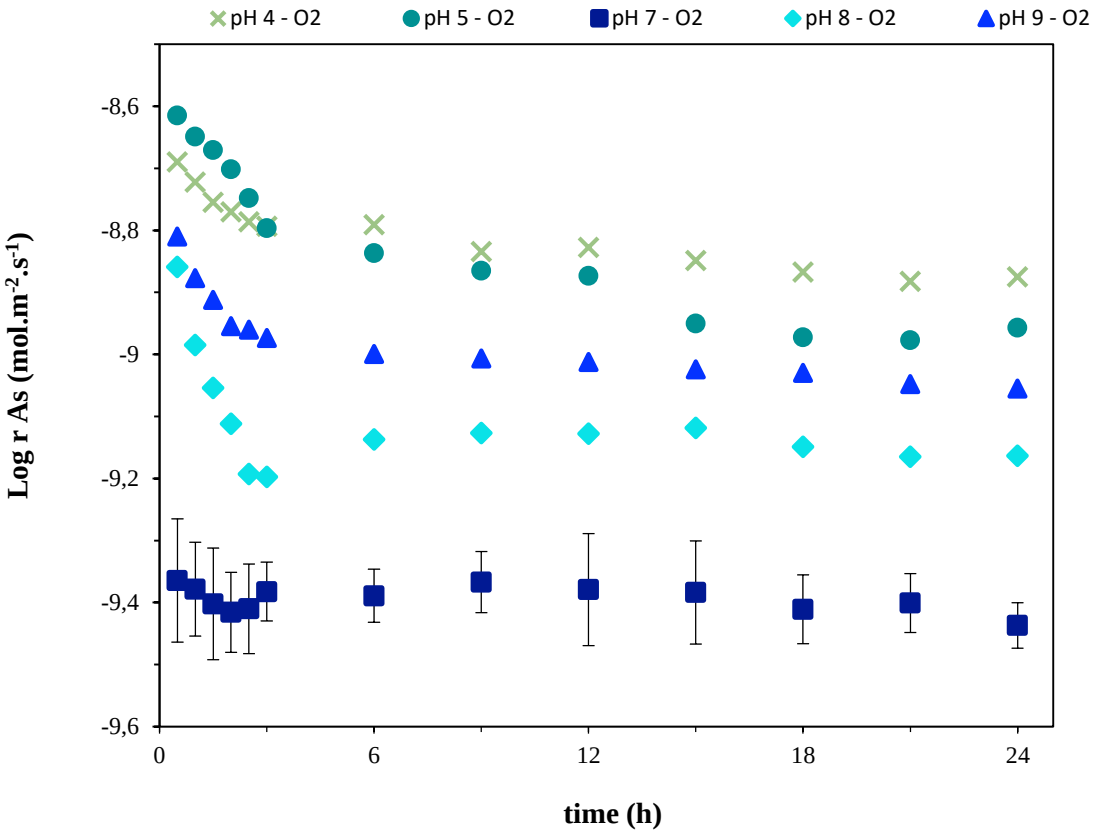

Figure 4-15: Effect of pH on the arsenic release rate from arsenopyrite fresh surface in an oxygen-saturated medium at 25°C ± 2 for pH $_{initial}$ = 4.0 ± 0.1, 5.0 ± 0.2, 7.0 ± 0.4, 8.0 ± 0.3 and 9.0 ± 0.1. pH $_{steady\ state}$ = 4.1 ± 0.2; 4.8 ± 0.2; 6.2 ± 0.4, 7.5 ± 0.2 and 8.1 ± 0.2, respectively. flow rate 1.00 ml.min^{-1} ± 0.05.

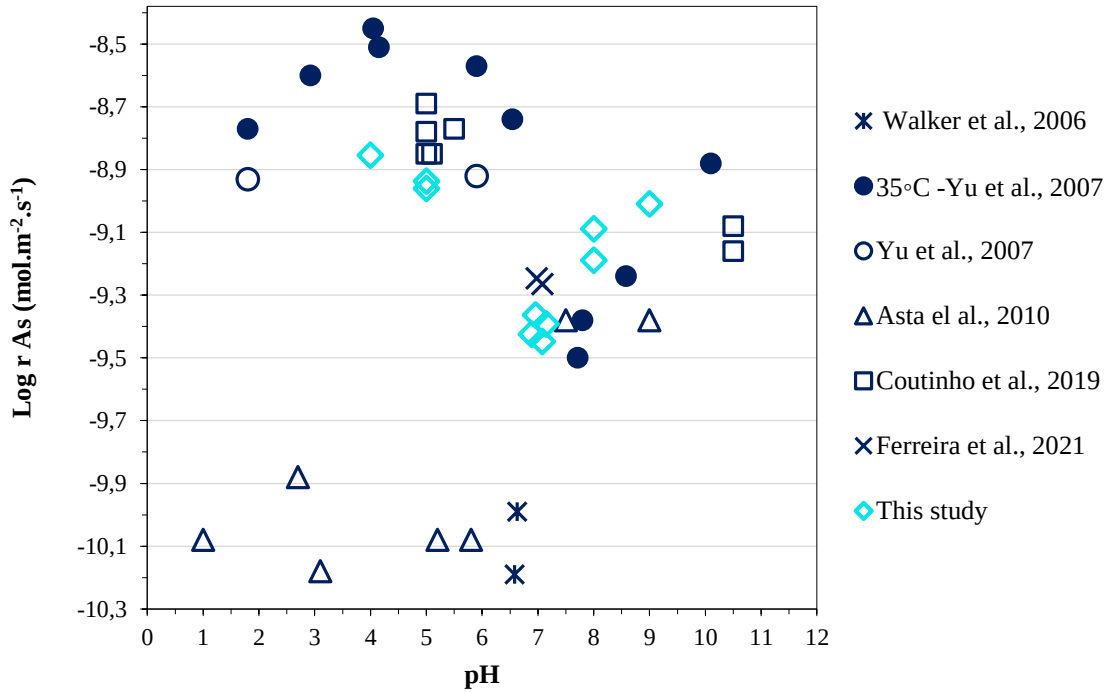

Figure 4-16: Oxidative dissolution rates of arsenopyrite vs $pH_{initial}$ obtained from this and previous studies; O_2 concentration between 6-9mg.L^{-1}; 25ºC, except when indicated. (Adapted from Asta et al., 2010 and Coutinho et al, 2019).

The lower reactivity at neutral pH is also in agreement with the arsenopyrite oxidation characteristics reported by Yu et al. (2007) and Craw et al. (2003). Both authors observed significant dissolution at pH <7 and pH >10 and the occurrence of a minimum oxidation rate at pH 7-8. Yu et al. (2007) suggest that this behavior may be the result of the switch in the main oxidant species, from dissolved Fe(III), at lower pH, to O_2, at higher pH. Another hypothesis presented by the author considers Fe(III) as the initial oxidant in the entire pH range. Thus, the minimum oxidation at neutral pH is a result of the lower solubility of iron oxyhydroxides, with concomitant sorption of As in the product layer, formed in a more alkaline medium.

By studying the dissolution of two different arsenopyrite rich samples (> 80%), Coutinho et al. (2019) also did not observe significant differences in the oxidation rates for experiments at pH 5 and 7 but determined a small decrease in the oxidation rate of arsenopyrite for experiments performed at pH 11. Under neutrality conditions (pH =7), an initial and sudden drop in pH occurs to approximately 4.5 and the $pH_{steady\ state}$ is established around 5.5, which is very close to experiments conducted with $pH_{initial}$ = 5.0. Under the latter condition, the pH is more stable ($pH_{steady\text{-}state}$ = 4.8). For the $pH_{initial}$ 11.0, Coutinho et al. (2019) also determined a

small decrease in the oxidation rate of arsenopyrite compared to the experiments at $pH_{initial}$ 5.0 and 7.0.

In opposition to the trends discussed above, Asta et al. (2010) determined similar reaction rates values in a pH range from 1 to 6, with an average rate equal to 10-10.1 ± 0.2 $mol.m^{-2}.s^{-1}$. The lower values determined by the authors (Figure 4-16) may be related to the long time established as steady state (hundreds of hours). Asta et al. (2010) suggest that the effect of the hydrogen ion concentration on the dissolution rate of arsenopyrite at acid pH is unsignificant.

Despite the lack of consensus in the literature on the effect of hydrogen ions on arsenopyrite oxidation, the rate values determined in the cited works and at the present study confirm the slow kinetics of the arsenopyrite dissolution.

Figure 4-17 shows de positive effect of oxygen on arsenic release from arsenopyrite oxidation under four $pH_{initial}$ ranges (5, 7, 8, and 9) at 25ºC. The study of the effect of oxygen on the sulfides oxidation is of great importance in the context of the tailings dam disposal as it is a dynamic environment exposing the particles to the air. Figure 4-17 also shows the As dissolution rate from the same experiments results as Fig 4a, but exhibits the calculated rates after reaching steady state condition. The positive effect of dissolved oxygen on the arsenic release is remarkable in all pH ranges. At $pH_{initial}$ 7, the mean calculated rate was 3.54 x 10^{-10} ± 0.03 mol $m^{-2}.s^{-1}$, and 7.93 x 10^{-11} ± 0.08 mol $m^{-2}.s^{-1}$ under oxygen-saturated and oxygen-depleted, respectively, which represents a decrease of about 350% in the As release rate.

The rate difference at $pH_{initial}$ 4 was even higher, being about 65-fold lower for the experiments conducted on oxygen deficiency (1.33x 10^{-9} under O_2 saturated versus 2.03 x10^{-11} in O_2 depleted condition). While the sulfide showed lower reactivity at pH 7 under an oxygen atmosphere, in the system conducted with O_2 depletion, the rates from pH 4 to 9 did not show significant differences albeit there is still a tending with lower reactivity at a neutral medium.

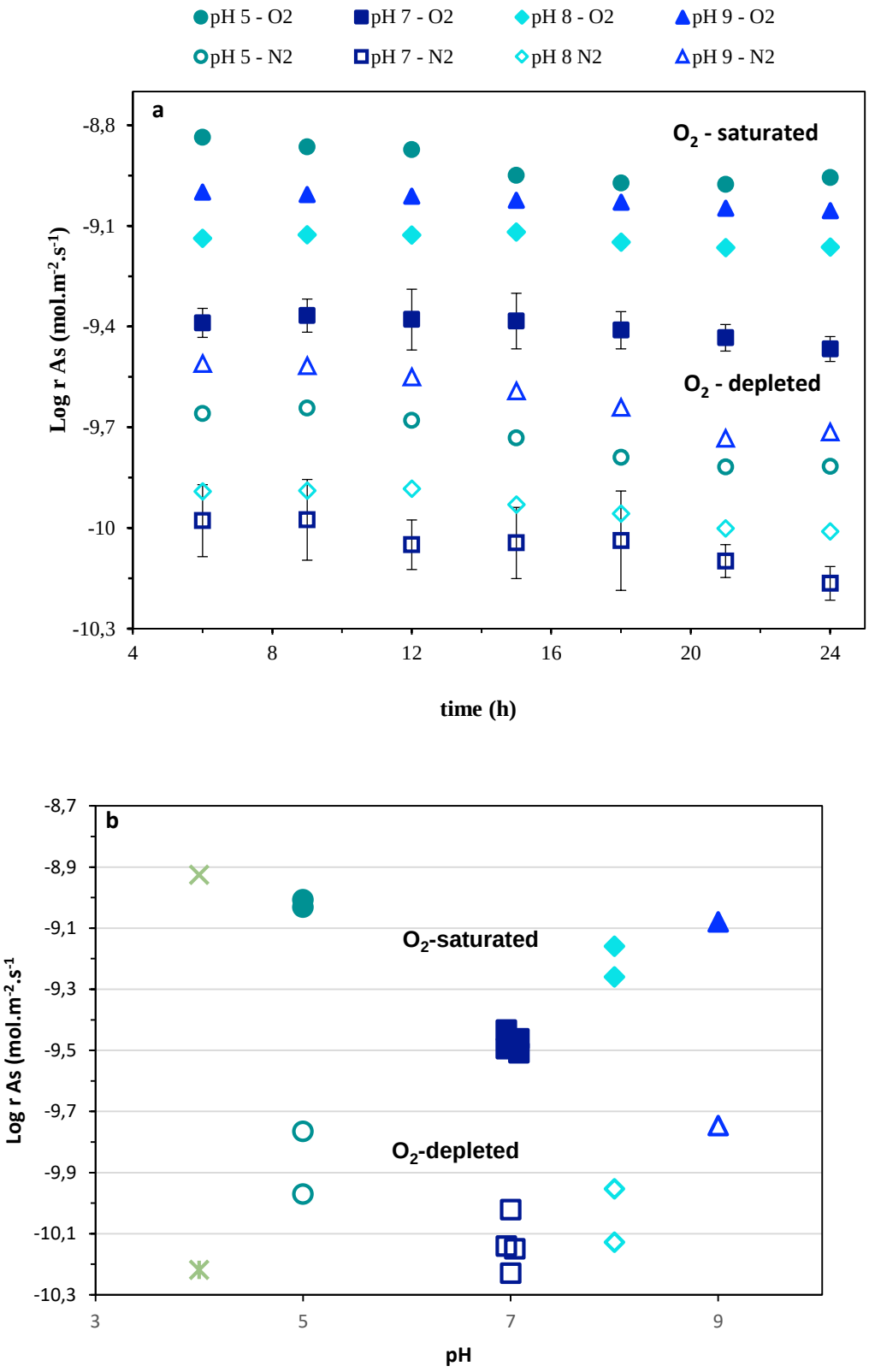

Figure 4-17: Arsenic dissolution rate from arsenopyrite under oxygen-saturated and oxygen-depleted at pH 5, pH 7, pH 8 and pH 9 as a function of time (b) Arsenic dissolution rate as a function of pH (range 4-9) after reaching the steady state (18h). T=25±2°C; Sample GH. The effect of oxygen is observed in all pH ranges.

The dependence the oxidation rates of arsenopyrite on the dissolved oxygen in acid pH was demonstrated by Yu et al. (2007), Asta et al. (2010), and McKibben et al. (2008) in the following pH ranges: 1.8 - 5.9; 1- 4 and 2.0 - 4.5, respectively. However, the reaction order to oxygen concentration determined by the authors was quite different: YU et al. (2007) found $mO_2 = 0.45$, which is inferior to that calculated by Asta et al. (2010) ($mO_2 = 0.76$) and higher than those of McKibben et al. (2008) ($mO_2 = 0.33$). In contrast with these studies, Walker et al. (2006) reported no oxygen dependence on the oxidation rate in the pH range from 6.3 to 6.7. Likewise, ranging from 100% N_2 to 100% O_2, Ferreira et al. (2021) reported an insignificant effect of oxygen at pH 7. In their work, the release of arsenic from FeAsS underwent a slight increase of about 1%.

1.10.2 Effect of pyrrhotite and arsenopyrite association

Figure 4-18 compares the release of Fe and S from the two pyrrhotite samples studied in this work (Virginia, US (V) and Minas Gerais, Brazil (MG)). The sulfur release (Figure 4-18) from the Pyh MG is 4.5 times higher than that from Pyh V. This difference is even larger that the difference (3.5x) in the samples' specific surface areas (Table 4-2), which was ascribed to the presence of iron and sulfur oxidation products identified in the Raman spectroscopy (section 4.1). The difference in the cumulative release of Fe and S (%) was, respectively, about ninety times and five times higher for the Pyh MG sample.

However, despite the remarkable difference in % sulfur release, the oxidation rates (Figure 4-18 b) at longer times of the two samples are similar ($10^{-9.41}$ vs $10^{-9.50}$ mol.m^{-2}.g^{-1} for Pyh MG and Pyh V, respectively – about 20% difference). This result is an indication that the surface layer of Fe and sulfur oxidized products identified on Pyh MG does not influence the oxidation of pyrrhotite, contrary to what occurs in the arsenopyrite sample (sample GH). The S release rates obtained in this study are close to those reported in the literature (about 10^{-10} mol.m^{-2}.g^{-1}) (Table 2-5). In terms of iron, the MG pyrrhotite sample showed a higher rate compared to the other pyrrhotite ($10^{-10.72}$ vs $10^{-11.38}$ (mol.m^{-2}.g^{-1}), respectively. For the Fe release, the rate values in the present work (approximately 10^{-11}) are substantially lower than those reported in the literature (range of 10^{-8} – 10^{-9} mol.m^{-2}.g^{-1}) (Table 2-5). The reasons for this difference are still unclear and need to be further investigated. Furthermore, Janzen et al. (2000), Mikhlin et al. (2000), and Mikhlin et al. (2002) suggest a preferential release of iron relative to sulfur in the oxidation or dissolution of pyrrhotite, however, in this study the opposite occurred (the release of sulfur was greater than that of iron) for all tests carried out with pyrrhotite.

With regards to the arsenopyrite-pyrrhotite association experiments, under oxygen-depleted condition, the As and S released raised from 0.12 to 0.15% and 0.15 to 0.18% (Figure 4-19), respectively when the sulfides were mixed at 1:1 proportion. This corresponds to a slight increase of 20% for As and S release. Because arsenopyrite has a higher rest potential – as discussed in the introduction – the greater release of arsenic due to the formation of galvanic couple is unexpected.

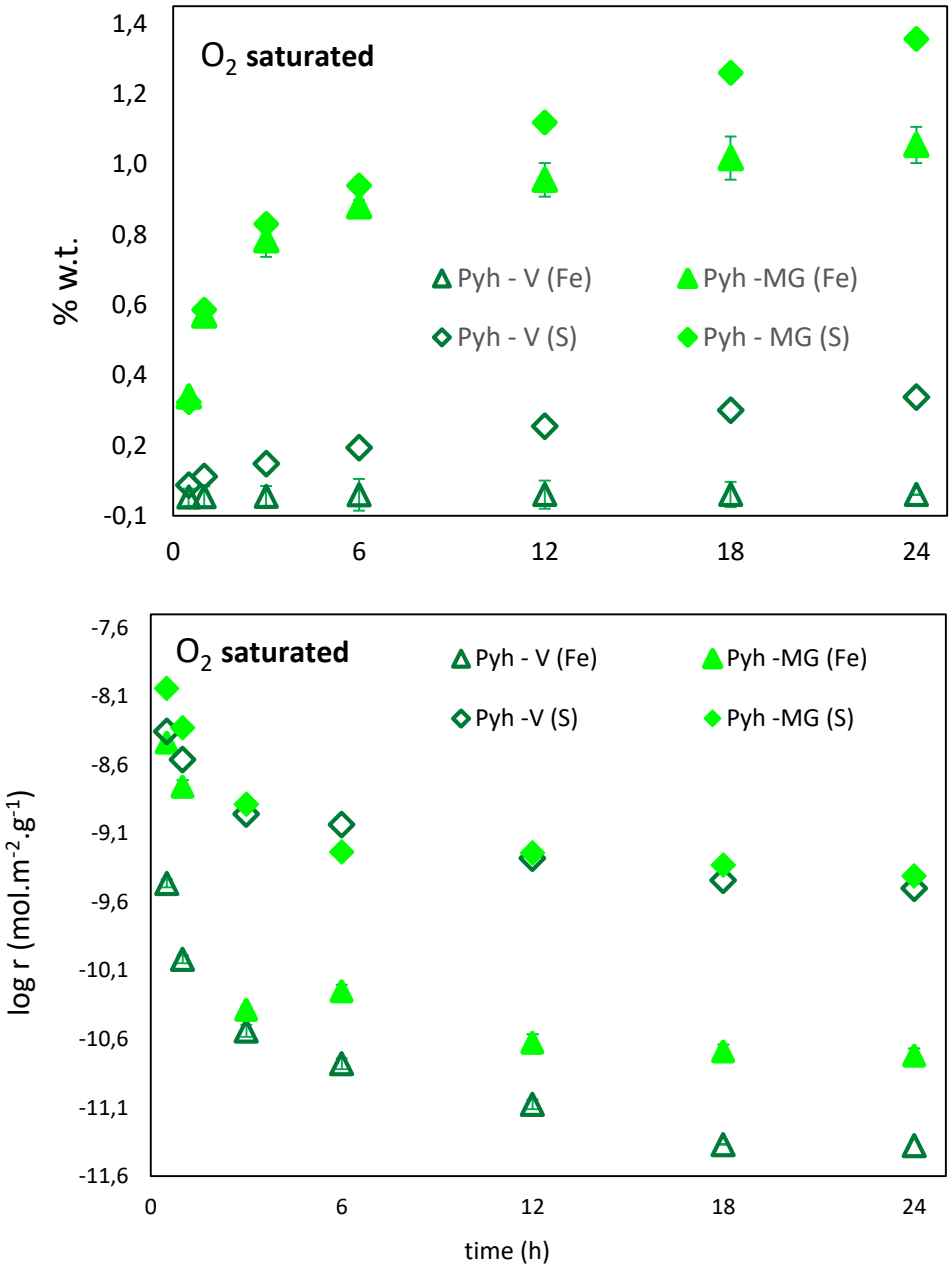

Figure 4-18: Iron and Sulfur released from two pyrrhotite samples (V and MG) under oxygen- saturated condition. (a) % w.t. (b) log rate (mol.m^{-2}.g^{-1}). Conditions: pH$_{initial}$ = 7.0 ±0.2 ; pH$_{steady-state}$ 6.5 (Pyh V experiments); pH$_{final}$ 5.2 ± 0.3 (Pyh MG experiments); flow rate = 1.00 ± 0.05 ml.min^{-1}.

The higher release of the toxic element was verified by Ferreira et al. (2021) at circumneutral pH when pyrite and arsenopyrite were associated. The authors showed that 5% wt. of FeS_2 within the reactor is enough to increase As released in 24 h around 75% under oxygen-saturated conditions. In those studies, the galvanic effect also occurred under oxygen-depleted conditions. Majuste et al. (2012) claim that a more pronounced galvanic effect occurs under the less oxidizing condition on the pyrite/chalcopyrite association. According to what was

highlighted in the introduction, there is no register of past studies on the oxidation kinetics for the galvanic association between arsenopyrite and pyrrhotite. Regarding the individual oxidation of pyrrhotite, the Pyh V sample released twice as much sulfur under oxygen saturated conditions (Figure 4-19b) compared to the release in the absence of oxygen (Figure 4-18 a), showing a positive effect of oxygen on pyrrhotite oxidation.

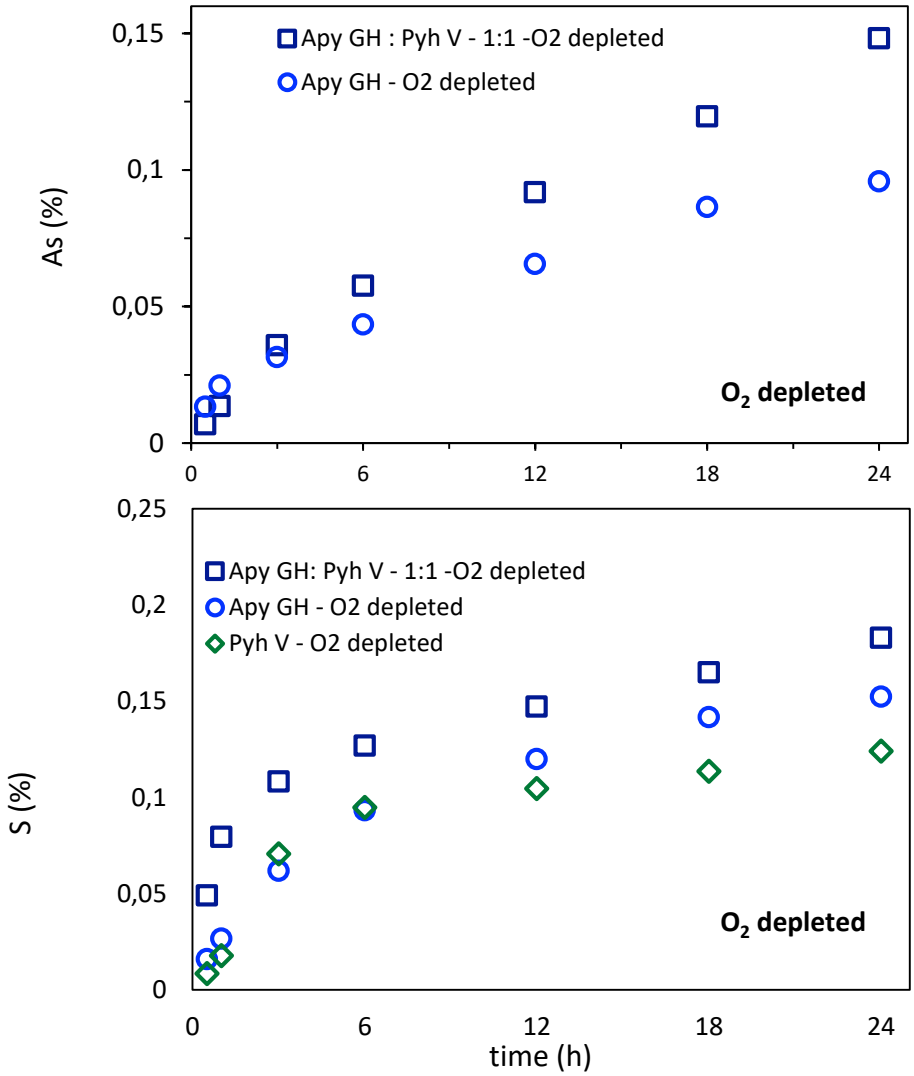

Figure 4-19: Effect of pyrrhotite coupling (50% w.t.) on the accumulated arsenic (a) and sulfur (b) release from FeAsS (sample GH) oxidation as a function of time. Duplicate experiments. Experimental conditions: oxygen depleted medium; T = 25 ± 2ºC; pH $_{initial}$ 7.0 ± 0.2; pH $_{final}$ 6.6 ± 0.2; flow rate = 0.93 - 1.04 ml.min^{-1}.

Under oxygen-saturated condition, the effect of pyrrhotite coupling on the accumulated As released from FeAsS (i.e., soluble As) at pH 7 were studied for both pyrrhotite samples (Figure 4-20). Also, two distinct proportions were investigated for the sample Pyh - V: i) Apy GH : Pyh V - 1:1; i.e., 50% of each sample; ii) Apy GH : Pyh V - 1:3; i.e., 25% arsenopyrite and 75% pyrrhotite. For Pyh MG – only 1:1 proportion was analysed.

Firstly, it is perceived that for Pyh V the association between the minerals provokes, again, a higher release of arsenic (Figure 4-20). For Apy GH :Pyh V- 1:1 experiment with oxygen, the mean accumulated As released reached (0.56 ± 0.07) % when the galvanic interaction was established. This corresponds to increases of around 37%, regarding the mean values determined for arsenopyrite oxidation without sulfides association. Although in lower intensity, the greater arsenic release was also determined for the Apy:Pyh - 1:3 test in the presence of oxygen – As dissolution reached (0.51 ± 0.05) % – , corresponding to an increase of 25 %.

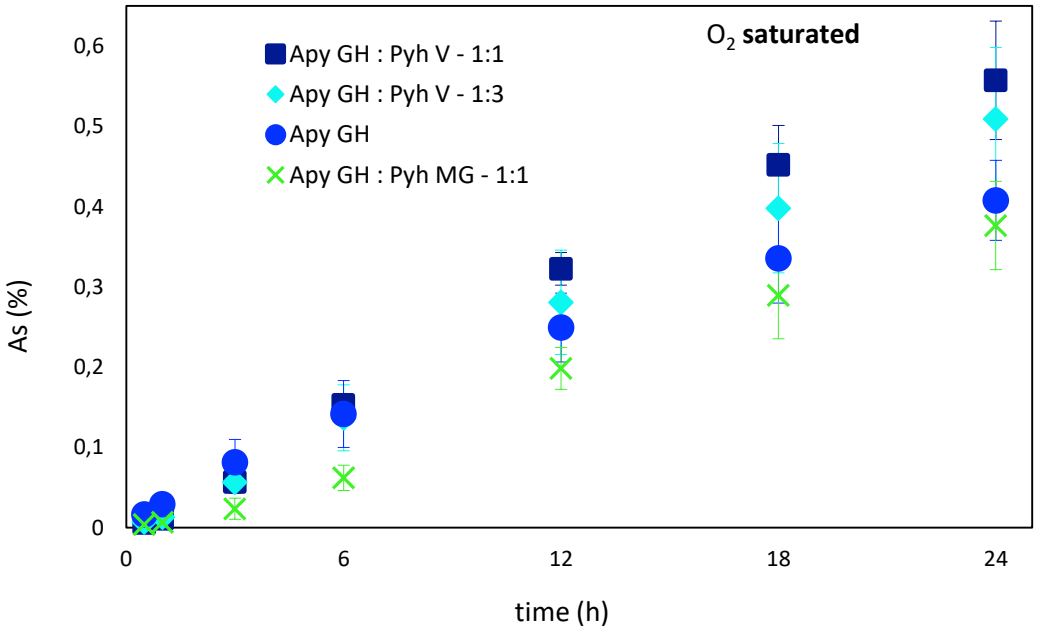

Figure 4-20: Effect of Pyh V sample coupling (50% w.t. and 75% w.t.) and Pyh MG sample coupling coupling (50% w.t.) on the accumulated arsenic release from FeAsS (GH) oxidation as a function of time. Experimental conditions: oxygen saturated medium; T = 25 ± 2ºC; pH $_{initial}$ 7.0 ± 0.2; pH $_{final}$ 6.5 (Apy GH; Apy GH: Pyh V experiments); pH$_{final}$ 5.2 ± 0.3 (Apy GH: Pyh MG) ; flow rate = 1.00 ± 0.05 ml.min^{-1}.

However, for the sample Pyh MG, the association between pyrrhotite and arsenopyrite showed a lower release of arsenic – (0.41 ± 0.05 (Apy GH) versus 0.38 ± 0.06 (Apy GH: Pyh MG -1:1). Also, this difference is very small and within the experimental error, as shown in Figure 4-20. It is important to emphasize that the Pyh MG sample has surface characteristics different from the Pyh-V, marked by a high specific surface area and iron oxide hydroxides layer. Despite that, the results for As release in this section were not significantly different concerning the associations with the Pyh V sample, which allows us to conclude that the oxidized surface layer on the MG pyrrhotite sample did not influence the rate of sulfide oxidation.

To conclude, although Apy GH - Pyh V experiments showed a trend towards a greater release of As, the difference range is narrow. In addition, the Apy GH - Pyh MG results showed an insignificant effect on As release. Thus, the joint analysis of the two pyrrhotite samples allows us to conclude that the effect of pyrrhotite on arsenopyrite oxidation is negligible. The results for sulfur release (Figure 4-21) also indicate a small change when the sulfides were associated.

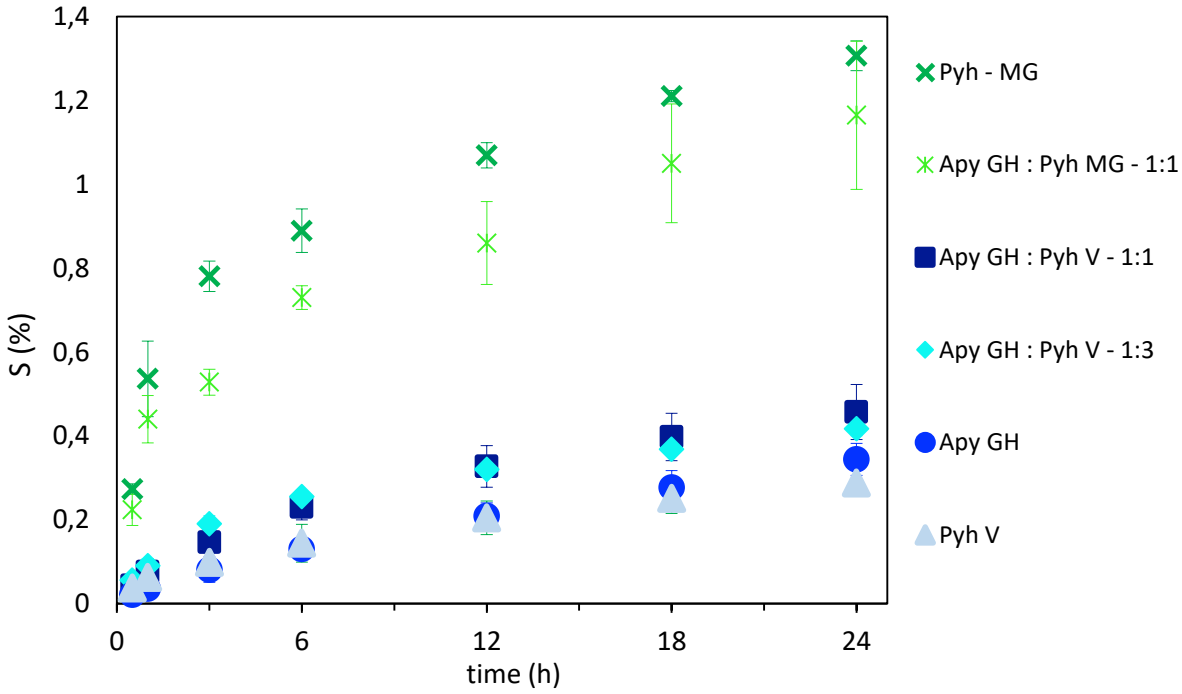

Figure 4-21: Effect of Pyh V sample coupling (50% w.t. and 75% w.t.) and Pyh MG sample coupling coupling (50% w.t.) on the accumulated sulfur release from FeAsS (GH) oxidation as a function of time. Experimental conditions: oxygen saturated medium; T = 25 ± 2ºC; pH $_{initial}$ 7.0 ± 0.2; pH $_{final}$ 6.5 (Apy GH; Apy GH: Pyh V experiments); pH$_{final}$ 5.2 ± 0.3 (Apy GH: Pyh MG) ; flow rate = 1.00 ± 0.05 ml.min^{-1}.

1.11 Environmental Implications

An important finding in the present study indicates that not only iron species already dissolved affect FeAsS dissolution, but also product layer of ferric oxyhydroxides under an oxygen medium. Strategies to decrease dissolved oxygen in the tailing dams (e.g., disposal under a water column, application of cover layers) have been applied to minimize the oxidation of sulfides (Ritcey, 2005, Malmström (2006), Pabst *et al*., 2018). Liu et al. (2008) claim that reducing the discharge amount of Fe(III) and other strongly oxidizing ions, is one of the important measures to improve the water environment in mining areas. Our results emphasize the importance of reducing the access of O_2, being effective both to reduce the diffusion of oxygen through the tailings, thus reducing the direct O_2 reaction, but also to prevent the oxidation of sulfides from the formation of the redox pair Fe(II)/Fe (III) at a circumneutral medium. The common association of arsenopyrite-pyrrhotite sulfides in tailings dams does not influence neither arsenic nor sulfur release.

5. CONCLUSION

i. The calculated rates for arsenic release from arsenopyrite were $10^{-9.0}$ and $10^{-9.5}$ mol.m^{-2}.s^{-1} for the stored and fresh minerals, respectively, suggesting that the removal of oxidation products prior to the experiment reduces the release rate in about five times at steady state conditions. This removal also favors to greater pH stability throughout the experiment and contributes to greater reliability of the oxidation rate results.

ii. It is proposed that oxidized product layer, when present, acts as a sink for the aqueous Fe(III), thus favoring arsenopyrite oxidation.

iii. Citrate showed a remarkable effect on sulfide oxidation (As and S release increased by about 300%), which is assumed to be a result of Fe(III)-citrate complexation, that in turn increases soluble ferric ion concentration at neutral conditions.

iv. Chloride ions complexation favors FeAsS oxidation by about 35%, even at conditions of low stability of the specie $FeCl_2^+$ at circumneutral pH.

v. Arsenopyrite has lower reaction rate at pH 7 – 3.54 x 10^{-10} ± 0.03 mol m^{-2}.s^{-1}, and 7.93 x 10^{-11} ± 0.08 mol m^{-2}.s^{-1} under oxygen-saturated and oxygen-depleted condition, respectively –, and the greatest dissolution rate occurs under acidic conditions.

vi. Oxygen has a positive effect on arsenic release from arsenopyrite at any pH condition.

vii. The oxidation rate of the two pyrrhotite samples is similar – $10^{-9.41}$ vs $10^{-9.50}$ mol.m^{-2}.g^{-1} – for Pyh MG and Pyh V, respectively at steady state condition. However, the initial rate and the % w.t. of sulfur released in 24h of experiments are very different (more than five times higher in the Pyh MG sample). Oxygen has a positive effect on the oxidation of pyrrhotite V.

viii. The association of arsenopyrite/pyrrhotite sulfides showed a negligible effect on arsenic and sulfur release for both pyrrhotite samples studied.

6. FURTHER STUDIES

i. To investigate through column tests the effect of pyrite/pyrrhotite association and the effect of mixing the three most common sulfides in gold mining tailings (pyrite, arsenopyrite, and pyrrhotite).

ii. To better characterize the surface of fresh and stored arsenopyrite samples and understand the difference between them.

iii. To better characterize pyrrhotite, focusing on understanding the low reactivity and low iron release of this sample, contrary to what is reported in the literature.

iv. To investigate humic acids as a material to cover or to mix with arsenopyrite particles, aiming to inhibit the sulfide oxidation.

7. REFERENCES

ABRAITIS, P.K., PATTRICK, R.A.D., KELSALL, G.H., VAUGHAN, D.J., (2004). Acid leaching and dissolution of major sulfide ore minerals: processes and galvanic effects in complex systems. Mineral. Mag. 68, 343–351.

ADAM, K., NATARAJAN, K.A., IWASAKI, I. (1984). Grinding media wear and its effect on the flotation of sulphide minerals. Int. J. Miner. Process. 12, 39-54.

ALMEIDA, C. M. V. B., & GIANNETTI, B. F. (2003). The electrochemical behavior of pyrite-pyrrhotite mixtures. Journal of Electroanalytical Chemistry, 553, 27–34.

ARAUJO, S. F., CALDEIRA, C. L., CIMINELLI, V. S. T., SILVA, A., & AMORIM, C. C. (2019). Versatility of iron-rich steel waste for the removal of high arsenic and sulfate concentrations in water. Environmental Science and Pollution Research, 26(5), 4266–4276. https://doi.org/10.1007/s11356-018-3168-7

ASTA, M. P.; CAMA, J.; AYORA, C.; ACERO, P.; GIUDICI, G. (2010) Arsenopyrite dissolution rates in O_2-bearing solutions. Chemical Geology, vol. 273, p. 272-285,

ASTA, M. P.; PÉREZ-LÓPEZ, R.; ROMÁN-ROSS, G.; ILLERA, V.; CAMA, J.; COTTE, M.; TUCOULOU, R. (2013). Analysis of the iron coatings formed during marcasite and arsenopyrite oxidation at neutral-alkaline conditions. Geologica Acta, vol. 11, nº 4, p. 465-481.

BASU, A.; MAHATA, J.; GUPTA, S.; GIRI, A. K. (2001) Genetic toxicology of a paradoxical human carcinogen, arsenic: a review. Mutation Research, vol. 488, 171–194.

BELZILE, N., CHEN, Y. W., CAI, M. F., & LI, Y. (2004). A review on pyrrhotite oxidation. Journal of Geochemical Exploration, 84(2), 65–76.

BERTAUT, E. F. (1953). Contribution à l'étude des structures lacunaires: la pyrrhotine. Acta Crystallographica, 6(6), 557-561.

BHATTACHARYA, P.; WELCH, A. H.; STOLLENWERK, K. G.; MCLAUGHLIN, M. J.; BUNDSCHUH, J.; PANAULLAH, G. Arsenic in the environment: Biology and Chemistry. Science of the Total Environment, vol. 379, p. 109–120, 2007.

BUCKLEY, A.N., WOODS, R., 1985. X-ray photoelectron spectroscopy of oxidized pyrrhotite surfaces: I. Exposure to air. Appl. Surf. Sci. 22/23, 280–287.

BUCKLEY, A. N.; WALKER, G. W. The surface composition of arsenopyrite exposed to oxidizing environments. Applied Surface Science, vol. 35, p. 227-240, 1988.

BUGAJINSKI, J., GAMSJAGER, H., 1982. The kinetics of dissolution of monoclinic pyrrhotite in aqueous acid solutions. Monat. Chem. 113, 1087–1092.

BUNDSCHUH, J.; LITTER, M., CIMINELLI, V. S. T; MORGADA, M. E.; CORNEJO, L.; HOYOS, S. G.; HOINKIS, J.; ALARCÓN-HERRERA, M. T.; ARMIENTA, M. A.; BHATTACHARYA, P. (2010) Emerging mitigation needs and sustainable options for solving the arsenic problems of rural and isolated urban areas in Latin America - A critical analysis. Water Research, vol. 44, p. 5828-5845.

CAI, M.F., DANG, Z., CHEN, Y.W., BELZILE, N. (2005). The passivation of pyrrhotite by surface coating. Chemosphere 61, 659–667.

CALDEIRA, C. L.; CIMINELLI, V. S. T.; OSSEO-ASARE, K (2010). The role of carbonate ions in pyrite oxidation in aqueous systems. Geochimica et Cosmochimica Acta, vol. 74, p. 1777–1789.

CHEN, Chung Yuan; WANG, Yun Ju; YANG, Chao Fen (2009). Estimating low-toxic-effect concentrations in closed-system algal toxicity tests. Ecotoxicology and Environmental Safety, v. 72, n. 5, p. 1514-1522.

CHENG, X., IWASAKI, I., (1992). Effect of chalcopyrite and pyrrhotite interaction on flotation separation. Miner. Metall. Process. 9 (2), 73-79.

CHIRITA, P., DESCOSTES, M., SCHLEGEL, M.L., 2008. Oxidation of FeS by oxygen-bearing acidic solutions. J. Colloid Interface Sci. 321, 84–95.

CHIRIŢĂ, P., & RIMSTIDT, J. D. (2014). Pyrrhotite dissolution in acidic media. Applied Geochemistry, 41, 1–10.

CHOPARD, A., BENZAAZOUA, M., PLANTE, B., BOUZAHZAH, H., & MARION, P. (2015). Kinetic experiments to evaluate the relative oxidation rates of various sulfides and sulfosalts. Proceedings of the 10th International Conference on Acid Rock Drainage (ICARD) & IMWA Annual Conference, Santiago, Chile, (April), 10.

CIMINELLI, V. S.T.; OSSEO-ASARE, K. (1995) Kinetics of pyrite oxidation in sodium hydroxide solutions. Metallurgical and Materials Transactions B, vol. 26, p. 209-218.

CIMINELLI, V. S.T.; OSSEO-ASARE, K. Kinetics of pyrite oxidation in sodium carbonate solutions. Metallurgical and Materials Transactions B, vol. 26B, p. 677-685, 1995.

CIMINELLI, V. S. T. (2014) Arsenic in mining: Sources and stability. In: One century of the discovery of Arsenicosis in Latin America (1914-2014). London, p. 3-7.

CIMINELLI, V. S. T.; GASPARON, M.; NG, J. C.; SILVA, G. C.; CALDEIRA, C. L. Dietary arsenic exposure in Brazil: The contribution of rice and beans. Chemosphere, vol. 168, p. 996-1003, 2017.

CISNEROS-GONZÁLEZ, I., OROPEZA-GUZMÁN, M., GONZÁLEZ, I. E., WOODS, R., & DOYLE, F. (2000). Electrochemistry in mineral and metal processing V. Electrochemistry in mineral and metal processing V.

CORKHILL, C. L.; VAUGHAN, D. J. Arsenopyrite oxidation – A review. Applied Geochemistry, vol. 24, p. 2342-2361, 2009.

CORRÊA, M L T; MELLO, J W V; RIBEIRO, A C; COSTA L M. Métodos de análises de sulfetos em amostras de rochas e sedimentos. Ver Brasil Ci. Solo, 26:103-115, 2002.

CRAW, D.; FALCONER, D.; YOUNGSON, J. H. Environmental arsenopyrite stability and dissolution: theory, experiment, and field observations. Chemical Geology, vol. 199, p. 71-82, 2003.

CRUZ, R., LUNA-SÁNCHEZ, R. M., LAPIDUS, G. T., GONZÁLEZ, I., & MONROY, M. (2005). An experimental strategy to determine galvanic interactions affecting the reactivity of sulfide mineral concentrates. Hydrometallurgy, 78(3–4), 198–208.

DE VILLIERS, J. P., LILES, D. C., & BECKER, M. (2009). The crystal structure of a naturally occurring 5C pyrrhotite from Sudbury, its chemistry, and vacancy distribution. American Mineralogist, 94(10), 1405-1410.

DENG, S., GU, G., HE, G., & LI, L. (2018). Catalytic effect of pyrite on the leaching of arsenopyrite in sulfuric acid and acid culture medium. Electrochimica Acta, 263, 8–16.

DENG, S., HE, G., WU, B., GU, G., (2020). Pyrite-promoted dissolution of arsenopyrite in the presence of Sulfobacillus thermosulfidooxidans. J. Mater. Res. Technol. 9 (4), 9362–9371.

DOS SANTOS, E. C., LOURENÇO, M. P., PETTERSSON, L. G. M., & DUARTE, H. A. (2017). Stability, Structure, and Electronic Properties of the Pyrite/Arsenopyrite Solid-Solid Interface-A DFT Study. Journal of Physical Chemistry C, 121(14), 8042–8051.

DRAHOTA, P.; FILIPPI, M. (2009) Secondary arsenic minerals in the environment: A review. Environment International, vol. 35, p. 1243–1255.

EKMEKÇI, Z., & DEMIREL, H. (1997). Effects of galvanic interaction on collectorless flotation behaviour of chalcopyrite and pyrite. International Journal of Mineral Processing, 52(1), 31–48.

ELLIOT, A. D. (2010). Structure of pyrrhotite 5C (Fe9S10). Acta Crystallographica Section B: Structural Science, 66(3), 271-279.

ELSETINOW, A. R., GUEVREMONT, J. M., STRONGIN, D. R., SCHOONEN, M. A. A., & STRONGIN, M. (2000). Oxidation of {100} and {111} surfaces of pyrite: Effects of preparation method. American Mineralogist, 85(3–4), 623–626.

FALLON, E. K., PETERSEN, S., BROOKER, R. A., & SCOTT, T. B. (2017). Oxidative dissolution of hydrothermal mixed-sulfide ore: An assessment of current knowledge in relation to seafloor massive sulfide mining. Ore Geology Reviews, 86, 309–337.

FERNANDO, W. A. M., ILANKOON, I. M. S. K., SYED, T. H., & YELLISHETTY, M. (2018). Challenges and opportunities in the removal of sulfate ions in contaminated mine water: A review. Minerals Engineering, 117, 74–90.

FERREIRA, P. M., MAJUSTE, D., FREITAS, E. T. F., CALDEIRA, C. L., DANTAS, M. S. S., & CIMINELLI, V. S. T. (2021). Galvanic effect of pyrite on arsenic release from arsenopyrite dissolution in oxygen-depleted and oxygen-saturated circumneutral solutions. Journal of Hazardous Materials, 412(January), 125236.

GLEISNER, M. (2005). Quantification of mineral weathering rates in sulfidic mine tailings under water-saturated conditions. Biogeochemistry. Stockholm University.

GUNSINGER, M. R., PTACEK, C. J., BLOWES, D. W., & JAMBOR, J. L. (2006). Evaluation of long-term sulfide oxidation processes within pyrrhotite-rich tailings, Manitoba. Journal of Contaminant Hydrology, 83(3–4), 149–170.

HARRIES, D. (2012). Structure and Reactivity of Terrestrial and Extraterrestrial Pyrrhotite. Universitaet Bayreuth (Germany).

HARRIES, D., POLLOK, K., & LANGENHORST, F. (2013). Oxidative dissolution of 4C- and NC-pyrrhotite: Intrinsic reactivity differences, pH dependence, and the effect of anisotropy. Geochimica et Cosmochimica Acta, 102, 23–44.

HOLMES, P.R., CRUNDWELL, F.K., 1995. Kinetic aspects of galvanic interactions between minerals during dissolution. Hydrometallurgy 39, 353–375.

HUANG, G., & GRANO, S. (2006). Galvanic interaction between grinding media and arsenopyrite and its effect on flotation: Part I. Quantifying galvanic interaction during grinding. International Journal of Mineral Processing, 78(3), 182–197.

HUGHES, M. F (2002). Arsenic toxicity and potential mechanisms of action. Toxicology Letters, vol. 133, p. 1–16.

ITO, H., FUJII, M., MASAGO, Y., WAITE, T. D., & OMURA, T. (2015). Effect of ionic strength on ligand exchange kinetics between a mononuclear ferric citrate complex and siderophore desferrioxamine B. Geochimica et Cosmochimica Acta, 154, 81-97.

IWASAKI, I., 1989. Bridging theory and practice in iron ore flotation, in: Advances in Coal and Mineral Processing Using Floatation. pp. 177–190.

JAMBOR, J.L., 1986. Detailed mineralogical examination of alteration products in core WA-20 from Waite Amulat tailings. CANMET Division Report MSL 86-137(IR). Dept. Energy Mines Resources, Canada.

JANZEN, M.P., 1996. Role of ferric iron, trace metal content, and crystal structure on pyrrhotite oxidation. MSc thesis. University of Waterloo. Canada. 175 pp.

JANZEN, M. P., NICHOLSON, R. V., & SCHARER, J. M. (2000). Pyrrhotite reaction kinetics: Reaction rates for oxidation by oxygen, ferric iron, and for nonoxidative dissolution. Geochimica et Cosmochimica Acta, 64(9), 1511–1522.

JOHNSON, D. B.; HALLBERG, K. B (2005). Acid mine drainage remediation options: a review. Science of the Total Environment, vol. 338, p. 3–14.

JONES, C. F., LECOUNT, S., SMART, R. S. C., & WHITE, T. J. (1992). Compositional and structural alteration of pyrrhotite surfaces in solution: XPS and XRD studies. Applied Surface Science, 55(1), 65–85.

JONES, R. A.; KOVAL, S. F.; NESBITT, H. W (2003). Surface alteration of arsenopyrite (FeAsS) by Thiobacillus ferroxidans. Geochimica et Cosmochimica Acta, vol. 67, nº5 ,p. 955-965.

KÖNIGSBERGER, L. C., KÖNIGSBERGER, E., MAY, P. M., & HEFTER, G. T. (2000). Complexation of iron (III) and iron (II) by citrate. Implications for iron speciation in blood plasma. Journal of inorganic biochemistry, 78(3), 175-184.

KOSLIDES, T.; CIMINELLI, V. S. T. (1992). Pressure oxidation of arsenopyrite and pyrite in alkaline solutions. Hydrometallurgy, vol. 30, p.87-106.

KOTO, K. I. C. H. I. R. O., MORIMOTO, N. O. B. U. O., & GYOBU, A. T. S. U. O. (1975). The superstructure of the intermediate pyrrhotite. I. Partially disordered distribution of metal vacancy in the 6C type, Fe11S12. Acta Crystallographica Section B: Structural Crystallography and Crystal Chemistry, 31(12), 2759-2764.

KWONG, Y.J., SWERHONE, G.W., LAWRENCE, J.R. (2003). Galvanic sulfide oxidation as a metal-leaching mechanism and its environmental implications. Geochem. Explor. Environ. Anal. 3 (4), 337e343.

LADEIRA, A. C. Q.; PANIAGO, E. B.; DUARTE, H. A.; CALDEIRA, C. L. (2014) Especiação Química e sua Importância nos Processos de Extração Mineral e de Remediação Ambiental. Cadernos Temáticos de Química Nova na Escola, n° 8, p. 18-23.

LIU, Q., LI, H., & ZHOU, L. (2008). Galvanic interactions between metal sulfide minerals in a flowing system: Implications for mines environmental restoration. Applied Geochemistry, 23(8), 2316–2323.

MALMSTRÖM, M. E., GLEISNER, M., & HERBERT, R. B. (2006). Element discharge from pyritic mine tailings at limited oxygen availability in column experiments. Applied Geochemistry, 21(1), 184–202.

MANDAL, B. K.; SUZUKI, K. T (2002). Arsenic round the world: a review. Talanta, vol. 58, p. 201–235, 2002.

MAJIMA, H. AND PETERS, E. (1968). Electrochemistry of sulfide dissolution in hydrometallurgical systems. Proc. Int. Min. Proc. Cong., Leningrad, 13pp.

MAJIMA, H., 1969. How oxidation affects selective flotation of complex sulfide ores. Can. Metall. Q. 8, 269–282.

MAJUSTE, D., CIMINELLI, V. S. T., OSSEO-ASARE, K., & DANTAS, M. S. S. (2012). Quantitative assessment of the effect of pyrite inclusions on chalcopyrite electrochemistry under oxidizing conditions. Hydrometallurgy, 113–114, 167–176.

MATSCHULLAT, J. Arsenic in the geosphere - a review. The Science of the Total Environment, vol. 249, p. 297-312, 2000.

MCGUIRE, M. M., BANFIELD, J. F., & HAMERS, R. J. (2001). Quantitative determination of elemental sulfur at the arsenopyrite surface after oxidation by ferric iron: Mechanistic implications. Geochemical Transactions, 2, 25–29.

MCKIBBEN, M.A., BARNES, H.L., 1986. Oxidation of pyrite in low temperature acidic solutions: rates laws and surface texture. Geochim. Cosmochim. Acta 50, 1509–1520.

MCKIBBEN, M. A.; TALLANT, B. A.; DEL ANGEL, J. K. Kinetics of inorganic arsenopyrite in acid aqueous solutions. Applied Geochemistry, vol. 23, p. 121-135, 2008.

MEHTA, A.P., MURR, L.E.(1983). Fundamental studies of contribution of galvanic interaction to acid-bacterial leaching of mixed metal sulfides. Hydrometallurgy 9, 235-256.

MIKHLIN, Y., VARNEK, V., ASANOV, I., TOMASHEVICH, Y., OKOTRUB, A., LIVSHITS, A., … PASHKOV, G. (2000). REACTIVITY OF PYRRHOTITE (FE9S10) SURFACES: SPECTROSCOPIC studies. Physical Chemistry Chemical Physics, 2(19), 4393–4398.

MIKHLIN, Y. L., KUKLINSKIY, A. V., PAVLENKO, N. I., VARNEK, V. A., ASANOV, I. P., OKOTRUB, A. V., … SOLOVYEV, L. A. (2002). Spectroscopic and XRD studies of the air degradation of acid-reacted pyrrhotites. Geochimica et Cosmochimica Acta, 66(23), 4057–4067.

MIKHLIN, Y., & TOMASHEVICH, Y. (2005). Pristine and reacted surfaces of pyrrhotite and arsenopyrite as studied by X-ray absorption near-edge structure spectroscopy. Physics and Chemistry of Minerals, 32(1), 19–27.

MIKUTTA, C., FROMMER, J., VOEGELIN, A., KAEGI, R., & KRETZSCHMAR, R. (2010). Effect of citrate on the local Fe coordination in ferrihydrite, arsenate binding, and ternary arsenate complex formation. Geochimica et Cosmochimica Acta, 74(19), 5574–5592.

MILLER, J. D., LI, J., DAVIDTZ, J. C., & VOS, F. (2005). A review of pyrrhotite flotation chemistry in the processing of PGM ores. Minerals Engineering, 18(8), 855–865.

MORAIS, M. A., GASPARON, M., DELBEM, I. D., CALDEIRA, C. L., FREITAS, E. T. F., NG, J. C., & CIMINELLI, V. S. T. (2019). Gastric/lung bioaccessibility and identification of arsenic-bearing phases and sources of fine surface dust in a gold mining district. Science of the Total Environment, 689, 1244–1254.

MOSES, O.; KIRK, D.; HERMAN S.; MILLS, L. Aqueous pyrite oxidation by dissolved oxygen and by ferric iron. Geochimica et Cosmochimica Acta, vol 51, p. 1561 - 1571, 1987.

MOSES, O.; HERMAN S. (1991) Pyrite oxidation at circumneutral pH. Geochimica et Cosmochimica Acta, vol 55, p. 471 - 482.

MUZEUM, A. (1990). Pyrrhotite superstructures. Part I: Fundamental structures ofthe Ne (N 2 , 3 , 4 and 5) type ISTvANDODONY. 7000.

MYCROFT, J. R., NESBITT, H. W., & PRATT, A. R. (1995). X-ray photoelectron and Auger electron spectroscopy of air-oxidized pyrrhotite: Distribution of oxidized species with depth. Geochimica et Cosmochimica Acta, 59(4), 721–733.

NAKAZAWA, H., & IWASAKI, I. (1985). Effect of Pyrite-Pyrrhotite contact on their floatabilities. Minerals and Metallurgical Processing, 2(4), 206–211.

NAKAZAWA, H., & IWASAKI, I. (1986). Galvanic contact between nickel arsenide and pyrrhotite and its effect on flotation. International Journal of Mineral Processing, 18(3–4), 203–215.

NAZARI, A.; RADZINSKI, R.; GHAHREMAN, AHMAD. Review of arsenic metallurgy: Treatment of arsenical minerals and the immobilization of arsenic. Hydrometallurgy, vol. 174, p. 258-281, 2017.

NEIL, W. C; JUN Y. Fe (III) Addition Promotes Arsenopyrite Dissolution and Iron(III) (Hydr)oxide Formation and Phase Transformation. Environmental Science & Technology Letters, 3, 30-35, 2016.

NESBITT, H. W., MUIR, I. J., PRATT, A. R. Oxidation of arsenopyrite by air and airsaturated, distilled water and implications for mechanisms of oxidation. Geochimica et Cosmochimica Acta, vol. 59, p. 1773–1786, 1995.

NICHOLSON, R.V., SCHARER, J.M. (1994). Laboratory studies of pyrrhotite oxidation kinetics. In: Alpers, C.N., Blowes, D.W. (Eds.), Environmental Geochemistry of Sulfide Oxidation. ACS Symposium Series, vol. 550, pp. 14–30. Washington.

NICOL M. J. AND SCOTT P. D. (1979) The kinetics and mechanism of the non-oxidative dissolution of some iron sulfides in aqueous acidic solutions. J. South African Institute of Mining and Metallurgy**,** 298 –305.

PABST, T., BUSSIÈRE, B., AUBERTIN, M., & MOLSON, J. (2018). Comparative performance of cover systems to prevent acid mine drainage from pre-oxidized tailings: A numerical hydro-geochemical assessment. Journal of Contaminant Hydrology, 214, 39–53.

PARTHASARATHY, H., BALTRUS, J. P., DZOMBAK, D. A., & KARAMALIDIS, A. K. (2014). A method for preparation and cleaning of uniformly sized arsenopyrite particles. Geochemical Transactions, 15(1).

PEIFFER S. AND STUBERT I. (1999) The oxidation of pyrite at pH 7 in the presence of reducing and nonreducing Fe(III)-chelators. Geochim. Cosmochim. Acta 63, 3171–3182.

POZZO, R.L., IWASAKI, I., 1989. Pyrite-pyrrhotite grinding media interactions and their effects on media wear and flotation. J. Electrochem. Soc. 136, 1734.

PRATT, A. R., NESBITT, H. W., & MYCROFT, J. R. (1996). The increased reactivity of pyrrhotite and magnetite phases in sulfide mine tailings. Journal of Geochemical Exploration, 56(1), 1–11.

QIAN, G., FAN, R., SHORT, M. D., SCHUMANN, R. C., LI, J., ST, R. C., & GERSON, A. R. (2018). The Effects of Galvanic Interactions with Pyrite on the Generation of Acid and Metalliferous Drainage. Environmental Science and Technology, 52(9), 5349–5357.

QING YOU, L., HEPING, L., & LI, Z. (2007). Study of galvanic interactions between pyrite and chalcopyrite in a flowing system: Implications for the environment. Environmental Geology, 52(1), 11–18.

RABIEH, A., EKSTEEN, J. J., & ALBIJANIC, B. (2017). The effect of grinding on cyanide leaching of gold in the presence of pyrrhotite. Hydrometallurgy, 173(April), 115–124.

RITCEY, G. M. (2005). Tailings management in gold plants. Hydrometallurgy, 78(1-2 SPEC. ISS.), 3–20.

ROMANO, G.Y., 2012. Kinetics of Pyrrhotite Oxidation in Seawater: Implications for Mining Seafloor Hotsprings. Master Thesis. University of California Riverside.

SANCHEZ, V. M.; HISKEY, B. J. Electrochemical behaviour of arsenopyrite in alkaline media. Mineral & Metallurgical Processing, p. 1–6, 1991.

SCHAUFUSS, A.; NESBITT, H; SCIANI J.; HOECSHT H.; BANCROFT. G.; SZARGAN R. (2000). Reactivity of surface sites on fractured arsenopyrite (FeAsS) toward oxygen. Am. Mineral, vol 85, 1754–1766.

SHARMA, M. K., & KUMAR, M. (2020). Sulfate contamination in groundwater and its remediation: an overview. Environmental Monitoring and Assessment, 192(2).

SILVA, A. M., KONG, X., PARKIN, M. C., CAMMACK, R., & HIDER, R. C. (2009). Iron (III) citrate speciation in aqueous solution. Dalton Transactions, (40), 8616-8625.

SILVA, J. C. M., DE ABREU, H. A., & DUARTE, H. A. (2015). Electronic and structural properties of bulk arsenopyrite and its cleavage surfaces-a DFT study. RSC Advances, 5(3), 2013–2023.

SILVA, J. C. M., DOS SANTOS, E. C., HEINE, T., DE ABREU, H. A., & DUARTE, H. A. (2017). Oxidation Mechanism of Arsenopyrite in the Presence of Water. Journal of Physical Chemistry C, 121(48), 26887–26894.

SIMATE, G. S., & NDLOVU, S. (2014). Acid mine drainage: Challenges and opportunities. Journal of Environmental Chemical Engineering, 2(3), 1785–1803.

SINGH, R.; SINGH, S.; PARIHAR, P.; SINGH, V. P.;PRASAD, S. M. (2015) Arsenic contamination, consequences and remediation techniques: A review. Ecotoxicology and Environmental Safety, vol 112, p. 247-270.

SMEDLEY, P. L.; KINNIBURGH, D. G (2002). A review of the source, behavior and distribution of arsenic in natural waters. Applied Geochemistry, vol. 17, 517-568.

THOMAS, J.E., JONES, C.F., SKINNER, W.M., SMART, R.ST.C., 1998. The role of surface sulfur species in the inhibition of pyrrhotite dissolution in acid conditions. Geochim. Cosmochim. Acta 62, 1555–1565.

THOMAS, J.E., SMART, R.S.C., SKINNER, W.M., 2000. Kinetic factors for oxidative and non-oxidative dissolution of iron sulfides. Miner. Eng. 13, 1149–1159.

THOMAS, J.E., SKINNER, W.M., SMART, R.S.C., 2001. A mechanism to explain sudden changes in rates and products for pyrrhotite dissolution in acid solution. Geochim. Cosmochim. Acta 65, 1–12.

TOKONAMI, M., NISHIGUCHI, K., & MORIMOTO, N. (1972). Crystal structure of a monoclinic pyrrhotite (Fe7S8). American Mineralogist: Journal of Earth and Planetary Materials, 57(7-8), 1066-1080.

URBANO, G., MELÉNDEZ, A. M., REYES, V. E., VELOZ, M. A., & GONZÁLEZ, I. (2007). Galvanic interactions between galena-sphalerite and their reactivity. International Journal of Mineral Processing, 82(3), 148–155.

URBANO, G., REYES, V. E., VELOZ, M. A., GONZÁLEZ, I., & CRUZ, J. (2008). Pyrite-arsenopyrite galvanic interaction and electrochemical reactivity. Journal of Physical Chemistry C, 112(28), 10453–10461.

WALKER, F. P.; SCHREIBER, M. E.; RIMSTIDT, J. D. Kinetics of arsenopyrite oxidative dissolution by oxygen. Geochimica et Cosmochimica Acta, vol. 70, p. 1668–1676, 2006.

WANG, S.; JIAO, B.; ZHANG, M.; ZHANG, G.; WANG, X; JIA, Y. (2018). Arsenic release and speciation during the oxidative dissolution of arsenopyrite by O_2 in the absence and presence of EDTA. Journal of Hazardous Materials, vol. 346, p. 184-190.

WILLIAMSON, A. RIMSTIDT, D. (1994) The kinetics and electrochemical rate-determining step of aqueous pyrite oxidation. Geochimica et Cosmochimica Acta, vol. 58, 5443-5454.

WORLD HEALTH ORGANIZATION (WHO), 2016. Disponível em: <http://www.who.int/mediacentre/factsheets/fs372/en/>, acessado em agosto de 2017.

WORLD HEALTH ORGANIZATION (WHO). Environmental health criteria 224, arsenic and arsenic compounds. Inter-organization program for the sound management of chemicals. Geneva; 2001.

YU, Y.; ZHU, Y.; WILLIAMS-JONES, A. E.; GAO, Z.; Li, D. (2004). A kinetic study of the oxidation of arsenopyrite in acidic solutions: implications for the environment. Applied Geochemistry, vol. 19, p. 435-444.

YU, Y.; ZHU, Y.; GAO, Z.; GAMMONS.; LI, D. (2007) Rates of Arsenopyrite Oxidation by Oxygen and Fe (III) at pH 1.8-12.6 and 15-45 °C. Environmental Science & Technology.

ZHANG, Y., & ZHOU, M. (2019). A critical review of the application of chelating agents to enable Fenton and Fenton-like reactions at high pH values. Journal of Hazardous Materials, 362, 436–450.

ZHENG, K., LI, H., WANG, S., FENG, X., WANG, L., & LIU, Q. (2020). Arsenopyrite weathering in sodium chloride solution: Arsenic geochemical evolution and environmental effects. Journal of Hazardous Materials, 392.

8. APPENDIX

APPENDIX A. ADDITIONAL CHEMICAL ANALYSIS INFORMATION

1. Digestion procedure

Acqua regia solutions prepared by mixing analytical grade 37% HCl and 65% HNO3 (Química Moderna Indústria and Comércio Ltda, São Paulo, Brazil) in a v/v ratio of 3:1, according to a procedure following acid digestion based on method 3050b in (Correa et al., 2002).

An amount of 20mg of sample (in triplicate), 9mL of HNO_3 and 3mL HCl were weighed into Teflon digestion vessels (50mL) and digested. On the following day and after reaching room temperature (~25ºC), the extracted solutions were transferred to FalconTM tubes, and made up to 50mL with deionized 18MΩ.cm water. The vessels were washed at least three times with deionized water to ensure the complete recovery of the extracted solution. The resultant solutions were stored at 4ºC until further analysis. The elements were analyzed by inductively coupled plasma optical emission spectrometry (ICP-OES) (Perkin Elmer, Optima 7300DV, Shelton, CT USA) according to the conditions described in Table A1. As quality assurance and quality control, two standard reference materials (NIST SRM 2710a and CANMET/ CCRMPTill3) were analyzed together with each batch of 10 samples. Lutetium ($1mg.L^{-1}$) was used as an internal standard element to monitor matrix effects and sensitivity drifts of the ICP-OES instrument.

The method of digestion by lithium metaborate fusion was used to analyze sulfur from the solid samples. A 100mg sample is weighed into a platinum crucible and 600mg LiBO2 is added and mixed well. Graphite crucibles are heated at 950°C for 50min, removed from the oven, and allowed to cool slightly. The melt is brought into solution with 4% HNO3 and quantitatively transferred to a 250mL plastic volumetric flask (Bartenfelder and Karathanasis, 1988).

2. ICPOES- Instrumental Conditions

Tabela A-1: ICP - OES (Perkin Elmer Optima 7300DV) instrumental conditions

Parameter	**Condition**
Radiofrequency (W)	1300
Internal Spike	Lu 1 $mg.kg^{-1}$
Nebulizer	LowFlow*, Burgener Miramist**
Chamber	Scott*, Cyclonic Spray**
Nebulizer Ar flow ($mL.min^{-1}$)	0.80
Alumina injector (mm)	2.0
Plasma Ar flow ($L.min^{-1}$)	15
Auxiliary Ar gas ($L.min^{-1}$)	0.8
Sample flow ($mL.min^{-1}$)	1.3
λ (nm)	As 193.7, Fe 238.2 and S 181,975

**Analysis from digestion – fusion and acqua regia)*

***Direct analysis to solution from oxidation experiments*

3. ICPMS- Instrumental Conditions

Tabela A-2: ICP-MS (PerkinElmer - NexION 300X) instrument operational parameters

Parameters	Conditions
Nebulizer type	Meinhard Concentric Glass
Peristaltic pump speed (rpm)	20
Nebulizer gas flow (L/min)	0.95
Auxiliary gas flow (L/min)	1.2
Plasma gas flow (L/min)	18
ICP RF Power (W)	1600 W
Reaction gas flow – DRC mode (mL/min)	As: oxygen - 0.5
	S: oxygen - 0.8
Colision gas flow – KED mode m(L/min)	Fe: helium - 3.8

APPENDIX B. SAMPLE CHARACTERIZATION

1. SEM - Scanning Electron Microscopy

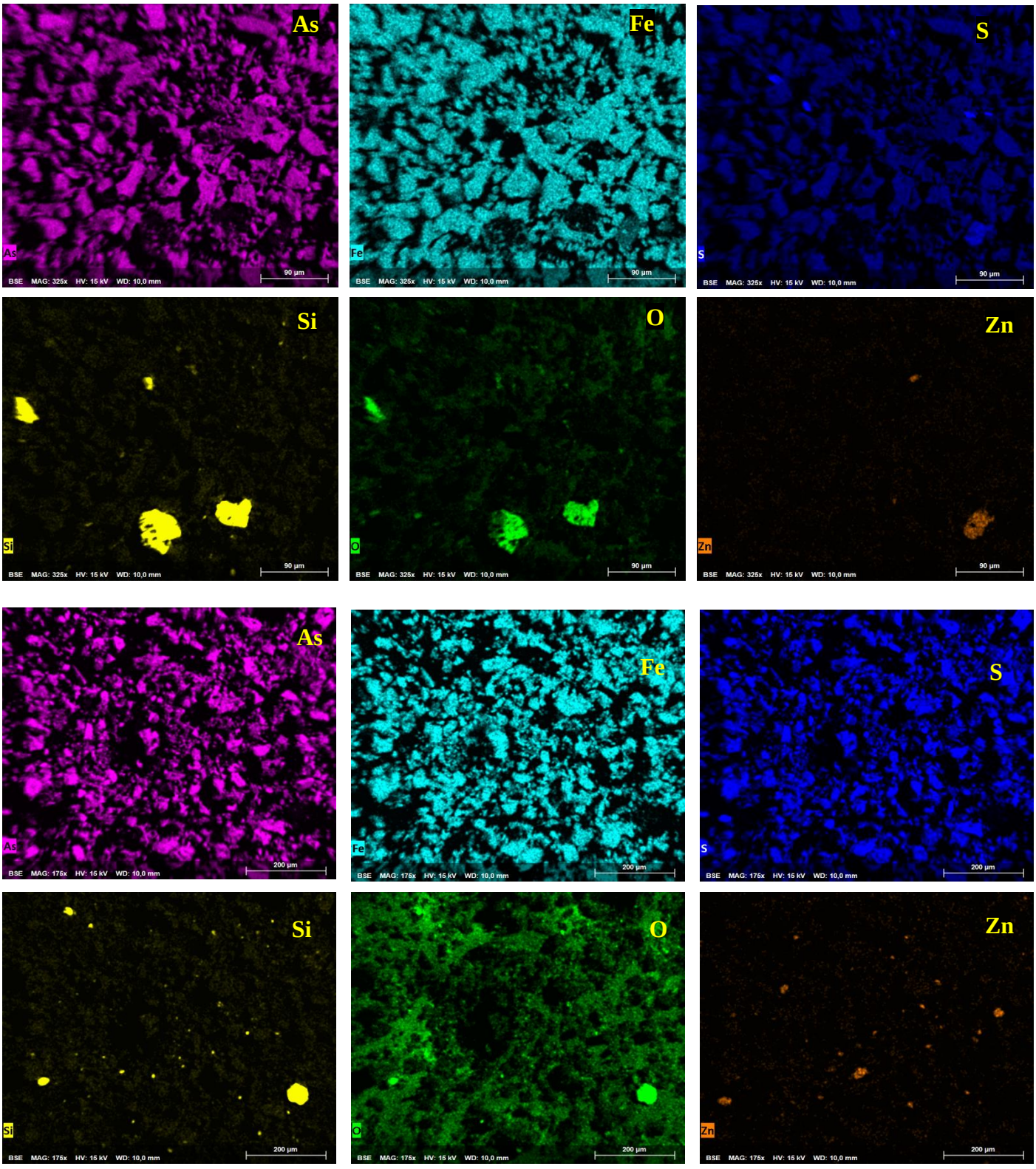

Figure 8-1 : Arsenopyrite (sample H) elemental composition map by EDS of fresh – 90 µm scale (a) and stored – 200 µm scale (b). The stored sample indicates a higher oxygen amount on the surface.

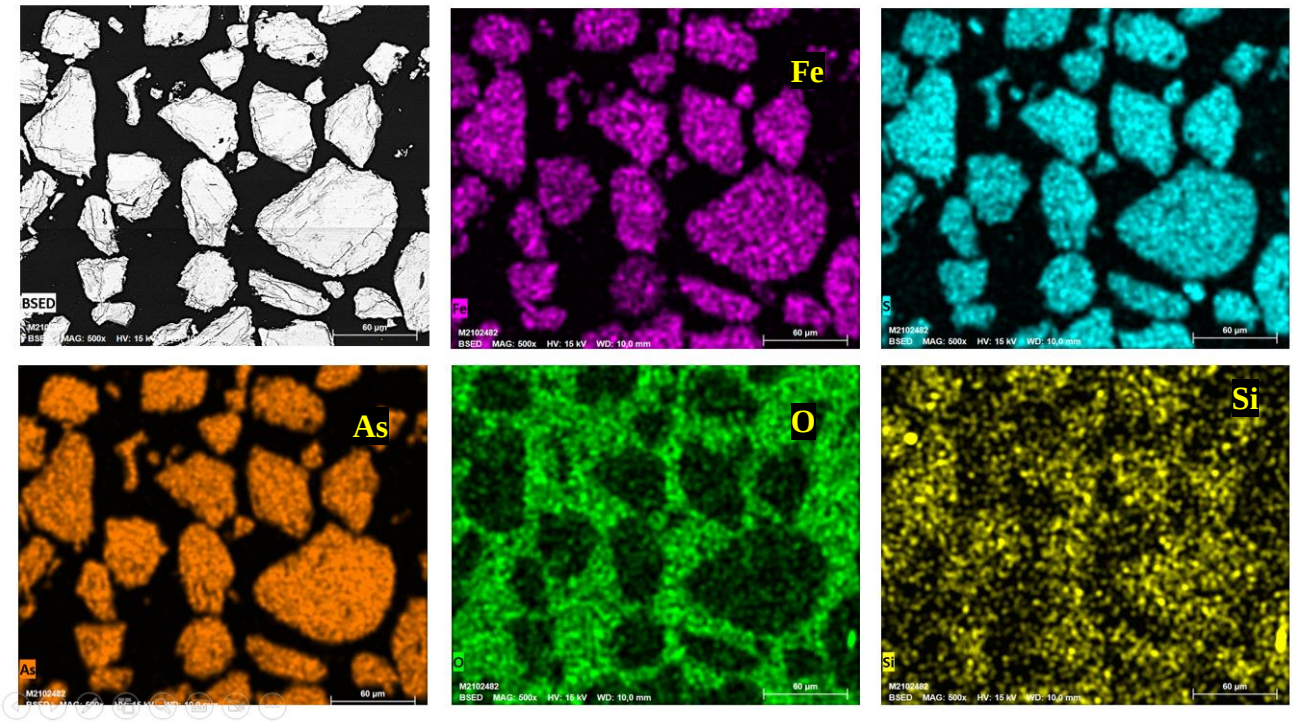

Figure 8-2: Arsenopyrite (sample GH - fresh) elemental composition map by EDS – 60 µm scale.

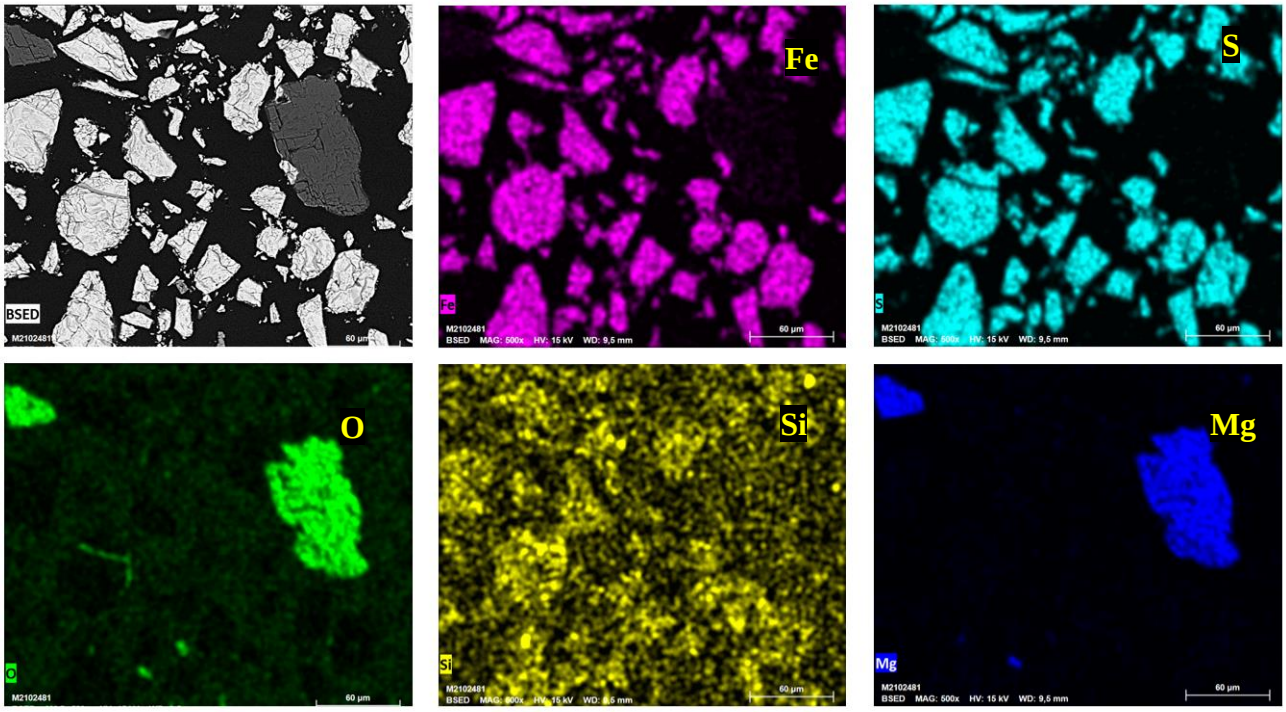

Figure 8-3: Pyrrhotite (sample V) elemental composition map by EDS – 60 µm scale.

2. **Granulometric Distribution**

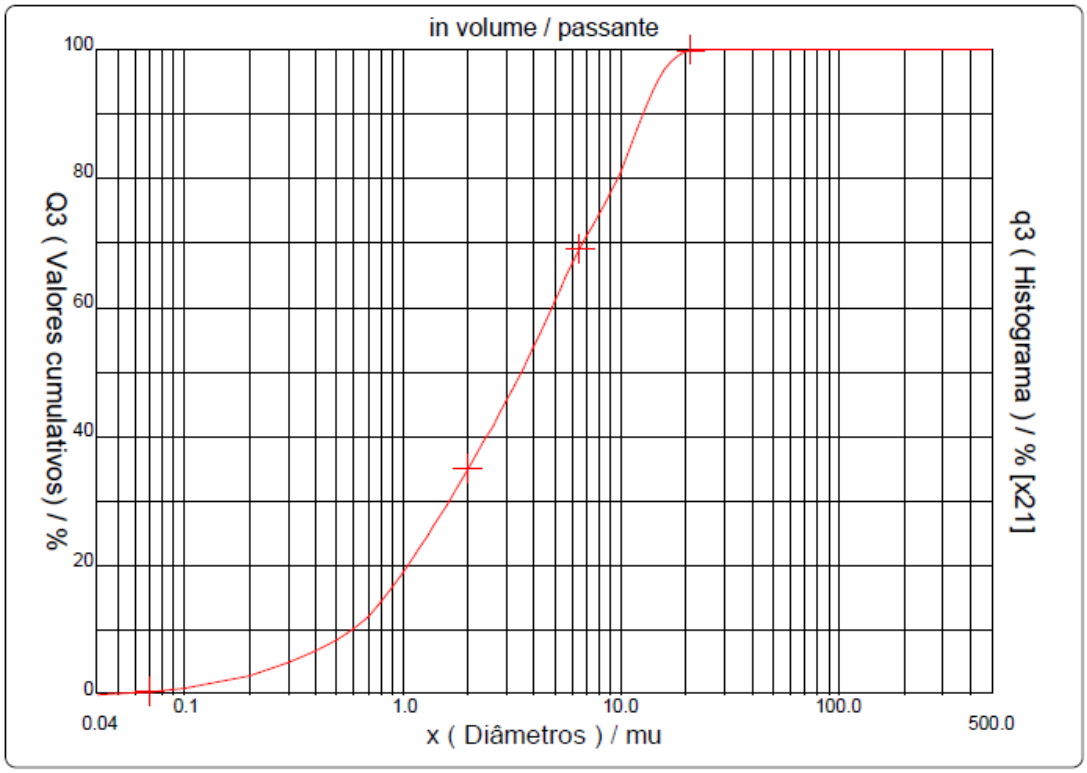

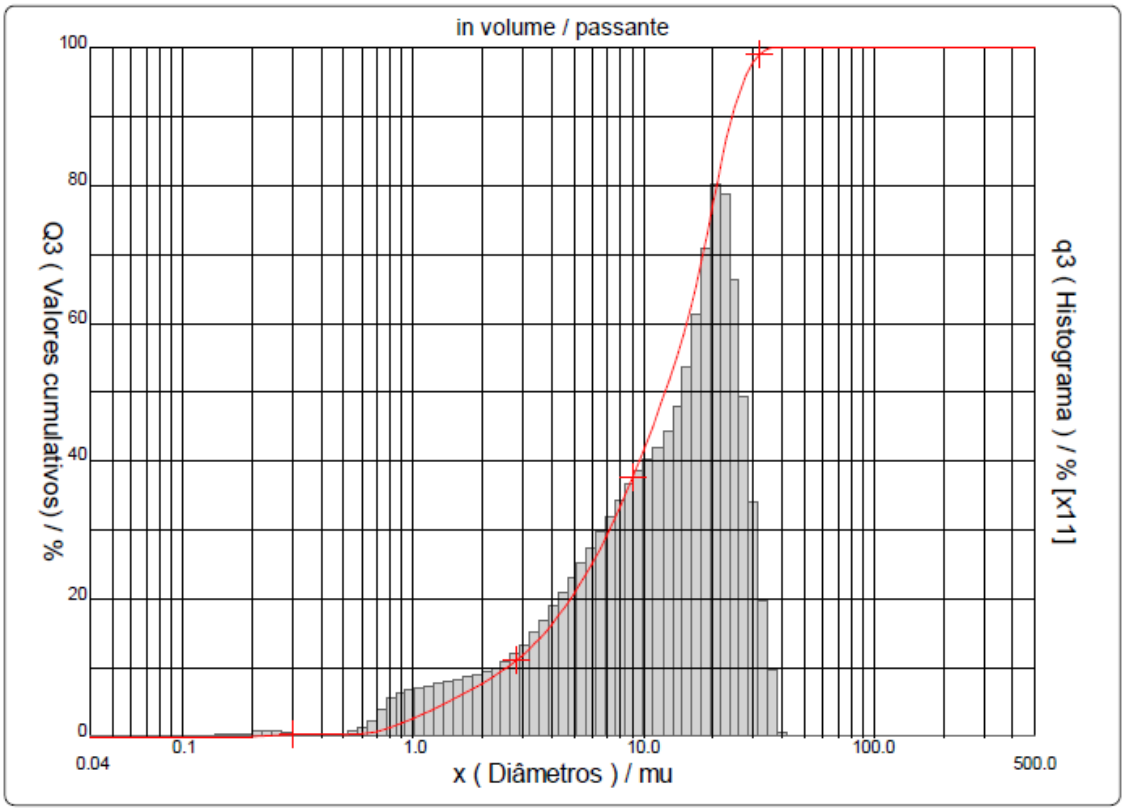

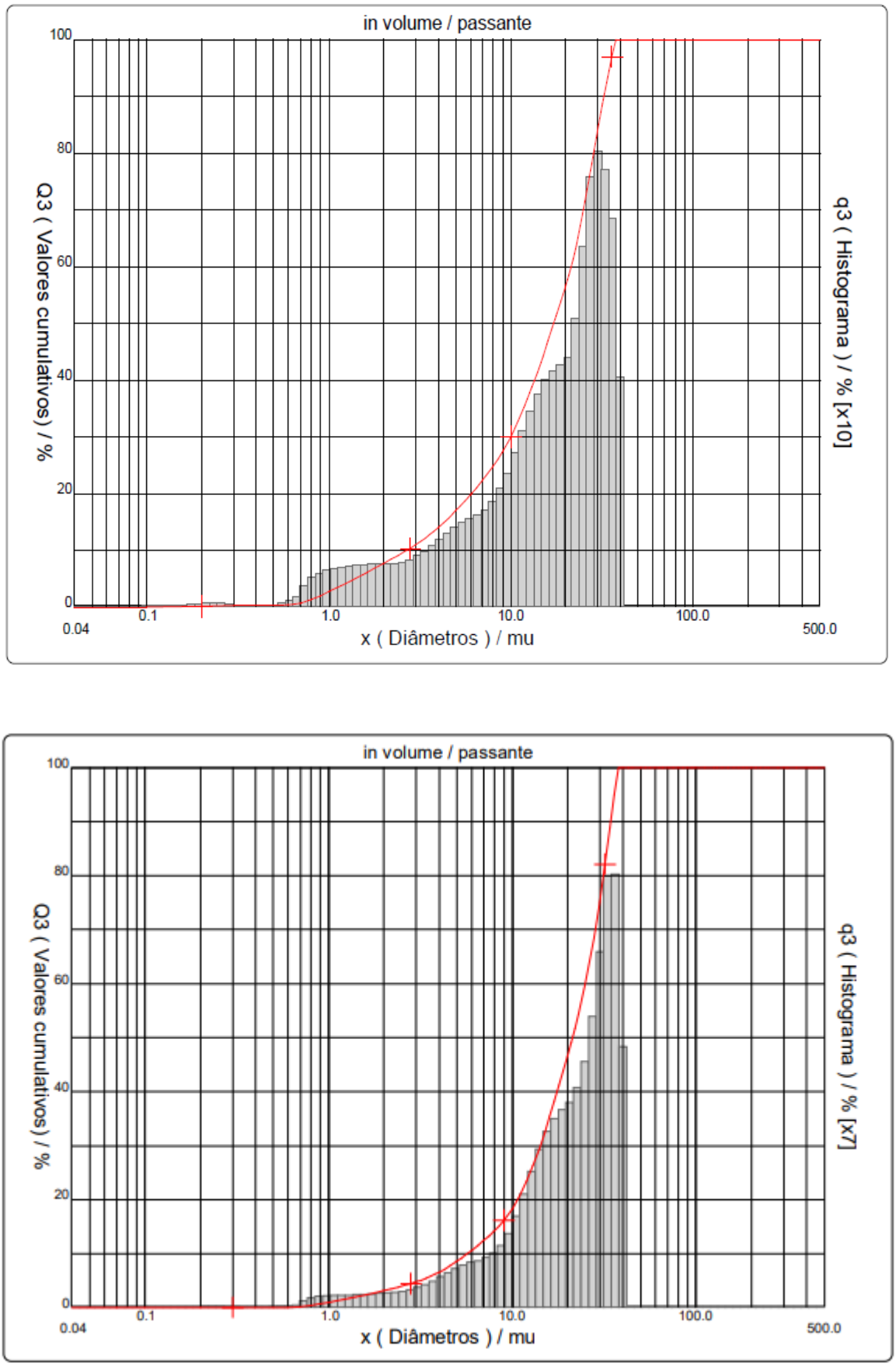

Figure 8-4 : Granulometric distribution histogram obtained by CILAS of the samples Apy H (a); Apy GH (b); Pyh V (c) and Pyh MG (d).

APPENDIX C. GRAPHIC RESULTS OF OXIDATION EXPERIMENTS UNDER FLOW-THROUGH REACTOR

1. **Experiments conducted at 40** °C

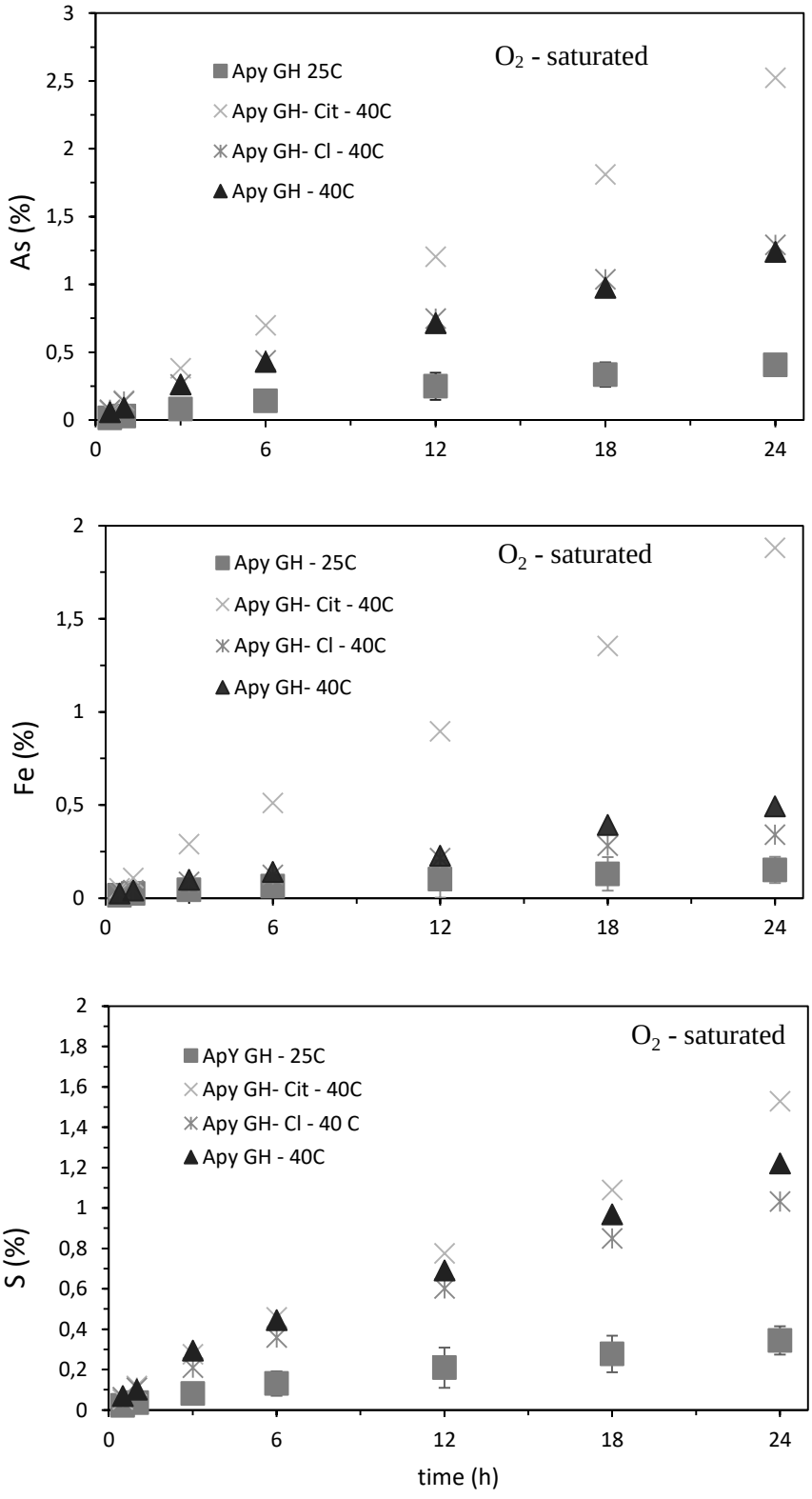

Figure 8-5: Combined effect of temperature (25 and 40 ºC) and ligand ions (chloride and citrate - 1mmol) on accumulated arsenic (a) iron (b) sulfur release (c) under oxygen- saturated condition from FeAsS (sample GH) oxidation as a function of time. Experimental conditions: $pH_{initial}$ 7.0 ± 0.2, flow rate 1.00 ml.min^{-1} ± 0.05.

2. Pyrite-pyrrhotite association

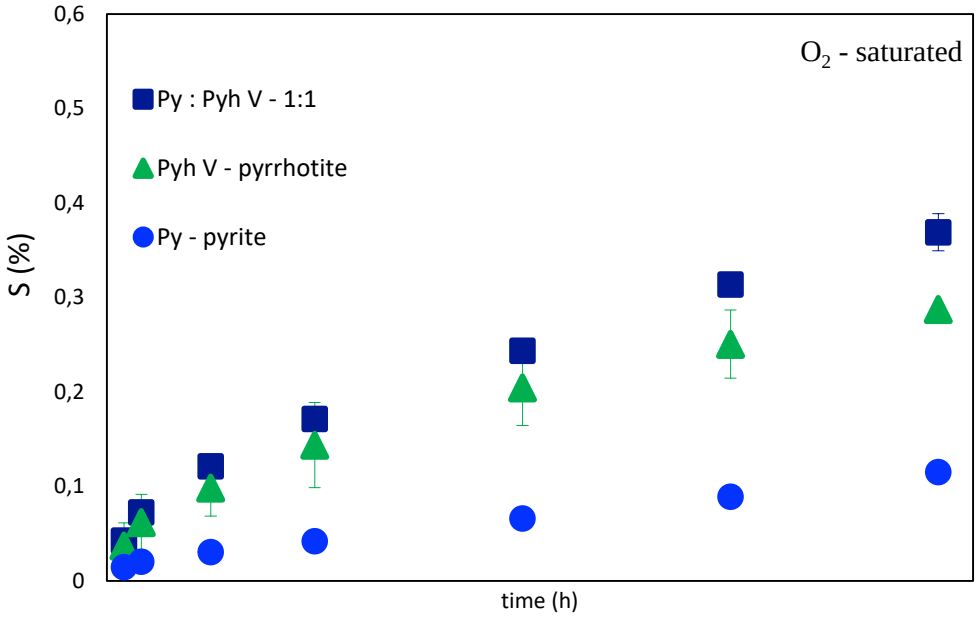

Figure 8-6: Effect of Pyh V sample coupling (50% w.t.) on the accumulated sulfur release from pyrite (FeS_2) oxidation as a function of time. Experimental conditions: oxygen saturated medium; T = 25 ± 2ºC;$pH_{initial}$ = 7.0. As expected, a higher release of sulfur occurred when the minerals were associated, indicating galvanic effect. The pyrite sample is the same used for Ferreira et al. (2021) (49–5884; Zacatecas, Mexico) and is estimated as 96.4% wt. FeS_2.

3. Concentration graphs (ppm) of the main results of this study

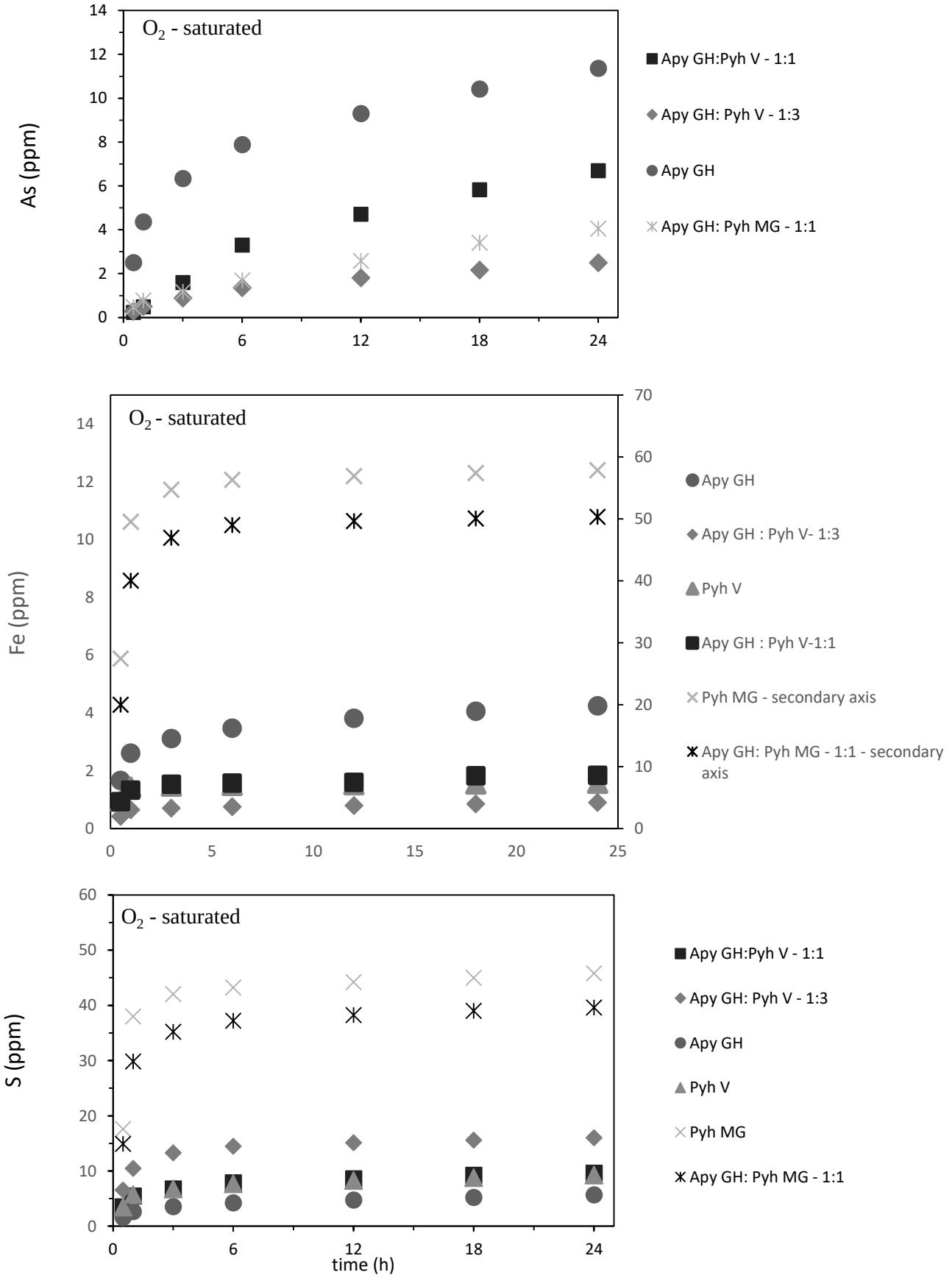

Figure 8-7: Effect of Pyh V sample coupling (50% w.t. and 75% w.t.) and Pyh MG sample coupling (50% w.t.) on the arsenic (a) iron (b) sulfur release (ppm) (c) under oxygen- saturated condition from FeAsS (sample GH) oxidation as a function of time. Experimental conditions: $pH_{initial}$ 7.0 ± 0.2, flow rate 1.00 ml.min^{-1} ± 0.05.

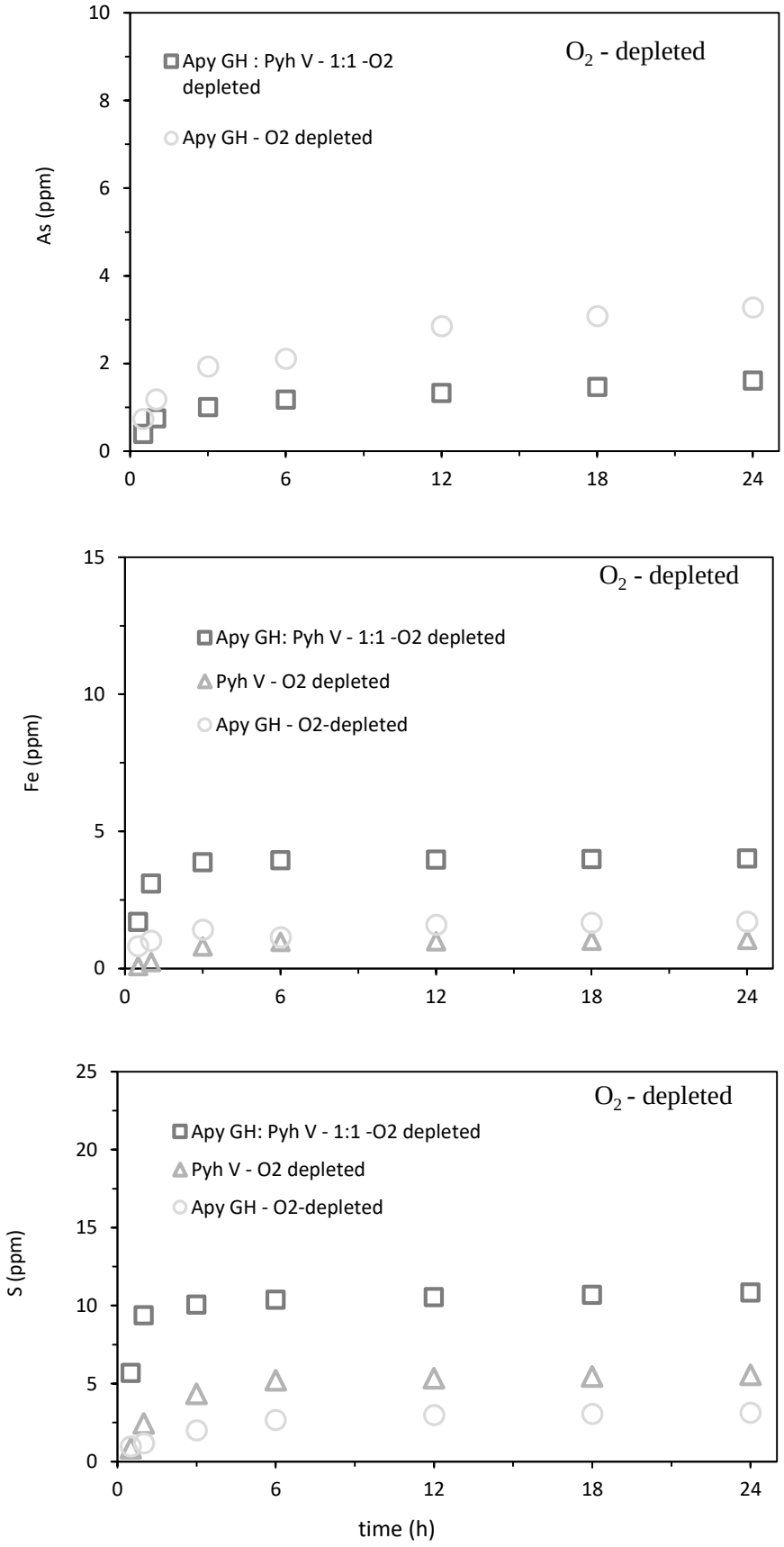

Figure 8-8: Effect of Pyh V sample coupling (50% w.t. coupling on the arsenic (a) iron (b) sulfur release (ppm) (c) under oxygen- depleted condition from FeAsS (sample GH) oxidation as a function of time. Experimental conditions: $pH_{initial}$ 7.0 ± 0.2, flow rate 1.00 ml.min^{-1} ± 0.05.

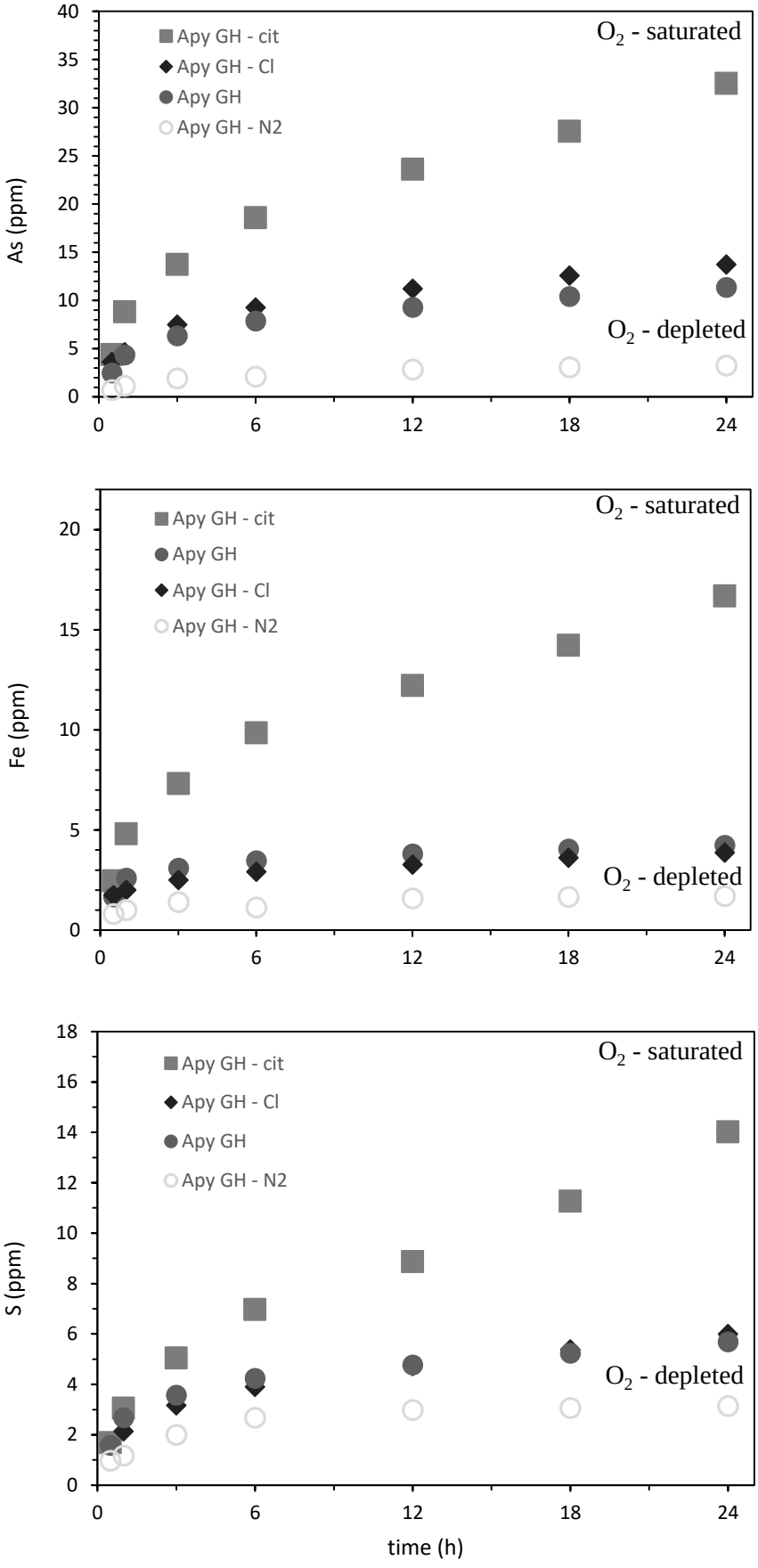

Figure 8-9: Chloride and citrate (1mmol) effect on accumulated arsenic (a) iron (b) sulfur release (ppm) (c) under oxygen-saturated and oxygen depleted condition from FeAsS (sample GH) oxidation as a function of time. Experimental conditions: $pH_{initial}$ 7.0 ± 0.2, flow rate 1.00 ml.min^{-1} ± 0.05.

APPENDIX D. SHAKER EXPERIMENTS

4. Addition of ferrous and ferric sulfates in the feed solution of the arsenopyrite oxidation experiment

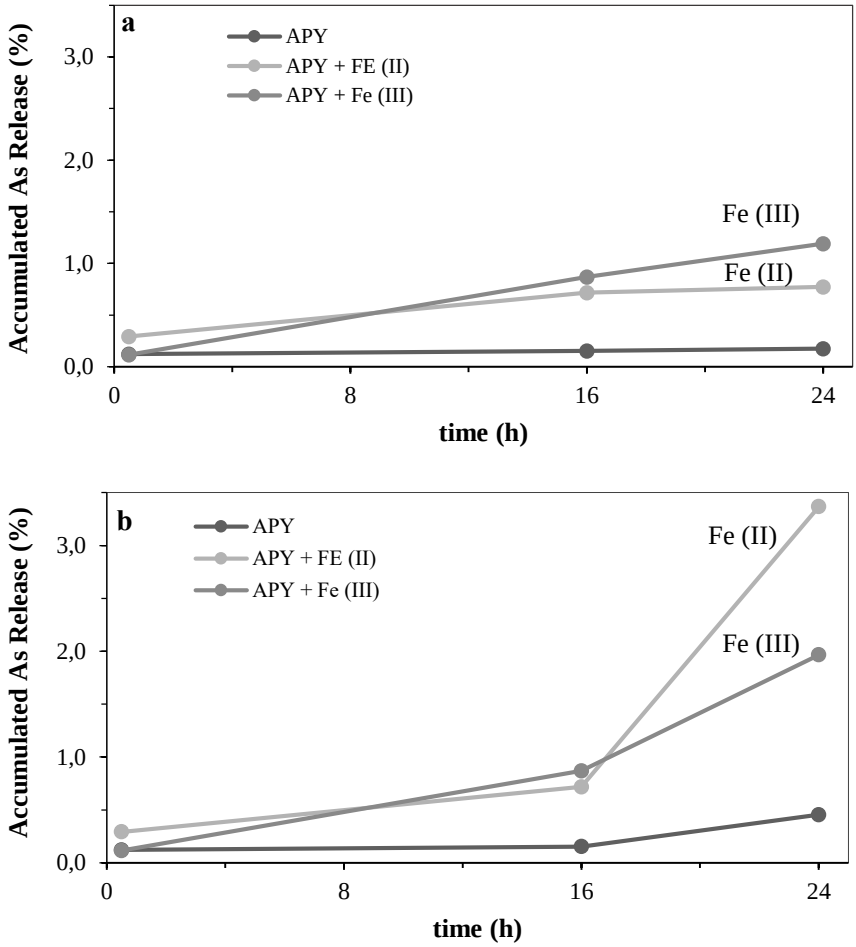

Figure 8-10: : **Effect of Fe (II) and Fe (III) addition on arsenic release; pH 5; T=25±2ºC; d50 = 13 μm. (a) Arsenic (%) released (b) Arsenic (%) released + acid cleaning of products. From graphic (a), the addition of Fe (II) increases approximately four times the arsenic release from the washed sample and, despite ferric iron precipitation (pH 5), is about six times higher when Fe (III) was added. After washing the leach product with HCl (graphic b), the total As released was seven and four times higher for the system conducted with Fe (II) and with Fe (III), respectively. It is suggested that the greater release of Arsenic under these conditions may be related to the oxidation of Fe (II) to Fe (III) by oxygen during the experiments. Thus, making the oxidant (Fe (III)) available in soluble form for the reaction.**

APPENDIX E.

Table E-1: Selected species and respective thermodynamic data from the Eh-pH diagram of the aqueous species of inorganic arsenic at 25ºC and arsenopyrite, 1bar, for $[As]_{total}$=10µmol.L^{-1} (Figure 2-1) (Source: *software HSC Chemistry* 9.0).

Species	ΔG_f^o (kcal.mol^{-1})
$FeAsO_4$	-184.607
FeAsS	-11.888
Fe_2O_3	-177.540
Fe_3O_4	-241.956
FeO*OH	-117.237
$Fe(OH)_2$	-116.389
$Fe(OH)_3$	-168.088
$Fe_2O_3*H_2O$	-233.230
$FeAsO_{4(aq)}$	-177.815
$HAsO_{2\ (aq)}$	-96.266
$H_3AsO_{3\ (aq)}$	-152.867
$H_3AsO_{4\ (aq)}$	-183.226
$AsO_2^{-}{}_{(aq)}$	-83.614
$AsO_3^{-3}{}_{(aq)}$	-106.935
$AsO_4^{-3}{}_{(aq)}$	-154.452
$FeAsO_4^{-}{}_{(aq)}$	-186.630
$HAsO_3^{-2}{}_{(aq)}$	-125.166
$HAsO_4^{-2}{}_{(aq)}$	-170.552
$H_2AsO_3^{-}{}_{(aq)}$	-140.425
$H_2AsO_4^{-}{}_{(aq)}$	-180.094
$SO_4^{-2}{}_{(aq)}$	-177.907

Table E-2: Selected species and respective thermodynamic data from the Eh-pH diagram of the aqueous species of inorganic iron at 25 ºC, 1 bar. $[Fe]_{(aq)} = 10^{-4}$ M systems; $[Cl]_{(aq)} = 10^{-3}$ M ideal solutions. Eh (V). (Figure 4-12) (Source: *software HSC Chemistry* 7.0).

Species	**ΔG_f^o (kcal.mol^{-1})**
$FeCl_2$	-72.15
$FeCl_3$	-79.39
Fe_2O_3	-177.11
Fe_3O_4	-241.96
FeO*OH	-116.93
$Fe(OH)_2$	-117.58
$Fe(OH)_3$	-168.64
$Fe_2O_3*H_2O$	-233.32
FeO	-58.73
FeOCl	-86.10
Cl^-	-31.37
Fe^{3+}	-4.11
Fe^{2+}	-21.88
$FeCl^{2+}$	-37.50
$FeCl^+$	-53.03
$FeCl_2^+$	-86.27
FeO^+	-53.09
FeO_2^-	-92.64
$FeOH^{2+}$	-57.83
$FeOH^+$	-65.85
$FeOH_2^+$	-108.08